CD47 impedes Antiviral Alveolar Macrophage Responses during Influenza A Virus Infection

Inaugural-Dissertation

zur

Erlangung des Doktorgrades

Dr. rer. nat.

Der Fakultät für

Biologie

an der

Universität Duisburg-Essen

Vorgelegt von

Christina Wenzek

Aus Bochum

Oktober 2020

Die in der vorliegenden Arbeit zugrunde liegenden Experimente wurden am Institut für medizinische Mikrobiologie der Universität Duisburg-Essen durchgeführt.

1. Gutachter: Prof. Dr. Jan Buer
2. Gutachter: Prof. Dr. Ulf Dittmer
3. Gutachter: /

Vorsitzender des Prüfungsausschusses: Prof. Dr. Sven Brandau

Tag der mündlichen Prüfung: 23.02.2021

DOI: 10.17185/duepublico/74145
URN: urn:nbn:de:hbz:464-20210323-113912-6

Table of Contents

List of Abbreviations

Abbreviation	Denotation
ACVR1C	Activin A Receptor, Type I C
ADCC	Antibody-Dependent Cell-Mediated Cytotoxicity
AEC	Alveolar Epithelial Cell
AEC II	Alveolar Type II Epithelial Cell
APC	Antigen Presenting Cell
ARDS	Acute Respiratory Distress Syndrome
Arg	Arginase
BALF	Broncho-Alveolar Lavage Fluid
BNIP3	BCL2/Adenovirus E1B 19 kDa Protein-Interacting Protein 3
C4a	Complement Component 4a
cAMP	Cyclic Adenosine Monophosphate
CCL	C-C Motif Chemokine Ligand
CCR	C-C Motif Chemokine Receptor
CD	Cluster of Differentiation
cGMP	Cyclic Guanosine Monophosphate
cRNA	Complementary RNA
CTL	Cytotoxic T Lymphocyte
CVV	Candidate Vaccine Virus
CXCL	C-X-C Motif Chemokine
CXCR	C-X-C Motif Receptor
DAMP	Damage Associated Molecular Pattern
DC	Dendritic Cell
cDC	Conventional DC
pDC	Plasmacytoid DC
moDC	Monocyte-Derived DC
tipDC	TNF/iNOS Producing DC
DPI	Days Post Infection
ECM	Extracellular Matrix
EDNRB	Endothelin Receptor Type B
ELISA	Enzyme-linked Immunosorbent Assay
EOMES	Eomesodermin
FACS	Fluorescence-Activated Cell Sorting
Fas-L	Fas Ligand
FSC	Forward Scatter
FSC-A	Area
FSC-H	Height
GC	Germinal Center
G-CSF	Granulocyte-Colony-Stimulating Factor

Abbreviation	Denotation
GzmB	Granzyme B
HA	Hemagglutinin
HBA	Hemoglobin-α
HBB	Hemoglobin-β
HSV-2	Herpes-Simplex-Virus-2
IAP	Integrin-Associated Protein
IAV	Influenza A Virus
IFN	Interferon
Ig	Immunoglobulin
Ig-SF	Immunoglobulin-Superfamily
IL	Interleukin
i.n.	intranasal
iNOS	Inducible Nitric Oxide Synthase
i.p.	intraperitoneal
ISG	Interferon Stimulated Gene
ITAM	Immunoreceptor Tyrosine-Based Activation Motif
ITIM	Immunoreceptor Tyrosine-Based Inhibition Motif
KLF	Krüppel-Like Factor
KO	Knockout
LCMV	Lymphocytic Choriomeningitis Virus
LN	Lymph Node
MΦ	Macrophages
aMΦ	Alveolar Macrophages
iMΦ	Interstitial Macrophages
MACS	Magnetic-Activated Cell Sorting
MFI	Mean Fluorescence Intensity
MHC	Major Histocompatibility Complex
MX1	Myxovirus Resistance Protein 1
NA	Neuraminidase
NEP	Nuclear Export Protein
NK cell	Natural Killer cell
NLRP3	NOD like receptor family PYD-containing protein 3/Cryopyrin
NO	Nitric Oxide
NP	Nucleoprotein
NS-1	Non-Structural Protein 1
OAS	Oligoadenylate Synthetase
PA	Polymerase Acidic Protein
PAMP	Pathogen Associated Molecular Pattern
PB	Polymerase Basic Protein
PB1-F2	Polymerase Basic Protein-frame-2

Abbreviation	Denotation
PRR	Pathogen Recognition Receptor
qRT-PCR	Quantitative Real-Time Polymerase Chain Reaction
SELP	Selectin Platelet
RIG-I	Retinoic Acid-Inducible Gene I
SHP	SH2 domain-containing protein tyrosine phosphatase
SIRP	Signal Regulatory Protein
SPA/SPD	Surfactant Protein A/D
SSC	Sideward Scatter
TGF-β	Tumor Growth Factor-β
TLR	Toll-like Receptor
TNF-α	Tumor Necrosis Factor-α
TRAIL	TNF-Related Apoptosis-Inducing Ligand
T_{reg}	Regulatory T cell
TSP-1	Thrombospondin-1
VEGFR2	Vascular Endothelial Growth Factor Receptor-2
vRNP	Viral Ribonucleoprotein
WT	Wildtype

List of Figures

List of Tables

1 Introduction

Human lower respiratory tract infections are among the top ten causes of death worldwide. In most cases these infections can be connected to influenza viruses. Although the human immune system can cope with the infection in many cases, 290,000 – 650,000 people die of respiratory diseases linked to seasonal flu annually (Iuliano et al., 2018; WHO, 2018). Besides the burden of seasonal epidemics, the pandemic potential of influenza viruses poses a huge threat to public health. In 1580 the first generally accepted influenza pandemic was recorded and since then at least 14 pandemics occurred. The most recent was the swine flu in 2009 and the most severe pandemic was the Spanish-flu in 1918, which caused the death of up to 50 million people. New pandemic influenza virus strains were shown to arise periodically and thus the menace of a new pandemic influenza virus is ever-present (Johnson and Mueller, 2002; Kon and Rai, 2016; Potter, 2001). Until now, prevention and treatment of influenza virus infections are limited due to the high variability and mutation rate of the virus. Hence, it is of essence to extend our knowledge of the virus and its related immune responses in order to discover new treatment options.

1.1 Influenza A Virus (IAV)

Initially, the influenza virus was isolated from pigs in 1931 and the first human isolate was obtained in 1933 (Shope, 1931b, 1931a; Smith et al., 1933). Influenza viruses are classified as negative-sense single stranded RNA (ssRNA) viruses with a segmented genome, which represent the family of *Orthomyxoviridae*. Four species of influenza viruses have been defined to date, influenza virus A, B, C and D. Only type A and B viruses can cause severe diseases in humans, with influenza A viruses (IAV) being more common than type B (WHO, 2017, 2020). Moreover, IAV are the sole origin of pandemics among the different influenza virus species (Zambon, 2001). Therefore, this work focuses on IAV.

1.1.1 Structure

IAV are pleomorphic enveloped viruses of filamentous to spherical shape. Spherical viruses have a size of about 120 nm whereas filaments have a diameter of 80-100 nm. However, these filaments can differ greatly in length ranging from 20 µm to over 50 µm (Chu et al., 1949; Harris et al., 2006; Mosley and Wyckoff, 1946). The envelope is formed by the former host cell membrane and three transmembrane proteins. Hemagglutinin (HA) and neuraminidase (NA) build trimeric and tetrameric complexes, respectively, which stick out of the surface of the virion. So far, 18 different HA and 11 different NA subtypes have been identified, which together determine the subpopulation of the virus, e.g. H1N1 or H2N3 (Centers for Disease Control and Prevention, 2019; Varghese et al., 1983; Wilson et al., 1981). Besides HA and

NA, the envelope is interspersed with the M2 ion channel. The inner leaflet of the envelope is connected to the matrix protein M1, which forms a scaffold and anchors the transmembrane proteins. Within the envelope lies the nuclear export protein (NEP; also known as non-structural protein 2 = NS2) as well as the viral ribonucleoprotein (vRNP) complex (Harris et al., 2006; Pinto et al., 1992; Richardson and Akkina, 1991). The vRNP complex consists of polymerase basic proteins 1 (PB1) and 2 (PB2), polymerase acidic protein (PA) as well as nucleoproteins (NP) which are bound to the RNA genome (Inglis et al., 1976; Murti et al., 1988). The viral genome is divided into 8 segments of different length. The structural proteins PB1, PB2, PA, HA, NA and NP are encoded on one segment each whereas the M1 and M2 protein as well as the non-structural protein 1 (NS1) and NEP arise from a single segment by alternative splicing (Davies and Barry, 1966; Hirst, 1962; Lamb and Choppin, 1979, 1981; McGeoch et al., 1976) (Figure 1-1). Apart from NS1, two further non-structural proteins are formed using alternative open reading frames within the PB1 gene, PB1-frame-2 (PB1-F2) protein and PB1 N40 protein (Chen et al., 2001; Wise et al., 2009). In contrast to structural proteins that build the virion, non-structural proteins are mainly virulence factors, which counteract immune responses against IAV (Mibayashi et al., 2007; Wise et al., 2009).

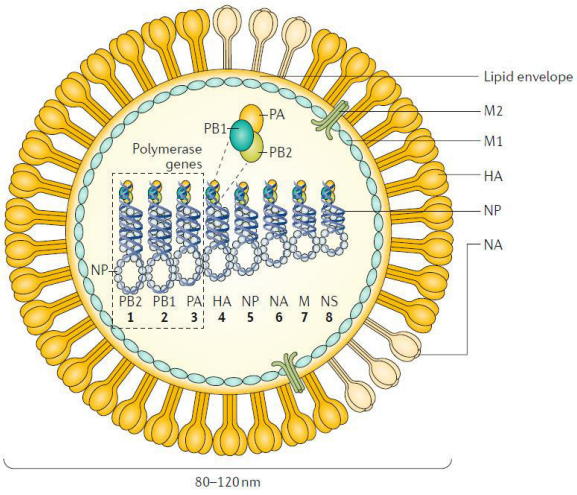

Figure 1-1: Schematic structure of influenza A viruses. The virion of influenza A viruses (IAV) is composed of an outer membrane envelope which encases the viral capsid. The envelope is interspersed with neuraminidase (NA), hemagglutinin (HA) and M2 ion channel proteins. M1 matrix proteins at the inner leaflet of the membrane anchor the transmembrane proteins and form a scaffold. Inside, the viral RNA genome is stored together with the nucleoprotein (NP) as well as the polymerase basic proteins 1 (PB1) and 2 (PB2) and the polymerase acidic protein (PA) in viral ribonucleoprotein (vRNP) complexes. The genome of IAV is divided into 8 segments of different length each encoding one structural protein or the non-structural proteins (NS) (Krammer et al., 2018).

1.1.2 Replication Cycle

IAV primarily infects airway and alveolar epithelial cells (AEC) via HA, which binds to sialic acid residues of glycoproteins. Two major types of sialic acids can be distinguished, α(2,3) and α(2,6), of which the latter are the main targets of human IAV (Connor et al., 1994; Winternitz et al., 1920). Upon interaction the virion is taken up by the cell via receptor-mediated endocytosis. Within the formed endosomes the acidic environment leads to conformational changes of HA and thereby induces fusion of the viral and endosomal membrane (Bullough et al., 1994; Lakadamyali et al., 2003; White et al., 1982). Furthermore, the low pH leads to the activation of the M2 ion channel, which in turn drives the acidification of the viral core. As a consequence of this, the vRNP complexes are released from the M1 scaffold and escape into the cytoplasm of the host cell (Bui et al., 1996; Pinto et al., 1992; Zhirnov, 1990). After transition into the nucleus, transcription of the viral genome is induced by a process called cap-snatching. To this end, the PB2 subunit of the viral polymerase complex (PB1, PB2 and PA) binds to a 5' methylated cap of a cellular mRNA. Subsequently, the PA subunit cleaves the 5' cap of the host mRNA, which functions as a primer for the PB1 subunit to initiate transcription of viral mRNAs. Finally, the virus highjacks the cellular translation system to produce viral proteins based on the newly synthesized mRNAs (Dias et al., 2009; Dou et al., 2018; Matsuoka et al., 2013). Besides transcription, replication of the viral genome takes place in the nucleus by a two-step process. First, the negative sense RNA is converted into positive sense complementary RNA (cRNA) by the viral polymerase complex. This cRNA is then used as a template to produce new viral RNAs which together with the newly synthesized viral proteins reconstitute vRNP complexes (Hay et al., 1977; Vreede et al., 2004; York et al., 2013). Subsequently, new vRNP complexes are exported from the nucleus by interaction with NEP and the M1 protein (O'Neill et al., 1998; Shimizu et al., 2011). Together with the newly synthesized structural proteins the vRNP complexes are trafficked to the apical plasma membrane. Here, the viral components colocalize in lipid rafts and thereby induce the budding of new viral particles (Figure 1-2). The newly formed viral progenies are captured at the cell surface by host sialic acids which trap the HA on the virion. Finally, the release of new viral particles is triggered by hydrolysis of the sialic acids via NA (Howley and Knipe, 2020; Kundu et al., 1996; Palese and Compans, 1976; Palese et al., 1974; Rodriguez Boulan and Sabatini, 1978). Altogether, the viral life cycle takes around 5 hours until the first new viral particles are released leading to a fast onset of clinical symptoms (Sidorenko and Reichl, 2004).

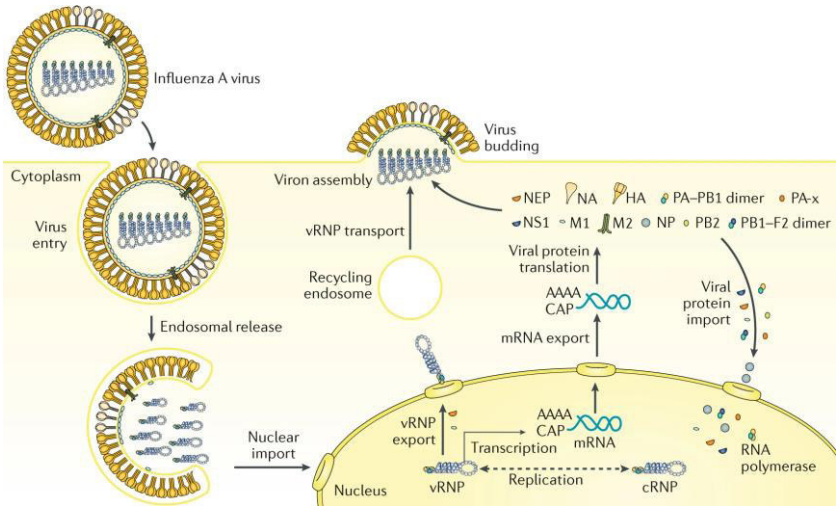

Figure 1-2: Replication cycle of influenza A viruses. Binding of viral hemagglutinin (HA) to sialic acids on host cells induces the uptake of viral particles by endocytosis. Within the endosome acidification triggers uncoating of the virus as well as the escape of the viral genome (vRNP) into the cytoplasm. Subsequently, the vRNPs are translocated into the nucleus where transcription and replication of the genome takes place. Viral mRNAs exploit the cellular translation system to induce synthesis of viral proteins. Some proteins such as nucleoprotein (NP) or polymerase proteins (PA, PB1 and PB2) traffic to the nucleus to build new vRNP which are transported to the plasma membrane thereafter. Together with the remaining viral proteins vRNPs colocalize in lipid rafts and induce budding of new viral particles (Krammer et al., 2018).

1.1.3 Clinical Course and Pathology

Transmission of IAV occurs mainly via droplet infection and is favored by low temperature and low humidity leading to a seasonal presence of the virus in temperate regions (Lowen and Steel, 2014; Shaman and Kohn, 2009). Upon infection the period of incubation ranges from one to five days. Clinically the infection manifests as a sudden onset of a variety of symptoms including high fever, coryza, cough, headache, myalgias and lassitude. During an uncomplicated influenza these symptoms last for seven up to ten days until full recovery (Hayden et al., 1998; Taubenberger and Morens, 2008) (Figure 1-3). However, in some cases infection can run a fatal course. Infants and elderly as well as immunocompromised patients and pregnant women are at high risk of developing a severe IAV infection. During fatal influenza pulmonary as well as extrapulmonary complications emerge. The former are characterized by a dysfunction of the respiratory system up to the development of an acute respiratory distress syndrome (ARDS). Respiratory insufficiency is mainly associated with primary viral or secondary bacterial pneumonia. Extrapulmonary lesions of IAV infection include inflammation of muscular, cardiac as well as cerebral tissue (Howley and Knipe, 2020; Kuiken and Taubenberger, 2008; MacCallum, 1921). Besides host factors, the viral strain determines the severity of the disease. For example, low pathogenic influenza strains mainly affect the upper respiratory tract, whereas fatal IAV infections involve the lower airways (van Riel et al., 2007; Schrauwen et al., 2014).

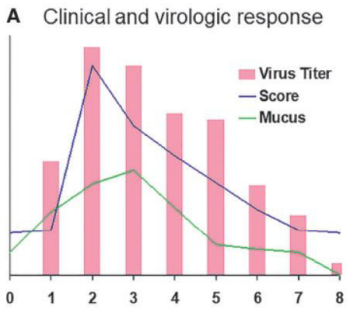

Figure 1-3: Clinical course of an influenza A virus infection. Upon inoculation influenza A viruses (IAV) quickly replicate in the respiratory tissues followed by a sudden onset of illness (score) one day after initial detection of the virus. The peak of virus titer coincides with the first symptoms and steadily decreases from then on. About six days after the viral peak the virus is cleared from the respiratory system. As the virus titer decreases so does the severity of symptoms which leads to recovery approximately five days after onset of illness. In connection with the course of virus levels increased mucus production can be detected at the onset of viral replication which decreases with reduced virus titer (Howley and Knipe, 2020).

The major hallmark of IAV-induced pathology is the death of infected epithelial cells (Winternitz et al., 1920). At the close of viral replication, the host cell dies approximately 12 hours post infection by pathogen-induced cell death (Baccam et al., 2006; Downey et al., 2018). Thus, mild as well as severe IAV infections lead to an initial shrinkage and vacuolization of epithelial cells which culminate in the desquamation into the luminal space (Hers and Mulder, 1961; Winternitz et al., 1920). Within the upper airways ciliated and goblet cells of the pseudostratified epithelium are the main target of IAV (Hui et al., 2018). Loss of these epithelial cells leads to a denudation of the basal cells (Figure 1-4) and is accompanied by mucosal inflammation and edema as well as cellular infiltrates of mononuclear cells and lymphocytes (Kuiken and Taubenberger, 2008; Walsh et al., 1961). In contrast to this, IAV infection of the lower respiratory tract targets alveolar type II epithelial cells (AEC II) (Weinheimer et al., 2012). AEC II display a cuboidal shape and are mainly located at the edge of the alveoli. Besides their function as surfactant producing cells, they may differentiate into alveolar type I epithelial cells (AEC I), which make up the surface of the alveoli and are responsible for gas exchange (Crapo et al., 1982; Danto et al., 1995; Fuchs et al., 2003; Phelps and Floros, 1988; Weibel, 1973) (Figure 1-4). IAV infection can culminate in a complete loss of the alveolar epithelium leading to the formation of hyaline membranes. Moreover, pathological lesions such as inflammation, edema, congestion, and hyperemia in the submucosal as well as interstitial tissues up to intra-alveolar edema and hemorrhage appear. During severe influenza pathological changes are predominantly accompanied by mononuclear cell infiltrates (Howley and Knipe, 2020; MacCallum, 1921; Taubenberger and Morens, 2008). Despite the recruitment of immune cells, the immune system cannot cope with the infection leading to severe complications up to death. In order to prevent severe IAV infections prophylactic as well as therapeutic treatment strategies have been developed.

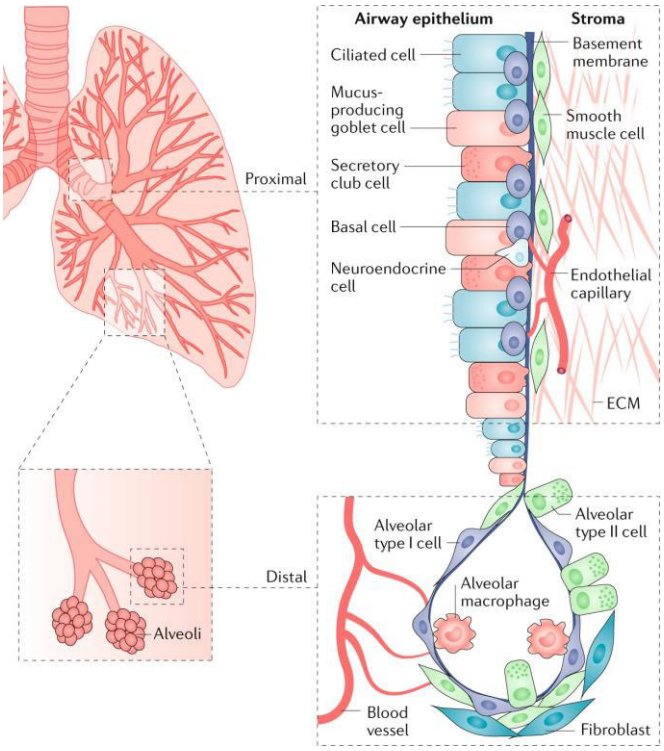

Figure 1-4: Schematic structure of the airway epithelium. The respiratory system can be divided into an upper / proximal and into a lower / distal part that are lined by a single layer of epithelial cells. Since both segments of the lung must meet distinct functional requirements, they vary greatly in structure. The proximal airways are sealed by a pseudostratified epithelial layer that separates the airway lumen from the stroma. The epithelium consists of ciliated cells, goblet cells, club cells, basal cells, and neuroendocrine cells, which sit on the basement membrane. Ciliated, goblet and club cells stick out into the airway lumen and cover the basal cells leading to the pseudostratified structure. The stroma of the upper respiratory tract is composed of smooth muscle cells, endothelial capillaries, and an extracellular matrix (ECM). In contrast to this, the distal part of the lung is encompassed by alveolar type I and type II cells, that are organized in a simple squamous layer. In order to facilitate gaseous exchange, the alveolar walls are connected to the vascular capillaries. Moreover, the interstitial tissue in the lower airways is built out of fibroblasts and smooth muscle cells (Altorki et al., 2019)

1.1.4 Vaccination and Therapy

Different types of vaccines are available to prevent IAV infection. Most commonly, inactivated influenza vaccines are utilized. Those are generated by propagation of the virus in embryonated chicken eggs. Since human influenza viruses display inefficient growth in chicken eggs, reassortment of the circulating influenza strains with a laboratory-adapted influenza strain (e.g. A/PR8/34) is performed. The resulting candidate vaccine viruses (CVVs) express the HA and NA genome segments of the predicted circulating influenza strains. Following propagation, the virus is chemically inactivated and purified. Initially, whole inactivated viruses were used for vaccination which were replaced by split or subunit vaccines to reduce adverse effects (Francis et al., 1944). Both are generated by disruption of the viral particle via solvents and subsequent purification of viral proteins. While split vaccines contain all viral proteins, subunit vaccines only include HA and NA of the virus (Soema et al., 2015). Recent vaccines are composed of either three or four different CVVs

combined in a tri- or quadrivalent vaccine, respectively. As some studies showed that egg-based growth of CVVs can lead to an adaption of the virus to the avian system and thus impair vaccine efficacy, cell culture systems have been established to propagate the virus (Howley and Knipe, 2020; Skowronski et al., 2014; Zost et al., 2017). Furthermore, recombinant technology is used to obtain inactivated subunit vaccines. Likewise, classical reassortment as well as recombinant technology are utilized to generate live attenuated influenza vaccines. Different attenuated donor viruses for type A and B influenza strains have been established and enable the generation of quadrivalent vaccines (Grohskopf et al., 2019; Howley and Knipe, 2020). In comparison to inactivated vaccines, live attenuated vaccines were shown to have higher efficacy in children whereas no significant differences have been observed for adults (Ashkenazi et al., 2006; Belshe et al., 2007; Osterholm et al., 2012). The current vaccination strategies are mainly directed against the HA and NA proteins of influenza viruses. However, their efficacy is highly limited. On the one hand, antigenic drift by mutations in the viral HA and NA genome segments leads to the development of new influenza strains and thus allows escape from immunological memory (Hirst, 1943; Smith et al., 2004). On the other hand, reassortment of different virus strains upon coinfection can introduce major antigenic changes in viral HA and NA. This antigenic shift not only allows evasion of vaccine-derived immunity but also natural prior immunity. Thus, antigenic shift is associated with the occurrence of new pandemic influenza viruses (Burnet et al., 1953; Novel Swine-Origin Influenza A (H1N1) Virus Investigation Team, 2009; Scholtissek et al., 1978; Smith et al., 2009). Hence, influenza vaccines depend on an exact prediction of circulating influenza strains in the subsequent season. Furthermore, the efficacy of influenza virus vaccines is especially limited in the high-risk groups for severe influenza virus infection (Sullivan et al., 2019). Thus, apart from preventing infection treatment strategies against acute influenza virus infection are of need.

Treatment of severe IAV infections is realized by the inhibition of viral replication at different stages. First antiviral compounds used for influenza treatment were M2 ion channel inhibitors (e.g. amantadine, rimantadine), which block the uncoating and release of the viral genome. However, these drugs only affect IAV but not type B viruses. Moreover, most IAV strains have developed resistance against M2 inhibitors making them ineffective for IAV treatment (Bright et al., 2006; Hay et al., 1985; Hayden et al., 1980; Heider et al., 1981). Another antiviral drug used to treat influenza are NA inhibitors, which limit the release of new viral particles (e.g. oseltamivir, zanamivir). Although these inhibitors work for type A and type B viruses, their efficiency is limited due to the occurrence of resistant strains (Mendel et al., 1998; Sheu et al., 2008; Treanor et al., 2000). Most recent antiviral compounds against IAV

are polymerase inhibitors (e.g. baloxavir marboxil, favipiravir) which suppress the activity of the viral PA subunit, that catalyzes the cap snatching of IAV to initiate viral transcription. However, first viruses have already developed resistance against the new inhibitors during clinical trials (Hayden et al., 2018; Takashita et al., 2018).

The high mutation rate of influenza viruses limits the efficiency of vaccines as well as antiviral drugs. Hence, investigation of new strategies to treat severe IAV infection remains an urgent need. Besides the direct restriction of IAV replication, recent strategies also include the modulation of immune responses as pathological changes of IAV infection cannot only be ascribed to the virus, but also to excessive immune responses. Hence, improved viral clearance as well as reduced immunopathology are both aspects of the immuno-modulatory therapy.

1.1.5 Immune Responses against IAV

Pathogens like IAV but also other microorganisms including bacteria, fungi and parasites challenge the human body every day. Since not all microorganisms cause severe disease like IAV the human body has to identify and clear harmful microorganisms among the innocuous ones. This task is accomplished by the immune system. The immune system can be divided into an innate and adaptive compartment. The innate immunity is the first line of defense against invading pathogens and provides fast though unspecific elimination. In contrast to this, the adaptive immunity provides a specific but slow response. Together, the innate and adaptive immune responses accomplish the recognition and elimination of pathogens as well as the regulation of immune response and the immunological memory.

1.1.5.1 Innate Immune Responses

The initial innate immune barrier of the respiratory system is formed by the mucosal layer sealing the epithelial cells. This airway mucus mainly consists of mucin proteins which are organized in oligomers. Moreover, mucins contain large amounts of sialic acid residues which facilitate the interaction with IAV. Binding of HA to mucin sialic acids traps the virus and allows mucociliary clearance (Burnet, 1951; Ehre et al., 2012; Klein et al., 1992; McAuley et al., 2017; Ridley et al., 2014). In addition to mucins, antimicrobial peptides are secreted into the airway lumen including β-defensins as well as the cathelicidin LL37, which induce viral aggregation and disrupt the membrane integrity of IAV, respectively (Barlow et al., 2011; Jiang et al., 2012; LeMessurier et al., 2016; Tripathi et al., 2013, 2015). In the alveolar space pulmonary surfactant substitutes the airway mucus. Surfactant proteins as well as surfactant lipids build the lining fluid among which surfactant proteins A (SPA) and D (SPD) are mainly known to interact with IAV. The former functions as a decoy like mucins, while SPD binds to

glycans on HA leading to an inhibition of viral entry as well as aggregation which triggers phagocytic clearance by tissue resident alveolar macrophages (aMΦ) (Hartshorn et al., 1994, 1997; LeVine et al., 2001).

aMΦ are the first professional innate immune cells to encounter IAV as they reside in the alveolar lumen. They form a distinct subset of MΦ, which derive during embryogenesis and form a self-renewing population (Guilliams et al., 2013; Hashimoto et al., 2013). During IAV infection aMΦ internalize and degrade viral aggregates or opsonized viral particles (Benne et al., 1997; Huber et al., 2001). As part of the innate immune system, they are able to recognize viral structures and induce inflammatory responses. Different pathogen recognition receptors (PRRs) detect conserved structures of the virus called pathogen associated molecular patterns (PAMPs), which are common to a class of microorganisms. For example, Toll-like receptor 7 (TLR7) realizes incoming viral RNA in endosomes (Lund et al., 2004; Zhang et al., 2015), whereas retinoic acid-inducible gene I (RIG-I) recognizes cytoplasmic RNA which is generated during IAV replication (Pichlmair et al., 2006; Rehwinkel et al., 2010). Furthermore, TLR3 is activated during influenza virus infection by a ligand unknown so far (Goffic et al., 2006; Guillot et al., 2005). Upon activation these receptors induce the expression of pro-inflammatory mediators which orchestrate the recruitment and activation of further immune cells. These mediators include cytokines and chemokines such as interleukin 6 (IL-6), tumor necrosis factor α (TNF-α), IL-1β, C-C motif chemokine ligand 2 (CCL2) and C-X-C motif chemokine 1 (CXCL1) (Wang et al., 2012). Furthermore, activation of NOD-like receptor family PYD-containing protein 3/Cryopyrin (NLRP3) by IAV leads to the formation of an inflammasome complex which triggers the maturation of IL-1β and IL-18 (Allen et al., 2009; Thomas et al., 2009). Besides the induction of pro-inflammatory immune responses, PRR signaling creates an antiviral state in infected and surrounding cells by the induction of type I and type III interferons (IFNs) (Figure 1-5). These IFNs in turn induce the expression of a variety of IFN stimulated genes (ISGs) which limit viral replication trough different mechanisms. For example, myxovirus resistance protein 1 (MX1) inhibits the nuclear translocation of the IAV genome after endosomal escape (Horisberger et al., 1983; Xiao et al., 2013). In contrast to this, oligoadenylate synthetase 1 (OAS1) interacts with the RNase L to induce degradation of viral and cellular RNA (Chakrabarti et al., 2011; Kerr and Brown, 1978). aMΦ were shown to be the main source of type I IFNs during IAV infection (Divangahi et al., 2015; Kumagai et al., 2007). Thus, aMΦ are the master regulators of early immunity and define the path of the downstream immune responses (Kim et al., 2013; Schneider et al., 2014; Tumpey et al., 2005). Apart from that, aMΦ participate in IAV clearance by restricting viral replication upon direct infection of the MΦ (Rodgers and Mims,

1982). Furthermore, aMΦ play an essential role for clearance of dying or dead infected epithelial cells by efferocytosis in order to limit viral spread (Hashimoto et al., 2007).

In case IAV overcomes these initial defense mechanisms, it can infect AEC II. These cells are the main target of IAV allowing efficient viral replication (Weinheimer et al., 2012). However, upon infection they recognize the infiltrating virus like aMΦ and support antiviral as well as pro-inflammatory immune responses (Guillot et al., 2013; Herold et al., 2006; Stegemann-Koniszewski et al., 2016; Winternitz et al., 1920).

The first immune cells which are recruited to the site of infection are neutrophils. This mechanism depends on CXCL1 as well as IL-1β (Schmitz et al., 2005; Wareing et al., 2007). Within the infected lung neutrophils together with aMΦ clear dying or dead infected epithelial cells by efferocytosis (Hashimoto et al., 2007). Furthermore, activated neutrophils further promote their recruitment by a feed forward loop mediated by inflammatory cytokines such as TNF-α, IL1-β, IL-6 and CXCL1 (Brandes et al., 2013).

In addition to neutrophils, inflammatory monocytes are recruited to the infected tissue in a CCL2-dependent manner (Herold et al., 2006; Rosseau et al., 2000). Within the lung these monocytes further reinforce their recruitment by the secretion of CCL2. Moreover, they drive the expression of pro-inflammatory cytokines like TNF-α and inducible nitric oxide synthase (iNOS) (Lin et al., 2014). Besides their direct effects, monocytes can differentiate either into interstitial MΦ (iMΦ) or dendritic cells (DCs) upon activation. iMΦ are another subset of lung resident MΦ, which reside in the lung interstitium and originate from blood monocytes. During IAV infection iMΦ phagocytose viral particles and may serve as antigen presenting cells (APCs) in the infected tissue (Lin et al., 2008). Furthermore, iMΦ are able to migrate into the mediastinal lymph node (LN). However, their contribution to T cell priming within the LN and subsequent immune responses is unclear (Yamamoto et al., 2001).

Another cell type recruited during IAV infection are NK cells (Figure 1-5). Here, recruitment depends on C-X-C motif receptor 3 (CXCR3) and C-C motif chemokine receptor 5 (CCR5) which interact with their ligands CXCL9, CXCL10 and CCL5, respectively (Carlin et al., 2018). Upon arrival in the inflamed tissue NK cells detect HA expressed on infected cells and subsequently induce cytolysis of target cells via granzyme B (GzmB) (Gazit et al., 2006; Mandelboim et al., 2001). Moreover, they express IFN-γ which triggers the activation of other innate immune cells such as MΦ and DCs and thereby the secretion of T cell attracting chemokines such as CXCL9 and CXCL10 (Ge et al., 2012; Kos and Engleman, 1996).

Antigen presentation and T cell priming during IAV infection mainly rely on DCs. Lung resident cluster of differentiation (CD) 103^+ $CD11b^-$ conventional DCs (cDCs) protrude into the alveolar lumen and sample foreign antigens. Upon antigen encounter these intraepithelial

DCs migrate into the mediastinal lymph node (LN) to prime $CD4^+$ and $CD8^+$ T cells. Likewise, $CD11b^+$ cDCs, which are located in the lung interstitium, prime $CD4^+$ T cells in the mediastinal LN upon activation (Ho et al., 2011; Kim and Braciale, 2009; Moltedo et al., 2011). Epithelial- as well as MΦ-derived cytokines such as type I IFNs and IL-1β support the maturation and migration of cDCs, respectively (Montoya et al., 2002; Pang et al., 2013; Unkel et al., 2012). In addition to cDCs, plasmacytoid DCs (pDCs) are present in the lung interstitium. Their main function is the secretion of type I IFNs as they have only a weak potential to prime T cells (GeurtsvanKessel et al., 2008). However, it has been shown that pDCs are essential to generate a proper B cell response during IAV infection (Jego et al., 2003). Contrary to tissue resident DCs, the impact of monocyte-derived DCs (moDCs) on the induction of T cell responses is not clear yet. However, moDCs were shown to produce high amounts of pro-inflammatory TNF-α and iNOS leading to their alternative name TNF and iNOS-producing DCs (tipDCs) (Aldridge et al., 2009).

1.1.5.2 Adaptive Immune Responses

Priming of $CD8^+$ and $CD4^+$ T cells in mediastinal LN by DCs triggers their activation and migration to the inflamed lung (Lawrence and Braciale, 2004; Román et al., 2002) (Figure 1-5). Within the infected tissue $CD8^+$ cytotoxic T cells detect specific major histocompatibility complex (MHC) class I-antigen complexes on infected cells via the T cell receptor and subsequently eliminate infected cells. To this end, $CD8^+$ T cells induce apoptosis through the release of cytotoxic granules containing granzyme B (GzmB) and perforin. Apart from that, they express death receptor ligands such as Fas ligand (FasL) and TNF-related apoptosis-inducing ligand (TRAIL), which induce apoptosis of infected cells by interaction with their corresponding receptors. Moreover, $CD8^+$ T cells release pro-inflammatory cytokines like TNF-α and IFN-γ which on the one hand support their cytotoxic activity via increased MHC class I expression on target cells. On the other hand, these cytokines promote the activation of innate immune cells like MΦ and DCs (Brincks et al., 2008; Hamada et al., 2013; King and Jones, 1983; Lawrence and Braciale, 2004; Topham et al., 1997). Contrary to $CD8^+$ T cells, $CD4^+$ T cells provide only an insubstantial contribution to cytotoxicity. Instead, they differentiate into Th1 and T_{FH} cells. Th1 cells support $CD8^+$ cytotoxic T cell responses by the secretion of IFN-γ as well as the generation of memory cells. In contrast to this T_{FH} cells promote the activation and maturation of B cells (Hornick et al., 2019; Janssen et al., 2005; Topham and Doherty, 1998).

B cell responses during IAV infection can be divided into three phases: immediate, early, and late responses. Immediate B cell responses originate via innate-like B-1 cells, which arise from progenitors in fetal bone marrow and reside mainly in the peritoneal and pleural cavities

(Hayakawa et al., 1985). During IAV infection B-1 cells are activated among others by type I IFNs and thereupon migrate into the mediastinal LN. Here they start to secrete natural antibodies, mainly IgM, which interact with the complement system and promote Fc receptor-mediated clearance of viral particles by phagocytes (Baumgarth et al., 1999; Jayasekera et al., 2007). Since the activation of innate-like B-1 cells is independent of antigen recognition, secreted natural antibodies are non-specific, polyreactive and typically have low affinity to foreign antigens (Holodick et al., 2017). Early and late B cell responses, which are provided by follicular B cells within the mediastinal LN, facilitate a more specific response against IAV infection. Here, activation of B cells is based on the recognition of an infiltrating viral antigen by the B cell receptor (BCR). Depending on the affinity of the BCR to circulating antigens follicular B cells either differentiate into short-lived plasmablasts or translocate into germinal centers (GC) (Paus et al., 2006). Plasmablasts build the early humoral immunity via the secretion of IgM, IgA and IgG (Kavaler et al., 1991; Lam and Baumgarth, 2019). These antibodies are specific to IAV and support viral clearance by neutralization, complement activation and Fc receptor mediated phagocytosis. Moreover, these antibodies can boost NK cell responses through antibody-dependent cell cytotoxicity (ADCC) (DiLillo et al., 2016; He et al., 2017). In contrast to this GC responses mainly participate in immunological memory by the differentiation of long-lived plasma cells and memory B cells (Figure 1-5). Upon reinfection these cells provide immediate humoral immune responses while having a minor contribution to viral clearance during primary infection (Lam and Baumgarth, 2019).

Together the different immune cells described above work in concert to allow efficient viral clearance and thus limit virus-induced pathology. However, pro-inflammatory immune responses always come at the risk of excessive tissue damage and therefore can aggravate disease severity. Especially, immune responses involving either direct cytolysis of infected cells by $CD8^+$ T cells and NK cells or induced cell death by pro-inflammatory mediators like reactive oxygen species (ROS) are a major cause of immunopathology (Coates et al., 2018; Lin et al., 2008; Moskophidis and Kioussis, 1998; Snelgrove et al., 2006; Tumpey et al., 2005; Ye et al., 2017). Thus, a balance of pro- and anti-inflammatory responses is essential to maintain integrity of lung tissue and avoid excessive immune responses.

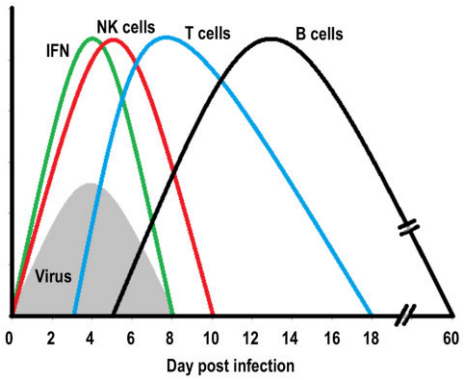

Figure 1-5: Schematic view of antiviral immune responses during influenza A virus infection. Initial immune responses upon influenza A virus (IAV) infection are mediated by interferons (IFN) which are secreted by different immune cells including alveolar macrophages and alveolar epithelial cells. The innate immune mediators orchestrate subsequent immune responses and peak around 4 days post infection (dpi). Natural killer (NK) cells are among the first immune cells recruited to the infected lung and increase till day 5 post infection. Subsequent to innate immune responses, adaptive immunity is initiated with T cells starting from day 3 post infection and B cells on day 5. T cell responses rise rapidly until day 7 post infection and last up to 18 dpi. In contrast to this, B cell responses grow steadily and culminate 14 dpi. Nevertheless, they last up to 60 dpi (Pommerenke 2012).

1.1.6 Homeostasis of the Pulmonary Immune System

The regulation of airway immune homeostasis is a multifactorial process, which takes place at each stage of antiviral immune responses. At the start of infection, the maintenance of immune homeostasis is controlled by the regulation of aMΦ activation. As mentioned above aMΦ are the first line of defense against invading pathogens and play an essential role in initiation of subsequent immune responses. Thus, limiting aMΦ activation by an anti-inflammatory environment, controls the extend of pulmonary immune responses. On the one hand cytokines like IL-10 and transforming growth factor β (TGFβ) constitute the anti-inflammatory milieu both of which are expressed by AEC II (Coker et al., 1996; Mayer et al., 2008; Meliopoulos et al., 2016). On the other hand, engagement of inhibitory receptors such as CD200 receptor (CD200R) or signal regulatory protein α (SIRPα) which are expressed on aMΦ induce hyporesponsiveness of the phagocytes. While CD200 is expressed on the cell surface of AEC II SPD, which interacts with SIRPα, is secreted into the alveolar lumen as part of the alveolar surfactant. In addition to SPD, CD47 is known to engage SIRPα and has been shown to be expressed on AEC II (Gardai et al., 2003; Janssen et al., 2008; Rosseau et al., 2000; Snelgrove et al., 2008). As a consequence, aMΦ activation requires multi-receptor signaling to overcome the inhibitory signals. Additionally, during IAV infection cell death of epithelial cells disrupts the suppressive environment in the respiratory system facilitating aMΦ activation.

During an acute IAV infection limiting pro-inflammatory immune responses is essential to achieve a balance of immune activation. Restriction of pro-inflammatory signaling is firstly

accomplished via the secretion of nitric oxygen (NO) by aMΦ. NO suppresses T cell proliferation as well as APC functions of pulmonary DCs and thus limits cytotoxic T cell responses (Holt, 1993; Kawabe et al., 1992; Upham et al., 1995). Additionally, aMΦ-derived TGF-β and retinoic acids trigger the differentiation of naïve T cells into regulatory T cells (T_{reg}). These T_{reg} in turn suppress effector T cell responses by soluble mediators such as IL-10 and TGF-β. Moreover, they compete for APC interactions as well as activating cytokines like IL-2 (Antunes and Kassiotis, 2010; Soroosh et al., 2013). Finally, efferocytosis of apoptotic cells from the alveolar lumen by aMΦ prevents the release of damage-associated molecular patterns (DAMPs) which otherwise activate a variety of immune cells (Grabiec and Hussell, 2016).

Besides balancing immune activation during acute phase of infection the mechanisms described above are involved in restoration of immune homeostasis after efficient viral clearance. Furthermore, contraction of immune responses is essential to re-establish homeostasis. Different mediators have been shown to take part in this process. For example, IFN-γ has been shown to inhibit the survival of $CD8^+$ cytotoxic T lymphocytes (CTLs) by the downregulation of pro-survival receptors (Prabhu et al., 2013). Furthermore, induced cell death of innate and adaptive effector cells is utilized to limit immune responses. Here, monocyte-derived MΦ were shown to be removed by Fas-FasL interaction whereas TRAIL expressing $CD4^+$ T cells are known to diminish $CD8^+$ CTL responses (Janssen et al., 2005, 2011). Apart from that, CD47 has been shown to take part in the resolution of immune responses by CD47-mediated cell death of $CD47^{low}$ effector T cells (Van et al., 2012).

1.2 CD47

CD47 was first identified in 1990 by Brown, Hooper and Gresham in placental tissue and on different hematopoietic cells as integrin-associated protein (IAP), which was involved in phagocytosis (Brown et al., 1990; Mawby et al., 1994). Independently, in 1992 Campbell *et al*. identified an antigen expressed by ovarian tumor cells (OA3) which has been shown to be identical to IAP (Campbell et al., 1992). To date, CD47 is best known for its function as a "*don't eat me*" signal and its expression on various cell types including tumor cells (Oldenborg et al., 2000; Veillette and Chen, 2018).

CD47 is a 50 kDa cell surface glycoprotein which belongs to the immunoglobulin (Ig) superfamily and is divided into three sections: (I) a C-terminal intracellular domain, (II) a penta-transmembrane domain, and (III) an IgV-like extracellular N-terminal domain (Lindberg et al., 1993) (Figure 1-6). Based on the length of the C-terminus, ranging from four to 34 amino acids four isotypes can be distinguished. The different isoforms show

tissue-specific expression, with isoform 2 being the most abundant (Reinhold et al., 1995). In general, CD47 displays a broad tissue expression and was found on both non-immune and immune cells (Brown et al., 1990; Mawby et al., 1994). Since the cytoplasmic C-terminus of CD47 lacks enzymatically active motifs, its functions depend on interacting proteins (Brown and Frazier, 2001).

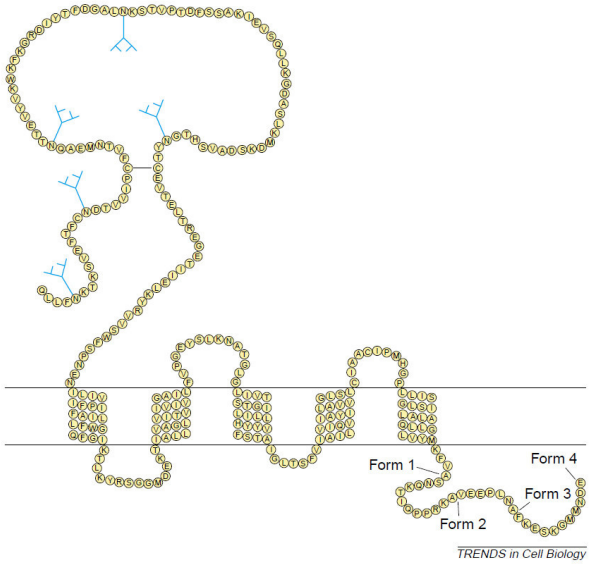

Figure 1-6: Schematic structure of the cell surface glycoprotein CD47. The integrin-associated cell surface protein CD47 is composed of three structural elements. The N-terminal domain of CD47 forms an IgV-like loop, that can be heavily glycosylated, followed by a transmembrane domain consisting of five membrane-spanning segments. Finally, the C-terminus builds an intracellular domain. Four isoforms of CD47 were detected which arise from alternative splicing of the C-terminal domain (Brown and Frazier, 2001).

1.2.1 CD47 Signaling and Interaction Partners

CD47 was initially described as an integrin-associated protein binding to different integrins, such as αvβ3, αIIbβ3 and α2β1 (Brown et al., 1990). Lateral binding occurs via the IgV-like domain of CD47 and regulates integrin activation (Fujimoto et al., 2003). Besides integrins, CD47 has been shown to associate with different proteins such as vascular endothelial growth factor receptor 2 (VEGFR2), Fas, and CD14. Signaling of these receptors depends on their interaction with CD47 (Kaur et al., 2010; Manna et al., 2005; Stein et al., 2016). In red blood cells CD47 has been shown to be associated with the Rh blood group antigen complex. However, no precise function has been attributed to CD47 within the complex (Lindberg et al., 1994; Oldenborg, 2004). Moreover, CD47 has been shown to form homotypic clusters, whose function is unclear yet (Drbal et al., 2000).

Besides its lateral interaction partners, the cytoplasmic domain of CD47 has been shown to bind BCL2 interacting protein 3 (BNIP3) and thus to trigger its accumulation within the cell (Lamy et al., 2003, 2007; Pettersen et al., 1999). Moreover, ubiquilin 1 and 2 associate with the C-terminal domain of CD47 and were shown to tether heterotrimeric G proteins to CD47

(N'Diaye and Brown, 2003; Wu et al., 1999). Apart from that, CD47 directly couples to heterotrimeric inhibitory G (G_i) proteins which transmit intracellular signaling via secondary mediators (Frazier et al., 1999). G_i proteins are known to suppress adenylate cyclase activity leading to reduced synthesis of the secondary mediator cyclic adenosine monophosphate (cAMP) (Alberts et al., 2014). This mechanism is mainly used to transmit signals derived from engagement of CD47 by extracellular ligands (Rebres et al., 2005). The main extracellular interaction partners of CD47 are thrombospondin 1 (TSP-1) and SIRPα.

1.2.1.1 Thrombospondin 1

TSP-1 is a 420 kDa homotrimeric glycoprotein which is part of the extracellular matrix (Baenziger et al., 1971; Margossian et al., 1981). It can be secreted by various cell types including platelets, endothelial cells, monocytes, leukocytes and fibroblasts (Jaffe et al., 1985; Lawler et al., 1978; Li et al., 2002; Raugi et al., 1982). Each of its subunits consists of an N-terminal and a C-terminal globular domain, that encompass an interchain disulfide bond, a procollagen homology domain as well as type I, II, and III repeats (Lawler and Hynes, 1986). Interaction with CD47 happens via the C-terminal domain of TSP-1, which engages the IgV-like domain (Gao and Frazier, 1994; Isenberg et al., 2006, 2009) and requires N-terminal glycosylation of CD47 (Kaur et al., 2011) (Figure 1-7 A).

Different signaling cascades are associated with CD47-TSP-1 interaction. On the one hand, CD47 ligation by TSP-1 induces conformational changes and thus activation of associated integrins (Fujimoto et al., 2003; Gao et al., 1996). On the other hand, binding of TSP-1 can trigger dissociation of CD47 from interaction partners such as VEGFR2 or CD14 limiting their function. Moreover, TSP-1 engagement induces the release of BNIP3 from CD47, which in turn induces apoptosis of the cell upon its translocation to mitochondria (Kaur et al., 2010; Lamy et al., 2003; Stein et al., 2016). Finally, CD47-TSP-1 interaction is a negative regulator of NO/cGMP signaling pathways (Green, 2013; Isenberg et al., 2009; Soto-Pantoja et al., 2015).

1.2.1.2 Signal regulatory protein α

SIRPα belongs to the SIRP family of paired receptors and has been shown to be mainly expressed by myeloid cells (Adams et al., 1998; Seiffert et al., 1999). Two other members of the SIRP family have been identified so far, SIRPβ and SIRPγ. The SIRP family receptors are characterized by three extracellular immunoglobulin superfamily (IgSF) domains as well as a single transmembrane domain (Fujioka et al., 1996; Ichigotani et al., 2000; Kharitonenkov et al., 1997). In contrast to this, the intracellular parts vary among the different family members. SIRPβ and SIRPγ have short cytoplasmic tails without own signaling motifs. However, SIRPβ

has been shown to associate with DNAX activation protein 12 (DAP12) mediating intracellular signaling via immunoreceptor tyrosine-based activation motifs (ITAMs) (Dietrich et al., 2000; Ichigotani et al., 2000; Kharitonenkov et al., 1997). Contrary to this, the intracellular domain of SIRPα contains inhibitory immunoreceptor tyrosine-based inhibition motifs (ITIMs) (Fujioka et al., 1996; Kharitonenkov et al., 1997). Among the three SIRP family receptors, only SIRPα and SIRPγ bind to CD47, with SIRPα showing higher affinity (Brooke et al., 2004; Seiffert et al., 2001). Interaction of SIRP family members and CD47 takes place via their IgV-like N-terminal domains (Hatherley et al., 2008) (Figure 1-7 B).

The impact of CD47-SIRP family receptor engagement on the CD47 bearing cell is not well understood. However, activation of SIRPα by CD47 ligation causes the recruitment of tyrosine phosphatases, such as SH2-domain-containing protein tyrosine phosphatase 1 (SHP1) and 2 (SHP2), to the ITIMs on the SIRPα cytoplasmic tail. These phosphatases transmit signals by dephosphorylation of various substrates triggering negative as well as positive signal transduction (Tsai and Discher, 2008; Veillette et al., 1998).

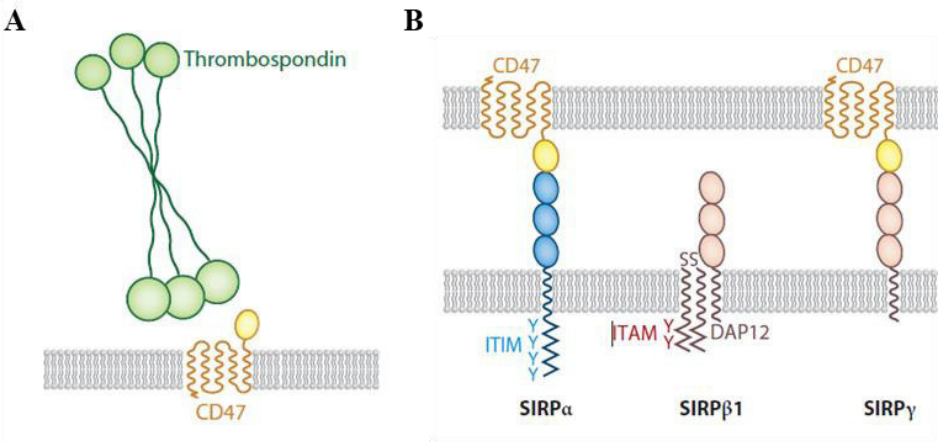

Figure 1-7: Interaction of CD47 and its ligands. The main extracellular interaction partners of CD47 are TSP-1 and two SIRP family receptors. (A) TSP-1 is a large homotrimeric glycoprotein, which is secreted by various cells. Interaction with its receptor CD47 happens via the C-terminal globular head that engages the IgV-like extracellular loop of CD47. (B) The SIRP family consist of three different receptors, SIRPα, SIRPβ, and SIRPγ, which are characterized by an extracellular N-terminus built of three immunoglobulin superfamily (IgSF) domains. SIRPα has a cytoplasmic tail bearing immunoreceptor tyrosine-based inhibition motifs (ITIMs), whereas SIRPβ and SIRPγ have short intracellular domains lacking signaling motifs. However, SIRPβ associated with DNAX activation protein 12 (DAP12) mediates intracellular signaling via immunoreceptor tyrosine-based activation motifs (ITAMs). Among the different SIRP family receptors only SIRPα and SIRPγ interact with CD47 by binding of the IgV-like N-terminal domains (adapted from Barclay and van den Berg 2014).

1.2.2 CD47 within the Immune System

Initial studies have identified CD47 as an integrin-associated protein involved in phagocytosis. Since then various functions of CD47 within the immune system have been described. Due to the ubiquitous expression of CD47 regulatory functions have been described for innate as well as adaptive immune responses.

Within the innate immune system CD47 is best known for its anti-phagocytic function on MΦ mediated by SIRPα (Oldenborg et al., 2000; Veillette et al., 1998). Apart from the function as a marker of self, CD47-SIRPα interaction inhibits cytokine and ROS production as well as the activation of the phagocytes (van Beek et al., 2012; Stein et al., 2016). Besides MΦ, CD47 has been shown to regulate NK cells and DCs. CD47 expression on NK cells inhibits their activation as well as cytolytic function (Kim et al., 2008). Likewise, DC activation, maturation and function are negatively regulated by CD47. On the one hand, anti-inflammatory regulation of DCs is mediated by SIPRα (Braun et al., 2006; Latour et al., 2001). On the other hand, CD47 engagement by TSP-1 has been shown to induce a negative feedback loop via the activation of latent TGF-β which in turn triggers the secretion of TSP-1 by DCs (Demeure et al., 2000; Doyen et al., 2003; Mittal et al., 2010). The impaired function of APCs like DCs also leads to a dysfunctional adaptive immune response. Besides this indirect effect, CD47 directly impedes effective T cell responses. Here engagement of CD47 by SIRPα as well as TSP-1 reduces the IL-12 responsiveness of T cells and thus the generation of Th1 responses (Avice et al., 2000; Bouguermouh et al., 2008; Latour et al., 2001). Moreover, CD47 expressed on T cells suppresses the early TCR mediated activation (Li et al., 2001). Apart from that, TSP-1 drives the differentiation of naïve T cells into T_{reg} (Grimbert et al., 2006; Mir et al., 2015; Xing et al., 2017). Finally, CD47 has been described to induce the apoptosis of different immune cells such as T cells and monocytes (Lamy et al., 2007; Mateo et al., 1999; Van et al., 2012). Thus, CD47 is an important anti-inflammatory regulator limiting the intensity and duration of immune responses.

Contrary to this, some pro-inflammatory functions of CD47 have been described. Interaction of CD47 and SIRPα were shown to facilitate recruitment of monocytes and neutrophils to the site of inflammation as well as DC recruitment to the LNs (Liu et al., 2001; Van et al., 2006; de Vries et al., 2002). Furthermore, CD47 mediates the recruitment of T cells to inflamed tissue by its interaction with both TSP-1 and SIRPα (Ticchioni et al., 2001). Likewise, CD47 supports the adhesion of T cells to APCs through the interaction with both SIRP family receptors and thus stimulates T cell proliferation and activation (Piccio et al., 2005; Ticchioni et al., 1997). Furthermore, TSP-1 binding of CD47 augments T cell activation by interference with VEGFR2 inhibitory signaling (Kaur et al., 2014)

Due to the diverse actions of CD47 within the immune system, the cell surface protein has been shown to be involved in the clearance of different infections. However, the precise impact of CD47 is controversial and is highly dependent on the pathogen, the site of infection and the cells involved in pathogen clearance. For example, CD47 supports clearance of systemic bacterial (*Escherichia coli* (*E.coli*)) as well as fungal (*Candida albicans*) infection

(Lindberg et al., 1996; Navarathna et al., 2015). Contrary to this, during *E.coli* induced pneumonia CD47 contributes to immunopathology by the recruitment of neutrophils (Su et al., 2008). Likewise, CD47 induced neutrophil recruitment aggravates *Staphylococcus aureus* (*S.aureus*) induced peritonitis and arthritis (Gresham et al., 2000; Verdrengh et al., 1999). During Plasmodium infection CD47 has been shown to inhibit phagocytosis of infected red blood cells and thus parasite clearance (Ayi et al., 2016; Banerjee et al., 2015). In line with this, pox viruses were described to express a CD47-mimic to inhibit clearance of infected cells (Cameron et al., 2005; Campbell et al., 1992). The direct role of CD47 during viral infections is less well known. Upon acute lymphocytic choriomeningitis virus (LCMV) infection CD47 has been shown to limit antiviral immune responses (Cham et al., 2020). In contrast to this, during chronic LCMV infection CD47 supports control of viral replication in an NK-cell dependent manner (Nath et al., 2018). Furthermore, CD47 has been described as a negative regulator of immune responses upon influenza vaccination (Lee et al., 2016). Hence, the impact of CD47 on antiviral immune responses is highly diverse.

1.3 Aim of the Study

Even though our knowledge of the immune system and many pathogens increases continually infectious diseases are still among the top 10 global causes of death. Especially lower respiratory infections which are mainly caused by influenza viruses are a severe threat to human health (WHO, 2018). Despite existing vaccines and antivirals, prevention and treatment of influenza virus infections are limited due to the high variability and mutation rate of the virus. Hence, novel treatment strategies against influenza viruses do not only focus on the virus itself but also on related immune responses as they have been shown to contribute to disease severity. Thus, among others the focus of influenza research lies on immuno-regulatory proteins. CD47 is a major regulator of innate and adaptive immune responses and mainly known as a “don’t eat me signal” during cancer. However, recent studies have also connected CD47 to antibacterial immune responses as well as influenza vaccination related immunity (Lee et al., 2016; Lindberg et al., 1996; Su et al., 2008). Interestingly, the impact of CD47 on protective immune responses is controversial depending on the pathogen and the site of infection. Moreover, the role of CD47 during primary influenza virus infection is still poorly understood. Therefore, the present study will determine the impact of CD47 on antiviral immune responses during acute influenza virus infection.

To this end, within the first part of this study the viral clearance of IAV as well as the associated innate and adaptive immune responses will be defined in wildtype (WT) and CD47 deficient mice upon intranasal infection with IAV (strain A/PR8/34). Here the role of CD47

for distinct immune cell subsets will be specified as well as their consequence for the disease severity. On the one hand, the focus of this study will lie on adaptive immune cells such as $CD4^+$ and $CD8^+$ T cells which are known to be involved in the final resolution of influenza virus infection (Iwasaki and Nozima, 1977; Topham and Doherty, 1998; Yap et al., 1978). On the other hand, the innate immune compartment including monocytes, MΦ, DCs, and neutrophils will be characterized as they have been shown to contribute to viral clearance as well as disease severity (Aldridge et al., 2009; Coates et al., 2018; Hashimoto et al., 2007; Tumpey et al., 2005). Furthermore, the contribution of its most prominent ligand SIRPα to the regulatory function of CD47 during acute IAV infection will be addressed in more detail by the use of SIRPα mutant mice as well as monoclonal SIPRα-blocking antibodies. In the last part of this study, the use of monoclonal CD47-blocking antibodies as a therapeutic treatment against severe IAV infection will be evaluated.

The obtained results of the present study may contribute to a better understanding of the immuno-regulatory function of CD47 during influenza virus infection. Moreover, they might offer a perspective for new treatment options against severe influenza virus infections.

2 Material and Methods

2.1 Materials

2.1.1 Appliances

Table 2-1: List of used appliances

Appliance	Manufacturer
7500 Fast Real-Time PCR System	Applied Biosystems (Foster City – California, USA)
autoMACS® Pro Separator	Miltenyi Biotec (Bergisch-Gladbach, Germany)
BD FACSAria II	BD Biosciences Pharmingen (Heidelberg, Germany)
BD FACSCantoTM II	BD Biosciences Pharmingen (Heidelberg, Germany)
BD LSR II	BD Biosciences Pharmingen (Heidelberg, Germany)
CO2 Incubator HERAcell® 150	Thermo Scientific (Darmstadt, Germany)
FastPrep-24TM Classic Instrument	MP Biomedicals Germany GmbH (Eschwege, Germany)
Heraeus Multifuge 3SR+ Centrifuge	Thermo Scientific (Darmstadt, Germany)
Luminex MAGPIX Instrument	Bio-Techne (Wiesbaden-Nordenstadt, Germany)
SunriseTM	Tecan Deutschland GmbH (Crailsheim, Germany)
T3000 Thermocycler	Biometra GmbH (Göttingen, Germany)
TGradient	Biometra GmbH (Göttingen, Germany)
Quantum CX5	VILBER LOURMAT Deutschland GmbH (Eberhardzell, Germany)
NanoDrop1000 Spectrophotometer	PEQLAB Biotechnologie GmbH (Erlangen, Germany)

2.1.2 Software

Table 2-2: List of utilized software

Software	Manufacturer
BD FACSDiva™ software v 8.0.1	BD Biosciences Pharmingen (Heidelberg, Germany)
BioVision	VILBER LOURMAT Deutschland GmbH (Eberhardzell, Germany)
GraphPad Prism 7	GraphPad Software, Inc. (La Jolla – California, USA)
Magellan™	Tecan Deutschland GmbH (Crailsheim, Germany)
xPONENT®	Bio-Techne (Wiesbaden-Nordenstadt, Germany)

2.1.3 Consumables

Table 2-3: List of the consumables which were used to perform the experiments

Consumables	Manufacturer
autoMACS® Columns	Miltenyi Biotec (Bergisch-Gladbach, Germany)
BD DiscarditTM II 2 ml / 10 ml	Becton Dickinson GmbH (Heidelberg, Germany)
BD MicrolanceTM 3	Becton Dickinson GmbH (Heidelberg, Germany)
CELLSTAR® Centrifuge Tubes 15 ml / 50 ml	Greiner Bio-One GmbH (Frickenhausen, Germany)
CELLSTAR® Filter Cap Cell Culture Flasks T-75	Greiner Bio-One GmbH (Frickenhausen, Germany)
CELLSTAR® 34mmune34ll culture plates 12 wells 24 wells 48 wells	Greiner Bio-One GmbH (Frickenhausen, Germany)
CELLSTAR® 96 well plates	Greiner Bio-One GmbH (Frickenhausen, Germany)
Falcon™ Cell Strainers 70 µm / 100 µm	Thermo Scientific (Darmstadt, Germany)
Microplate, 96 well, PS, U-bottom, clear	Greiner Bio-One GmbH (Frickenhausen, Germany)
Nunc™ MaxiSorp™ ELISA Plates, Uncoated	BioLegend GmbH (Koblenz, Germany)

Consumables	Manufacturer
Lysing Matrix M Tubes (2 ml)	MP Biomedicals Germany GmbH (Eschwege, Germany)
Omnican® F	B. Braun Melsungen AG (Melsungen, Germany)
Tube, 1.3 ml, PP, 8.5/44 MM, round bottom, nature	Greiner Bio-One GmbH (Frickenhausen, Germany)
Vasofix® Safety 20G	B. Braun Melsungen AG (Melsungen, Germany)

2.1.4 Chemicals and Reagents

If not listed below the chemicals utilized were purchased form Carl Roth GmbH + Co. KG (Karlsruhe, Germany).

Table 2-4: List of used chemicals

Chemicals	Manufacturer
AutoMACS Pro Washing Solution	Miltenyi Biotec (Bergisch-Gladbach, Germany)
AutoMACS Running Buffer	Miltenyi Biotec (Bergisch-Gladbach, Germany)
Avicel® PH-101	Merck KGaA (Darmstadt, Germany)
Biozym Plaque Agarose	Biozym Scientific GmbH (Hessisch Oldendorf, Germany)
Brefeldin A (BFA)	Biorad Laboratories GmbH (München, Germany)
Corning® Matrigel® Matrix (GFR, phenol red-free)	Corning GmbH (Kaiserslautern, Germany)
ELISA Coating Buffer (5x)	BioLegend GmbH (Koblenz, Germany)
FACS Flow Sheath Fluid	BD Biosciences Pharmingen (Heidelberg, Germany)
FACS Clean Solution	BD Biosciences Pharmingen (Heidelberg, Germany)
FACS Rinse Solution	BD Biosciences Pharmingen (Heidelberg, Germany)
Ionomycin Calcium Salt	Sigma Aldrich (St. Louis – Missouri, USA)
Ketamin 10 % Injektionslösung	MEDISTAR Arzneimittelvertrieb GmbH (Ascheberg, Germany)
Fetal calf serum (FCS)	Biochrom GmbH (Berlin, Germany)

Chemicals	Manufacturer
LE Agarose	Biozym Scientific GmbH (Hessisch Oldendorf, Germany)
L-Glutamin	Sigma Aldrich (St. Louis – Missouri, USA)
Natrium-Chlorid-Lösung (0,9 %)	B. Braun Melsungen AG (Melsungen, Germany)
SeaPrep™ Agarose	Lonza Cologne GmbH (Köln, Germany)
TMB Substrate Set	BioLegend GmbH (Koblenz, Germany)
Xylaxin 2 %	Ceva Animal Health Pty Ltd (Glenorie, Australia)

Table 2-5: List of used reagents

Reagents	Manufacturer
Clodronate Liposomes & Control Liposomes (PBS)	Liposoma B.V. (Amsterdam, Netherlands)
Collagenase D	Roche Life Science (Mannheim, Gemany)
Corning® Dispase	Corning GmbH (Kaiserslautern, Germany)
DNase I from bovine prancreas	Merck KGaA (Darmstadt, Germany)
Dnase I	Roche Life Science (Mannheim, Gemany)
dATP Solution (100 mM)	Thermo Scientific (Darmstadt, Germany)
dCTP Solution (100 mM)	Thermo Scientific (Darmstadt, Germany)
dGTP Solution (100 mM)	Thermo Scientific (Darmstadt, Germany)
dTTP Solution (100 mM)	Thermo Scientific (Darmstadt, Germany)
Fetal Calf Serum (FCS)	Biochrom GmbH (Berlin, Germany)
Gibco™ HEPES (1M)	Thermo Scientific (Darmstadt, Germany)
Gentamicin	Sigma Aldrich (St. Louis – Missouri, USA)

Reagents	Manufacturer
Gibco™ Penicillin-Streptomycin	Thermo Scientific (Darmstadt, Germany)
Midori^{Green} Advance	NIPPON Genetics EUROPE GmbH (Düren, Germany)
M-MLV Reverse Transcriptase	Invitrogen (Karlsruhe, Germany)
M-MLV Reverse Transcriptase 5x Reaction Buffer	Promega (Mannheim, Germany)
Oligo(dT)$_{12-18}$ Primer	Invitrogen (Karlsruhe, Germany)
pHrodo™ Green *E.coli* BioParticles™	Thermo Scientific (Darmstadt, Germany)
Random Primers	Invitrogen (Karlsruhe, Germany)
TruStain fcX™ (anti-mouse CD16/32) Antibody	BioLegend GmbH (Koblenz, Germany)
Trypan Blue Solution, 0.4%	Thermo Scientific (Darmstadt, Germany)
Trypsin-EDTA solution 10x	Sigma Aldrich (St. Louis – Missouri, USA)
Vybrant® CFDA SE Cell Tracer Kit	Thermo Scientific (Darmstadt, Germany)

2.1.5 Kits

The concentration of cytokines the pulmonary lumen was determined by Luminex® Assay which were purchased from Bio-Techne (Wiesbaden-Nordenstadt, Germany).

Table 2-6: List of utilized Kits

Kits	Manufacturer
Anti-F4/80 MicroBeads UltraPure (mouse)	Miltenyi Biotec (Bergisch-Gladbach, Germany)
Foxp3 / Transcription Factor Staining Buffer Set	eBioscience NatuTec (San Diego-California, USA)
GoTaq® Flexi DNA Polymerase Kit	Promega (Mannheim, Germany)
NucleoSpin® RNA XS	MACHEREY-NAGEL GmbH & Co. KG (Düren, Germany)
Maxima SYBR Green qPCR Master Mix (2x)	Thermo Scientific (Darmstadt, Germany)

2.1.6 Buffers and Media

Table 2-7: List of purchased media

Medium	Manufacturer
Dulbecco's Modified Eagle Medium (DMEM)	Thermo Scientific
High glucose, pyruvate	(Darmstadt, Germany)
Low glucose, pyruvate	
Iscove's Modified Dulbecco's Medium (IMDM), GlutaMAX™ Supplement	Thermo Scientific
	(Darmstadt, Germany)
Opti-MEM™ Reduced Serum Medium, GlutaMAX™ Supplement	Thermo Scientific
	(Darmstadt, Germany)

Table 2-8: Composition of utilized buffers and media

Buffer/ Medium	Compounds
ACK buffer	8.29 g/l NH_4Cl
	1 g/l $KHCO_3$
	0.1 mM EDTA
DMEM AEC II	25 mM HEPES
	DMEM (low glucose)
DMEM AEC $II_{complete}$ (DMEM AEC II_c)	25 mM HEPES
	10 % heat-inactivated FCS
	50 U/ml Penicillin
	DMEM (low glucose)
$DMEM_{complete}$ ($DMEM_c$)	10 % heat-inactivated FCS
	100 µg/ml Streptomycin
	100 U/ml Penicillin
	2 mM L-Glutamin
	DMEM (high glucose)
DMEM Plaque Assay	0.05 % BSA
	0.2 µg/ml Trypsin
	0,1 mg/ml Gentamycin
	3 % Avicel
	$DMEM_{complete}$
FACS buffer	2 % heat-inactivated FCS
	2 mM EDTA
	PBS buffer
$IMDM_{complete}$	10 % heat-inactivated FCS
	100 µg/ml Streptomycin
	100 U/ml Penicillin
	25 µM 2-Mercaptoethanol
	IMDM

Buffer/ Medium	Compounds
PBS buffer (pH 7.0)	8 g/l NaCl
	0.2 g/l KCl
	1.44 g/l $Na_2HPO_4x2H_2O$
	0.2 g/l KH_2PO_4
	H_2O
TBE buffer	89 mM Tris
	89 mM Boric acid
	2 mM EDTA
	H_2O
TE buffer	10 mM Tris/HCl (pH 8.0)
	1 mM EDTA
	H_2O

2.1.7 Antibodies

For quantification of influenza virus-specific antibodies via Enzyme-linked Immunosorbent Assay (ELSIA) horseradish peroxidase coupled antibodies directed against the constant region of IgA, IgG, and IgM were used. The utilized antibodies were purchased from Southern Biotech (Birmingham-Alabama, USA)

The antibodies used for *in vivo* blockade of CD47 (InVivoMAb anti-mouse CD47, clone: MIAP301) and SIRPα (LEAF™ Purified anti-mouse CD172a, clone: P84) were obtained from BioXCell (West Labanon-New Hampshire, USA) and BioLegend GmbH (Koblenz, Germany), respectively.

For flow cytometric analysis of different cellular markers the fluorochrome linked antibodies listed below were used (Table 2-9). To discriminate between viable and dead cells the eBioscience™ Fixable Viability Dye (FVD) that is linked to the Fluorochrome eFluor™ 780 (Thermo Scientific - Darmstadt, Germany) was utilized. Detection of Biotin labelled antibodies was achieved by PerCP Streptavidin (BD Biosciences Pharmingen – Heidelberg, Germany).

Table 2-9: List of used antibodies

Target	Clone	Species	Linked Fluorochrome	Manufacturer
Arginase	polyclonal	sheep	APC	Bio-Techne (Wiesbaden-Nordenstadt, Germany)
CCR2	REA538	human	Pe-Vio770	Miltenyi Biotec (Bergisch-Gladbach, Germany)
CCR7	4B12	rat	PE	eBioscience NatuTec (San Diego-California USA)

Target	Clone	Species	Linked Fluorochrome	Manufacturer
CD3	145-2C11	hamster	PE	BD Biosciences Pharmingen (Heidelberg, Germany)
CD4	H129.19	rat	PE	BD Biosciences Pharmingen (Heidelberg, Germany)
CD4	GK1.5	rat	FITC	BD Biosciences Pharmingen (Heidelberg, Germany)
CD4	RM4-5	rat	PeCy7	BioLegend GmbH (Koblenz, Germany)
CD8a	53-6.7	rat	PB	BD Biosciences Pharmingen (Heidelberg, Germany)
CD11a	M17/4	rat	FITC	BioLegend GmbH (Koblenz, Germany)
CD11b	M1/70	rat	APC PeCy7 PB	BioLegend GmbH (Koblenz, Germany)
CD11b	M1/70	rat	PerCP-Cy5.5 PE	BD Biosciences Pharmingen (Heidelberg, Germany)
CD11c	HL3	hamster	APC FITC	BD Biosciences Pharmingen (Heidelberg, Germany)
CD11c	N418	hamster	PE	BioLegend GmbH (Koblenz, Germany)
CD16/32	93	rat	PE	eBioscience NatuTec (San Diego-California USA)
CD19	1D3	rat	PE	BD Biosciences Pharmingen (Heidelberg, Germany)
CD25	PC61	rat	V450	BD Biosciences Pharmingen (Heidelberg, Germany)
CD31	390	rat	PE	BioLegend GmbH (Koblenz, Germany)
CD45	30-F11	rat	PE PeCy7	BD Biosciences Pharmingen (Heidelberg, Germany)
CD47	MIAP301	rat	FITC PeCy7	BioLegend GmbH (Koblenz, Germany)
CD47	MIAP301	rat	BV421	BD Biosciences Pharmingen (Heidelberg, Germany)
CD49b	DX5	rat	APC	BioLegend GmbH (Koblenz, Germany)
CD49d	R1-2	rat	AF647	BD Biosciences Pharmingen (Heidelberg, Germany)

Target	Clone	Species	Linked Fluorochrome	Manufacturer
CD69	H1.2F3	hamster	Biotin	BD Biosciences Pharmingen (Heidelberg, Germany)
CD80	16-10A1	hamster	V450	BD Biosciences Pharmingen (Heidelberg, Germany)
CD86	GL1	rat	PeCy7	BD Biosciences Pharmingen (Heidelberg, Germany)
CD93	AA4.1	rat	APC	BioLegend GmbH (Koblenz, Germany)
CD103	M290	rat	PE	BD Biosciences Pharmingen (Heidelberg, Germany)
CD107a	1D4B	rat	PE	BD Biosciences Pharmingen (Heidelberg, Germany)
CX3CR1	SAO11F11	mouse	BV510	BioLegend GmbH (Koblenz, Germany)
EOMES	Dan11mag	rat	AF488	eBioscience NatuTec (San Diego-California USA)
F4/80	BM8	rat	APC PE FITC	Thermo Scientific (Darmstadt, Germany)
FoxP3	FJK-16s	rat	FITC	eBioscience NatuTec (San Diego-California USA)
Granzyme B	GB12	mouse	APC	Thermo Scientific (Darmstadt, Germany)
IFN-γ	XMG1.2	rat	BV510	BioLegend GmbH (Koblenz, Germany)
IL-2	JES6-5H4	rat	FITC	eBioscience NatuTec (San Diego-California USA)
iNOS	CXNFT	rat	PeCy7	eBioscience NatuTec (San Diego-California USA)
Ly6C	AL-21	rat	PeCy7	BD Biosciences Pharmingen (Heidelberg, Germany)
Ly6C	HK1.4	rat	PerCP PeCy7	BioLegend GmbH (Koblenz, Germany)
Ly6G	1A8	rat	APC	BioLegend GmbH (Koblenz, Germany)
MHC II	M5/144.15.2	rat	BV510	BioLegend GmbH (Koblenz, Germany)
NK1.1	PK136	mouse	FITC	BD Biosciences Pharmingen (Heidelberg, Germany)

Target	Clone	Species	Linked Fluorochrome	Manufacturer
NK1.1	PK136	mouse	PB	eBioscience NatuTec (San Diego-California USA)
SIRPα	P84	rat	PE APC PerCP-Cy5.5	BioLegend GmbH (Koblenz, Germany)
SIRPα	P84	rat	BV421	BD Biosciences Pharmingen (Heidelberg, Germany)
TNF-α	MP6-XT22	rat	APC	eBioscience NatuTec (San Diego-California USA)

2.1.8 Primer

Primers used in this study were obtained from Eurofins Genomics Germany GmbH (Ebersberg, Germany) and are listed below.

Table 2-10: List of utilized primers for quantitative real-time PCR

Target	Sequence (forward, reverse)	Concentration [nM]	T_A [°C]
CD47	5'-ATGGCACGGCCCCCTTTTGATTTC-3',	300	58
	5'-TGTTCCTTCCAGCTGTGAGTCGTG-3'	300	
Matrixprotein 1	5'-CTTCTAACCGAGGTCGAAACG-3',	300	55
	5'-AGGGCATTTTGGACAAAGTCGTCTA-3'	300	
RSP9	5'-CTGGACGAGGGCAAGATGAAGC-3',	900	58
	5'-TGACGTTGGCGGATGAGCACA-3'	50	
SIRPα	5'-CTCTGTGGACGCCTGTAA-3',	300	51
	5'-GATGCTGCTGCTGTTGTT-3'	300	
TSP-1	5'-TGCCCGCTCCACTCTGCCTTACT-3',	300	55
	5'-GCTCCTGCCTCCCCACATCTCA-3'	300	

2.1.9 Virus

The utilized influenza virus strain A/PR/8/34 (H1N1) was a kind gift of Prof. Dr. P. Stäheli (Institute of Virology, University Freiburg). It was initially isolated 1934 in Puerto Rico during an epidemic of respiratory infection. Adaption of the human pathogenic virus to the murine system was achieved by repeated passages in ferrets, mice, and chicken eggs. The obtained virus strain displays high pathogenicity with marked pulmonary lesions in mice (Beare et al., 1975; Francis, 1934) .

2.1.10 Cell lines

In the present study Madin-Darby Canine Kidney (*MDCK*) cells were used to determine the viral titer of influenza virus-infected mice. This cell line originates from a kidney of an adult female cocker spaniel and was established 1958 by S. Madin and N.B. Darby. The epithelial

cells show an adherent growth and are susceptible to a wide range of viruses, such as influenza virus, vesicular stomatitis indiana virus (VSV), and vaccinia virus (Gaush and Smith, 1968; Gaush et al., 1966).

2.1.11 Animals

During this study different mouse strains were utilized to perform the projected experiments. C57BL/6 mice were obtained from Envigo (Envigo RMS GmbH - Venray, Netherlands), whereas an initial homozygous couple of the knockout (KO) mouse strain B6.129S7-CD47^{tm1Fpl} (CD47$^{-/-}$) was obtained from Jackson Laboratory (JAX stock #003173; Jackson Laboratory - Bar Habor-Maine, USA). Thereafter, CD47$^{-/-}$mice have been bred and kept at the laboratory animal device of the university hospital Essen. SIRPα mutant (SIRPα$^{-/-}$) mice were kindly provided by Prof. Dr. Karl Lang (Institut für Immunologie, Universitätsklinikum Essen). For experiments mice were aged between 6 to 8 weeks and kept under specific pathogen free (SPF) conditions.

The utilized KO mouse strain B6.129S7-CD47^{tm1Fpl} is deficient for the integrin-associated surface protein CD47. For this purpose, a neomycin resistant cassette was inserted into exon 2 of the corresponding gene, which encodes for the signal peptide cleavage site and the IgV domain (1.2). C57BL/6J mice served as a genetic background for this KO strain. Despite the ubiquitous expression of CD47 and its role as a marker of self, CD47 deficient mice display no obvious phenotypic and pathologic alternations in appearance, survival, or fertility. However, a reduced CD3^{+} lymphocyte number can be detected in blood of homozygous KO mice. Moreover, they have been shown to be more susceptible to bacterial infection with *Escherichia coli (E. coli*) (Lindberg et al., 1996).

2.2 Methods

2.2.1 Animal Experimental Methods

2.2.1.1 Influenza Virus Infection of Mice

Acute infection of mice with influenza virus strain A/PR8/34 was achieved by intranasal instillation of 75 PFU of IAV in 25 µl of PBS with 0.3 % BSA. Beforehand, mice were intraperitoneally anaesthetized with ketamine (100 mg/kg body weight) and xylazine (5 mg/kg body weight), which were diluted in an isotonic saline solution. At the level of tolerance, the diluted virus was administered.

2.2.1.2 In vivo Macrophage Depletion

Specific depletion of MΦ was achieved by the administration of dichloromethylene bisphosphonate (clodronate) containing liposomes. In contrast to free clodronate, that cannot pass cellular membranes, liposomes are easily taken up by MΦ leading to an accumulation of the contained clodronate in the cytoplasm. Inside the cell the clodronate is metabolized into a nonhydrolyzable ATP analog which disturbs the cell metabolism and thereby induces apoptosis of the phagocyte. (Lehenkari et al., 2002; van Rooijen and Sanders, 1994). Using different routes of application distinct subgroups of MΦ can be targeted. In this study, single intranasal instillation of 75 µl of clodronate containing liposomes was performed to deplete aMΦ from the alveolar lumen. Depletion of iMΦ was achieved by twice intraperitoneal administration of 200 µl of clodronate containing liposomes at an interval of 48 h. For intranasal application, the mice were anesthetized as mentioned above and treatment was performed at the level of tolerance.

2.2.1.3 Adoptive Transfer of Murine Alveolar Macrophages

Adoptive transfer of WT and CD47 deficient aMΦ was accomplished by an initial depletion of aMΦ in recipient mice (2.2.1.2). After 48 h aMΦ isolated from WT and KO donor mice were transferred intranasally into recipient mice. Isolation of murine aMΦ was achieved by repeated broncho-alveolar lavage (BAL). The lungs were flushed five times with 1 ml of PBS + 1 mM EDTA. The obtained cells were centrifuged (1200 rpm/10 min/4 °C) and resuspended in 500 µl of sorting buffer. Isolation of aMΦ was performed based on their autofluorescence and was done via the BD FACSAria II. For further use isolated aMΦ were centrifuged (1200 rpm/10 min/4 °C) and resuspended in 50 µl of PBS. Transfer of isolated aMΦ was performed by intranasal application. As described above, mice were anesthetized beforehand and aMΦ in 50 µl of PBS were transferred into each mouse at the level of tolerance.

Sorting Buffer

PBS
1 mM EDTA
2 % FCS
25 mM HEPES

2.2.1.4 In vivo Phagocytosis Assay

The *in vivo* phagocytic activity of WT and KO MΦ in the lung was determined by intranasal administration of 0.05 mg pHrodo™ Green *E. coli* BioParticles™ in 75 µl of PBS. Anesthesia of mice was performed with ketamine and xylazine as mentioned above. After 1 h the cells of the BAL fluid (BALF) were isolated for flow cytometric analyses (2.2.3.6). The pH-sensitive pHrodo® Green dye enables a specific determination of phagocytosed BioParticles®. At neutral pH the dye is non-fluorescent while it emits green light in the acidic environment of phagosomes.

2.2.1.5 In vivo Efferocytosis Assay

Clearance of dead cells by WT and KO aMΦ *in vivo* was analyzed by intranasal instillation of *ex vivo* infected AEC II (2.2.3.82.2.3.8) in 50 µl of PBS. Prior to transfer the AEC II were stained with Vybrant® CFDA SE Cell Tracer Kit. CFDA SE (CFSE) is a green fluorescent dye which is able to pass through the cell membrane and accumulate in the cytoplasm of viable cells. In the first step of staining the cells were washed with an adequate volume of Iscove's Modified Dulbecco's Medium (IMDM). Next, the cells were resuspended in 4 ml of IMDM and 2.5 µM of CFSE was added. The cells were incubated protected from light for 8 min at 37 °C. Afterwards, 4 ml of FCS were added to stop the staining reaction (5 min/37 °C). Finally, 5 ml of FACS buffer was added, the cells were centrifuged for 10 min at 1200 rpm and 4 °C. Thereafter the cells were resuspended in an adequate volume of FACS buffer and the number of cells was determined (2.2.3.9). Finally, the labelled cells were transferred in WT and KO recipient mice. Anesthesia of mice was performed with ketamine and xylazine as mentioned above. The uptake of fluorescent dead cells by aMΦ was assessed by flow cytometric analyses 1 h after administration.

2.2.1.6 In vivo Blockade of CD47 and its Ligand SIRPα

In order to specifically block CD47 *in vivo* during IAV infection, mice were treated with 100 µg of a monoclonal antibody directed against CD47 (2.1.7) in 100 µl PBS referring to Cham et al. 2020. Application was performed intraperitoneally (i.p.) each day from day three until day six post infection. *In vivo* blockade of SIRPα was accomplished by intravenous injection of 200 µg of a SIRP-blocking antibody (2.1.7) one day post infection.

2.2.2 Histological Methods

2.2.2.1 Histopathology

In order to investigate the disease severity in the lung upon influenza virus infection histopathologic analyses were performed. The lungs of infected mice were perfused with up to 10 ml of PBS through the right ventricle of the heart and filled with 4 % paraformaldehyde through the trachea. Next, the lungs were dissected and transferred into 50 ml Falcon tubes filled with 4 % paraformaldehyde. The subsequent steps of the histopathological analyses were kindly performed by Robert Klopfleisch (Institute of Veterinary Pathology, Freie Universität Berlin). The fixed tissues were embedded in paraffin and sectioned at a thickness of 4 µm with a microtome. The sections were stained with hematoxylin and eosin (H&E) and the pathological lesions in the lung tissue were examined at a magnification of 40. The pathological score of the lung sections was composed of different parameters listed below.

Table 2-11: Parameters of pulmonary lesions for histopathologic analyses

Score	Parameter
0-5	Inflammation (Lymphocytes / plasma cells)
0-5	Hyperplasia (type II pneumocytes)
0-3	Histiocytosis (aMΦ)
0-3	Neutrophils (alveoli / interstitium)
0-3	Necrosis

2.2.2.2 Immunohistochemistry

Immunohistochemical staining were performed to analyze the MΦ responses in the lungs of IAV-infected mice. To this end, the lungs were perfused and fixed as described above. The following steps were kindly performed by Dr. Florian Wirsdörfer (Institut für Zellbiologie, Universitätsklinikum Essen) as described previously (de Leve et al., 2017). Briefly, the fixed lungs were embedded in paraffin and sectioned with a thickness of 5 µm. Subsequently, the paraffin was removed from the sections and the samples were steam boiled in citrate buffer (pH 6). Endogenous peroxidase activity was blocked with 3 % H_2O_2 and MΦ were labelled based on the expression of Mac3. Visualization of labelled cells was accomplished via horseradish peroxidase (HRP) coupled secondary antibodies and a subsequent diaminobenzidine staining. Moreover, the sections were counterstained with hematoxylin.

2.2.3 Cytological Methods

2.2.3.1 Cell Culture

The cultivation of *MDCK* cells was performed in Dulbecco's Modified Eagle Medium$_{complete}$ ($DMEM_c$) (2.1.6) at 37 °C and 5 % CO_2.

2.2.3.2 Passaging of MDCK cells

For passaging the cells were washed with 10 ml PBS. As these cells grow adherently, they were detached from the culture flask by incubation with 2 ml of Trypsin-EDTA (1x) at 37 °C for 8-10 min. The reaction was stopped by addition of 10 ml $DMEM_c$ and finally the cells were split in an adequate ratio and transferred into a new cell culture flask.

2.2.3.3 Freezing and Thawing of MDCK Cells

In the long term *MDCK* cells were stored in liquid nitrogen. To this end, the cells were detached from the culture flask and centrifuged for 5 min at 1000 rpm and RT. Pelleted cells were resuspended in an adequate volume of 10 % DMSO in FCS (c = 1 x 10^6 cells/ml) and transferred into cryotubes. Subsequently, the *MDCK* cells were placed at -80 °C overnight and finally, transferred into liquid nitrogen.

Thawing of the *MDCK* cells was done by addition of 10 ml pre-warmed $DMEM_c$. In order to get rid of the DMSO, cells were centrifuged for 8 min at 800 rpm and RT. Finally, the cells were resuspended in 20 ml of $DMEM_c$ and transferred into a cell culture flask.

2.2.3.4 Influenza Plaque Assay

The virus titer of IAV in infected tissue was quantified by Plaque Assay. To this end, the lungs of infected mice were dissected and transferred in 800 µl of PBS + 0.3 % BSA. Next, the infected tissue was homogenized via the FastPrep-24TM and Lysing Matrix M Tubes (2 ml) and the resulting homogenate was centrifuged for 8 min at 8000 rpm and 4 °C. Subsequently, the supernatant was collected stored at -80 °C until further use.

In the beginning of the plaque assay, 1.5 x 10^5 *MDCK* cells were seeded into each well of a 12-well plate and cultured for 24 h. Next, the *MDCK* cells were infected with 500 µl of lung supernatant which was serially diluted (10^{-1} – 10^{-4}) in Opti-MEM™ Medium + 0.3 % BSA. After 1 h the infected cells were sealed with DMEM Plaque Assay Medium containing 3 % Avicel. Avicel is a microcrystalline cellulose powder that forms an overlay on the *MDCK* cells and thereby prevents the spread of new viral particles into the medium. As a result of this new viruses are restricted to neighboring cells leading to circular areas of infected cells called plaques. Due to the lytic replication cycle of IAV the plaques are visible as voids in the cell layer. After 3 days of incubation, *MDCK* cells were fixed with 4 % PFA (30 min/RT) and stained with a 0.5 % crystal violet solution (10 min/RT). Finally, the cells were washed with

PBS and the plates were dried for analyses. The number of infectious particles can be determined by counting of plaques and the amount of plaque forming units (PFU) in 1 ml is calculated by following formula:

$$PFU = 2 \times \left(\frac{n_1 \times d_1 + n_2 \times d_2 + \ldots + n_x \times d_x}{x} \right)$$

n = counted plaques

d = dilution factor

2.2.3.5 Influenza Suppression Assay

The suppressive activity of BALF samples from influenza virus-infected WT and CD47 KO mice was determined based on a plaque assay. Initially, 1.5 x 10^5 *MDCK* cells per well were seeded on a 12-well plate and cultured for 24 h. On the next day, the *MDCK* cells were pre-treated for 30 min at RT with 250 µl of the BALF from WT and KO mice, which was diluted 1:3 in Opti-MEM™ Medium. Subsequently the cells were infected with 1000 PFU of A/PR8/34 influenza virus in 250 µl of Opti-MEM™ Medium + 0.6 % BSA. After 1 h the infected cells were sealed with DMEM Plaque Assay Medium and incubated for 72 h. Next, the *MDCK* cells were fixed and stained as described before (2.2.3.4). Finally, the suppressive activity of the BALF samples was calculated. To this end, the PFU of the pre-treated *MDCK* cells was normalized to the amount of infectious viral particles in a medium-treated control.

2.2.3.6 Isolation of Pulmonary Immune Cells from Mice

In order to isolate immune cells from the alveolar lumen a BAL was performed. To this end, the lungs were flushed two times with 0.5 ml of PBS via the trachea. After centrifugation (5 min/1500 rpm/4 °C) the supernatant was stored at -20 °C for cytokine and antibody analysis (2.2.4.6). The cells were resolved in 1 ml of ACK buffer and lysis of erythrocytes was stopped after 3 min by addition of 5 ml FACS buffer. The cells were again centrifuged and resuspended in an adequate volume of FACS buffer for further analysis.

Asides from this, immune cells were isolated from the pulmonary tissue. Initially, the lungs were perfused with up to 10 ml of PBS through the heart. Subsequently, the lungs were dissected and chopped into small pieces. Digestion of the tissue was performed for 45 min at 37 °C in 3 ml of digestive solution. Afterwards, the organs were squeezed through a 70 µm strainer. The filtrate was centrifuged for 5 min at 1500 rpm and 4 °C. Afterwards, remaining erythrocytes were lysed by incubation in 2 ml of ACK buffer for 3 min at RT. Lysis was stopped by the addition of 8 ml FACS buffer and the cells were centrifuged. Finally, the cells were resolved in 2 ml of FACS buffer and used for further analysis.

Digestive Solution:

0,5 mg/ml DNase I
0,16 mg/ml Collagenase D
5 % heat-inactivated FCS
IMDM

2.2.3.7 Isolation of Immune Cells from Murine Spleen

To isolate cells from a murine spleen, the organ was dissected and rinsed with 10 ml of ACK buffer. The solute cells were filtrated with a 70 µm strainer and thereafter transferred to a 15 ml tube. After centrifugation for 5 min at 1500 rpm and 4 °C the cells were resuspended in an adequate volume of FACS buffer.

2.2.3.8 Isolation of Murine Alveolar Epithelial Cells Type II

Isolation of AEC II was performed as previously described by Gereke et al. 2012. Briefly, the lungs were perfused with up to 10 ml PBS via the heart. Afterwards, the lungs were filled with 2 ml of Corning® Dispase through the trachea and further 0.5 ml of 1 % Biozym Plaque Agarose were added. The agarose was polymerized for 2 min at 4 °C and the lungs with trachea were dissected and transferred in 2 ml of Corning® Dispase. After incubation for 45 min at RT, the lobes of the lung were separated and transferred in 7 ml of DMEM AEC II (2.1.6). Next, the lobes were rigorously minced and 100 µl of DNase I (Merck KGaA) as well as 14 µl of TruStain fcX™, that blocks the Fc receptor, were added to the medium. The samples were incubated for 10 min at RT on a rocker and the obtained cell suspension was sequentially filtered through a 100 µm, 70 µm, and 30 µm strainer. The filtrate was centrifuged for 12 min at 900 rpm and 4 °C followed by an erythrocyte lysis in 2 ml of ACK buffer. Lysis was stopped with 13 ml of DMEM AEC II_c (2.1.6) and cells were centrifuged. The obtained cell pellet was resolved in 600 µl of staining solution and incubated at 4 °C for 10 min. Afterwards, the cells were washed with DMEM AEC II_c and resolved in 500 µl of medium. The AEC II cells were sorted from the obtained suspension with the BD FACSAria II. Finally, isolated AEC II cells were plated on a 96-well plate, which was coated with 3 mg/ml Matrigel in DMEM with low glucose. Before further use the AEC II were allowed to rest for 12 h at 37 °C and 5 % CO_2 in DMEM AEC II_c.

Staining Solution:

CD19 PE	F4/80 APC
CD31 PE	CD93 APC
CD11b PE	CD11c APC
CD16/32 PE	DMEM AEC IIc
CD45 PE	

2.2.3.9 Determination of the Cell Number

The number of cells was determined using a Neubauer haemocytometer. In a first step, the cells were diluted in an adequate volume of 0.4 % Trypan Blue solution. This dye is unable to pass the cell membrane of viable cells, but it can enter dead cells. Thereby, dead and living cells were distinguished and the viable cells inside the squares of the haemocytometer were counted under the microscope. Each square has an area of 0.04 mm^2 and a depth of 1 mm and thus comprises a volume of 0.004 µl. By calculating the mean (m) of the counted cells the total cell number (T) can be determined via the following formula:

$$T = m \times d \times 10^4 \times V \qquad V = \text{volume}$$

$$d = \text{dilution factor}$$

2.2.3.10 AEC II ex vivo Infection Assay

In order to analyze the replication of IAV in normal and CD47 deficient AEC II an *ex vivo* infection assay was performed. To this end AEC II cells were isolated (1.2.2.7) and one day later infected with 1 / 0.5 / 0.25 / 0.125 x 10^3 PFU IAV diluted in DMEM AEC II_c (2.1.6). Next, cells were incubated for 48 h at 37 °C and thereafter lysed in 200 µl of RA1 buffer of the NucleoSpin® RNA XS kit for RNA isolation (2.1.5). Upon RNA isolation and cDNA synthesis the viral titer of IAV in infected AEC II was determined by qRT-PCR (2.2.4.5).

2.2.3.11 Immunofluorescence Staining of Cell Surface Markers

Specific staining of isolated cells was accomplished by labelling with different fluorophore linked antibodies (2.1.7). In a first step, the cells were transferred onto a 96-well microplate and centrifuged for 5 min at 1200 rpm and 4 °C. Afterwards, the antibodies were diluted in FACS buffer and 100 µl of the antibody solution were used per well to stain the cells (10 min/4 °C). In a next step, the cells were washed with 100 µl of FACS buffer. If the cells had been used for further intracellular immunofluorescence staining (2.2.3.12) the cells were washed with 100 µl of PBS instead. For analyses, the cells were resuspended in 200 µl of FACS buffer and transferred into 1.3 ml tubes.

2.2.3.12 Intracellular Immunofluorescence Staining

In general, intracellular proteins like cytokines or transcription factors were stained using the Foxp3 / Transcription Factor Staining Buffer Set. Initially, the cells were fixated for 30 min at RT in Fixation/Permeabilization buffer (1x). Afterwards, the cells were washed with 100 µl of Permeabilization buffer (5 min/1200 rpm/4 °C). In a next step, the cells were incubated for 30 min at RT with diluted antibodies in Permeabilization buffer (2.1.7). After washing the cells with 100 µl of Permeabilization buffer (5 min/1200 rpm/4 °C) the cells were resuspended in 200 µl of FACS buffer and transferred into 1.3 ml tubes.

2.2.3.13 Flow Cytometry

Analyses of stained cells were performed via the flow cytometers BD LSR II or BD FACSCanto™ II together with the BD FACSDiva™ software. The frequencies as well as the absolute number of the cells of interest were determined. Based on the obtained gate frequencies (% G) as well as the number of cells counted in the lung suspension (N) the total number of the cells of interest (X) was calculated as follows:

$$X = N \times (\%\,G1 \times \%G2 \times \ldots \times \%Gn)$$

2.2.4 Molecular Biological Methods

2.2.4.1 Isolation of RNA

In order to isolate RNA from murine lungs, the tissue was prepared as described before (2.2.3.4). Isolation of RNA was performed with 200 µl of pulmonary supernatant via the NucleoSpin® RNA XS Kit according to the manufacturer's instructions except a final elution in 20 µl of RNase free water. Subsequently, the concentration of the isolated RNA was photometrically determined with the NanoDrop™1000 spectrophotometer. RNA samples were stored at -20 °C until further use.

2.2.4.2 Synthesis of Complementary DNA

For further analysis, purified RNA was transcribed into complementary DNA (cDNA) by reverse transcription, that was first described in retroviruses (Baltimore 1970). This step allows an unspecific amplification of obtained RNA and thus support analysis of low amount transcripts. To this end, 1-2 µg of the obtained RNA was diluted in RNase free water to a total volume of 13 µl. Subsequently, the RNA was incubated for 10 min at 70 °C with 0.5 µl of Oligo(dT)$_{12\text{-}18}$ Primers and Random Primers each. Afterwards, 4 µl of M-MLV Reverse Transcriptase 5x Reaction Buffer, 1 µl of 10mM dNTP Mix, and 1 µl of M-MLV Reverse Transcriptase were added. For reverse transcription, the samples were incubated at 42 °C for 1 h. Finally, the enzyme was inactivated at 95 °C for 5 min and the cDNA samples were stored at -20 °C until further use.

2.2.4.3 Polymerase Chain Reaction

In order to quantify the cDNA level in a semi-quantitative way conventional Polymerase Chain Reaction (PCR) was used. During PCR, the process of DNA replication is hijacked to amplify specific parts of DNA, which are defined by two oligonucleotide primers. Initially, the double-stranded (ds) DNA is denatured into single-strands which are used as a matrix for replication. Next, specific primers are annealed to the single stranded DNA with annealing temperature (AT) being dependent on the primer sequence (Table 2-10). Afterwards, the DNA polymerase binds to the primer and starts to synthesize the complementary strand. By

repeating these cycles, the DNA is amplified exponentially. Here PCR was performed based on the GoTaq® Flexi DNA Polymerase Kit and in T3000 Thermocycler. The reaction mix and PCR program are listed below. Subsequently, the amount of generated DNA was visualized by an agarose gel electrophoresis (2.2.4.4).

PCR Reaction Mix:

1 µl	cDNA
4 µl	GoTaq Flexi Buffer 5x
1,2 µl	$MgCl_2$
1 µl	Primer Mix (5 pmol/µl)
0.1 µl	GoTaq Polymerase (5 U/µl)
Ad 20 µl	H_2O

qRT-PCR Program

Step	Temperature [°C]	Time	Cycles
Initial Denaturation	94	10 min	1
Denaturation	94	45 sec	
Annealing	T_A	45 sec	30
Extension	72	45 sec	
Final Extension	72	10 min	1
Storage	4	∞	

2.2.4.4 Agarose Gel Electrophoresis

During an agarose gel electrophoresis nucleotide fragments are separated based on their size. To this end, 1 % of LE Agarose was dissolved in TBE buffer and allowed to polymerize. Moreover, the Midori^{Green} Advance dye was added, which interacts with the backbone of DNA and emits green fluorescence upon UV-excitation when bound to DNA. Afterwards, the gel was transferred into a gel electrophoresis chamber and an electric voltage was applied to induce the migration of the negatively charged DNA to the positive pole. Finally, the separated DNA was visualized via the Quantum CX5 gel documentation system.

2.2.4.5 Quantitative Real-Time PCR

Quantification of relative gene expression levels in murine pulmonary samples was performed via quantitative real-time PCR (qRT-PCR). Contrary to a conventional PCR, the qRT-PCR allows the real-time monitoring of the amplified target. For this purpose, different types of fluorescent probes are available, such as hydrolysis probes, dual hybridization probes or DNA-intercalating dyes. In this setting SYBR® Green was used, which is part of the latter. During polymerization, the dye is incorporated into the dsDNA in a non-sequence-specific manner. While the SYBR® Green exhibits only minor fluorescence in its unbound mode, the

fluorescence increases upon binding to DNA. As a result of this, the fluorescence intensity correlates with the amount of the amplicon and thus is directly proportional to the initial amount of template DNA. Based on that, the amount of template DNA prior to amplification can be calculated by an absolute or a relative quantification (Arya et al., 2005).

In the beginning of qRT-PCR, cDNA samples were pre-diluted in water relative to the expression of the housekeeping gene ribosomal protein S9 (RPS9) which was determined by a conventional PCR (2.2.4.3). The Maxima SYBR Green qPCR Master Mix (2x) Kit was utilized for amplification and detection of the DNA. Moreover, specific primers for a gene of interest or the housekeeping gene RPS9 were added (2.1.8). The analysis of the qRT-PCR was performed via the 7500 Real-Time PCR System.

qPCR Reaction Mix:

1 µl	cDNA
10 µl	Maxima SYBR Green qPCR Master Mix (5 µM ROX)
5 µl	Primer Mix
Ad 20 µl	H_2O

qRT-PCR Program

Step	Temperature [°C]	Time	Cycles
Initial Denaturation	95	10 min	1
Denaturation	95	15 sec	
Annealing	T_A	30 sec	40
Extension	72	30 sec	
Dissociation	95	15 sec	
	60	1 min	1
	95	15 sec	
	60	1 min	

2.2.4.6 Quantification of Influenza A Virus-Specific Antibodies

The quantification of IAV-specific antibodies was performed by an Enzyme-linked Immunosorbent Assay (ELSIA). The ELISA is an immunological method, which detects the binding of a specific protein by an antibody via color reaction (Engvall and Perlmann, 1972; Van Weemen and Schuurs, 1971). In this study the ELISA was performed based on a protocol described before (Lee et al., 2016). Briefly, heat inactivated IAV (5 x 10^4 PFU) was coated to Nunc™ MaxiSorp™ ELISA Plates in 1x ELISA Coating Buffer over night at 4 °C. Subsequently, the plates were washed three times with washing buffer and incubated for 90 min at 37 °C with a blocking buffer to prevent unspecific interactions. Next, the plates were loaded with bronchoalveolar lavage fluid (BALF) of infected mice, which was

prediluted 1:10 in blocking buffer. After 90 min at 37 °C the plates were washed three times and antibodies specific to the Fc-domain of either IgA, IgM, or IgG were added. These antibodies were coupled to HRP which catalyzes the conversion of the TMB substrate. This chromogenic substrate is oxidized into a blue dye that changes to a yellow color after addition of the acidic stop solution. Thus, the amount of the specific target protein corelates with the adsorption intensity of the dye. The adsorption of the substrate was detected by Sunrise™ microplate reader and Magellan™ software.

Washing buffer:

PBS

0.05 % Tween 20

Blocking buffer:

PBS

0.05 % Tween 20

3 % BSA

2.2.5 Statistical Analysis

Statistical analyses of the obtained data sets as well as the graphical illustration were performed in GraphPad Prism 7 software. The results were analyzed for normality based on the D'Agostino & Pearson normality test. All shown data sets are depicted as the mean ± the standard error of the mean (SEM).

3 Results

Lower respiratory tract infections pose a severe threat to human health and are commonly associated with influenza viruses. So far, treatment of severe IAV infection is limited and investigation of new strategies remains an urgent need. The integrin-associated transmembrane protein CD47 is an immuno-regulatory cell surface protein, which is expressed by innate as well as adaptive immune cells. Due to its impact on various immune cell functions such as the activation, migration, or differentiation, it has been shown to be involved in the clearance of different pathogens. However, its effect is varying depending on the invading microorganism as well as the site of infection (1.2.2). Moreover, its role in antiviral immunity is still poorly understood. Thus, this study defines the impact of CD47 on antiviral immune responses during IAV infection of the respiratory system to gain a better understanding of its therapeutic potential.

3.1 CD47$^{-/-}$ Mice display Reduced Viral Load upon IAV Infection

3.1.1 IAV Infection augments the Expression of CD47

CD47 is expressed by a variety of cells including non-immune and immune cells. However, the amount of CD47 on the surface of individual immune cells (Latour et al., 2001) as well as its level in different tissues varies (Reinhold et al., 1995). In order to investigate its impact on antiviral immunity in the respiratory system, initially the expression of CD47 on pulmonary immune cells was assessed. Different immune cells were isolated from the lung of naïve C57BL/6 (WT) mice and the expression of CD47 on their cell surface was determined via flow cytometry. At steady state, neutrophils, NK cells, and different T cell subsets showed a minor expression of CD47 as compared to myeloid immune cells such as monocytes, MΦ, and DCs. Interestingly, the most abundant CD47-expression was found on the surface of MΦ (Figure 3-1 A). Within the respiratory system two different types of MΦ can be found. aMΦ reside in the alveolar lumen of the lung while iMΦ are located in the parenchymal tissue. To get a deeper insight into the impact of the cellular localization within the lung on the expression of CD47, both pulmonary MΦ subtypes as well as splenic MΦ were compared. Of the two pulmonary MΦ populations aMΦ showed the highest expression whereas iMΦ displayed similar levels to splenic MΦ (Figure 3-1 B). The cytokine milieu in the alveolar lumen is highly specialized and characterized by anti-inflammatory molecules such as IL-10 and TGF-β. This alveolar environment has been shown to participate in the homeostasis of resident immune cells such as aMΦ by controlling the expression of different immuno-regulatory receptors (e.g. CD200) (Snelgrove et al., 2008). To examine the possible impact of the alveolar environment on CD47 expression, F4/80^{+} MΦ were isolated from the

spleen of naïve mice via magnetic-activated cell sorting (MACS) and incubated with TGF-β or IL-10. Afterwards, CD47-levels on the MΦ were determined by flow cytometry. While TGF-β had a minor effect, IL-10 significantly triggered the expression of CD47 on splenic MΦ indicating a specific expression on immune cells in the alveolar lumen (Figure 3-1 C). To further support this hypothesis, the expression of CD47 on different pulmonary and splenic DCs was assessed. In line with the MΦ populations, splenic cDCs expressed low levels of CD47 compared to pulmonary DCs. Among those, $CD103^+$ DCs, which protrude into the alveolar lumen, showed the highest expression (Figure 3-1 D). These findings reveal a specifically high expression of CD47 on alveolar immune cells.

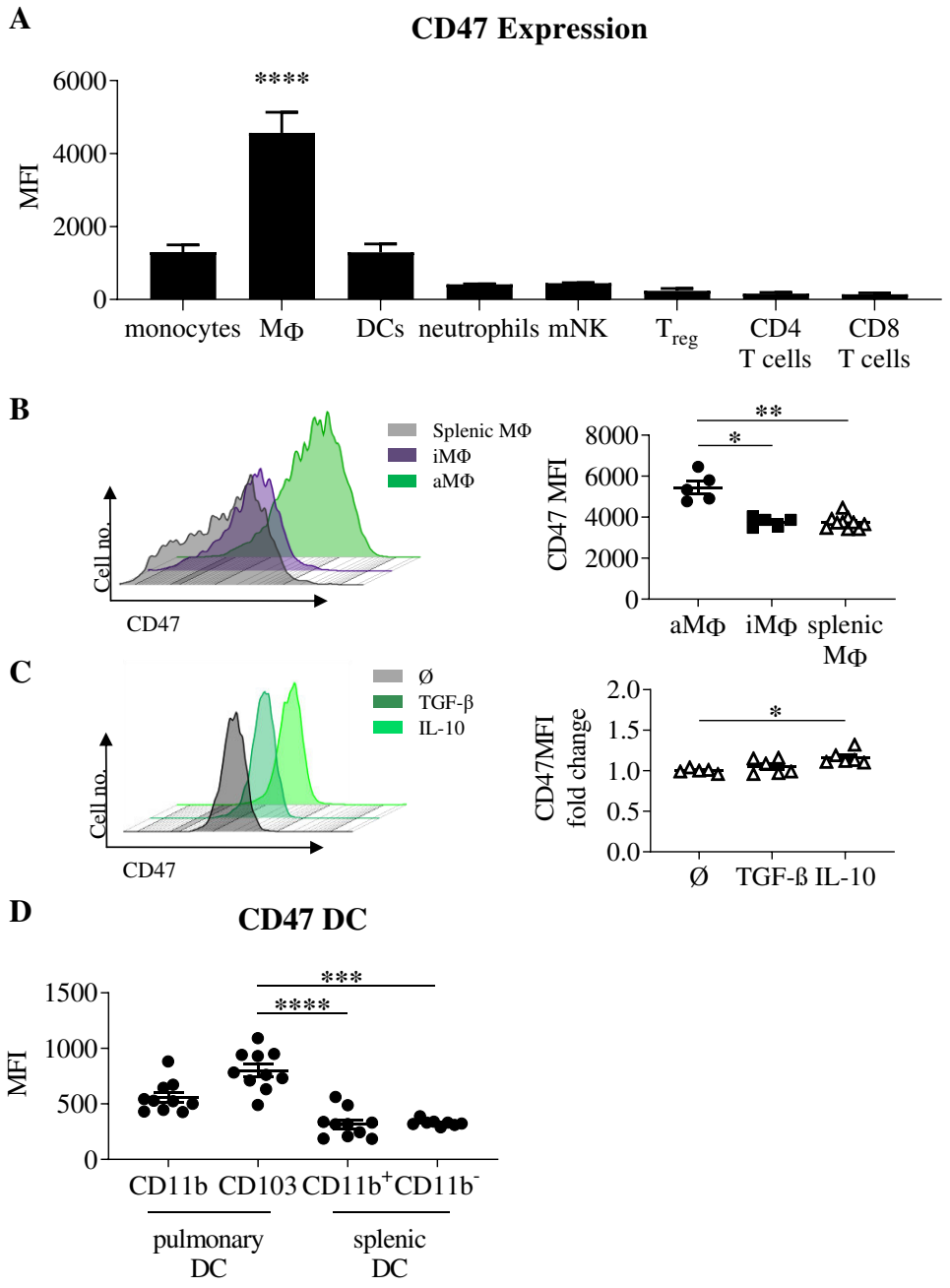

Figure 3-1: Site-specific expression of CD47 on alveolar immune cells. Pulmonary as well as splenic immune cells were isolated from naïve C57BL/6 mice and the expression of CD47 on different immune cells was assessed by flow cytometry as the mean fluorescence intensity (MFI). (A) The individual innate and adaptive

immune cells were identified as follows: NK1.1$^-$ CD11c$^-$ CD11b^{hi} monocytes, F4/80$^+$ macrophages (MΦ), CD11c$^+$ dendritic cell (DCs), Ly6G^{hi} CD11b^{hi} CD45$^+$ neutrophils, CD3$^-$ CD49b$^+$ NK1.1$^+$ natural killer (NK) cells, Foxp3$^+$ CD25$^+$ CD4$^+$ regulatory T cells (T_{regs}), CD4$^+$ T cells and CD8$^+$ T cells. (B) Moreover, CD11b$^-$ alveolar MΦ (aMΦ) and CD11b$^+$ interstitial MΦ (iMΦ) as well as (D) CD11b$^+$ CD11c$^+$, CD11b$^-$ CD11c$^+$ splenic cDCs and CD11b$^+$ CD103$^-$, CD11b$^-$ CD103$^+$ pulmonary DC subsets were distinguished. (C) Additionally, splenic MΦ were isolated from naïve wildtype mice via magnetic-activated cell sorting based on their expression of F4/80. Subsequently, isolated MΦ were incubated at 37 °C with either transforming growth factor-β (TGF-β) or interleukin-10 (IL-10). After 4 h the expression of CD47 on the cell surface was determined by flow cytometry as the fold change of the MFI normalized to an untreated control. Depicted are the results of two (B-D) or three (A) independent experiments (n = 5-10). For statistical analysis parametric One-way ANOVA was performed together with a post hoc Tuckey test (A) as well as nonparametric Kruskal Wallis test together with Dunn's test for correction of multiple comparison (B-D) (* = p<0.05, ** = p<0.01, *** = p<0.001, **** = p<0.0001).

To further investigate the role of CD47 during respiratory IAV infection, influenza virus strain A/PR8/34 was intranasally administered to WT mice (Figure 3-2 A). qRT-PCR analyses of the infected lungs revealed the upregulation of CD47 in the early phases of infection (Figure 3-2 B). Regarding the distinct immune cells, MΦ and neutrophils significantly enhanced the expression of CD47 on day three post infection. In the later course of infection, CD47 returned to basal levels in total lung tissue although T_{regs} and CD8$^+$ T cells exhibited an augmented expression on the surface seven days post infection (dpi) (Figure 3-2 C). In addition to CD47, its ligands SIRPα and TSP-1 were induced upon IAV infection. While the expression of SIRPα was significantly elevated in the lung at an early phase of infection, TSP-1 levels raised at a later phase (Figure 3-2 B).

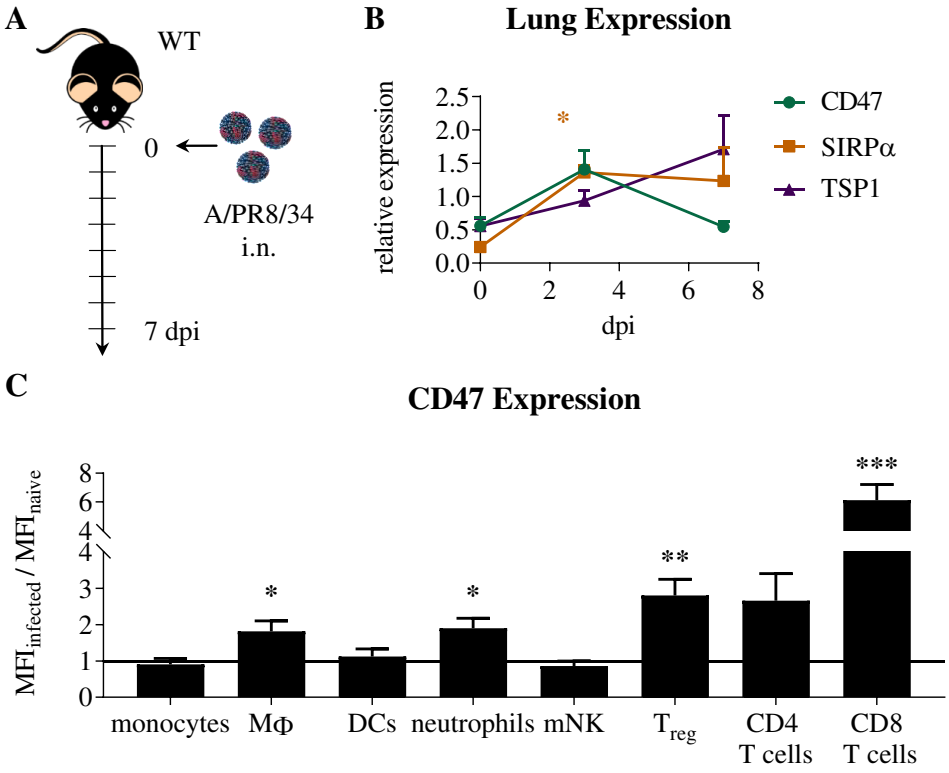

Figure 3-2: Increased expression of CD47 during influenza A virus infection. (A) C57BL/6 mice were infected intranasally (i.n.) with influenza virus strain A/PR8/34. On days three and seven after influenza virus infection the lungs were either used for gene expression (B) or flow cytometric analyses (C) of CD47 and its

ligands SIRPα and TSP-1. Innate immune cells including NK1.1^{-} CD11c^{-} CD11b^{hi} monocytes, F4/80^{+} macrophages (MΦ), CD11c^{+} dendritic cell (DCs), Ly6G^{hi} CD11b^{hi} CD45^{+} neutrophils and CD3^{-} CD49b^{+} NK1.1^{+} natural killer (NK) cells were analyzed three days post infection (dpi) whereas CD47 on adaptive immune cells (Foxp3^{+} CD25^{+} CD4^{+} regulatory T cell (T_{regs}), CD4^{+} T cells,CD8^{+} T cells) was assessed after seven days. The mean fluorescence intensity (MFI) of CD47 during infection was compared to the level on naïve cells. Depicted were the normalized MFI of infected cells relative to the naïve MFI. The graphs show the results of two (B) or three (C) independent experiments (n = 4-13). For statistical analysis nonparametric Kruskal Wallis test was performed together with a post hoc Dunn's test (B) as well as parametric One-way ANOVA together with Tuckey test for correction of multiple comparison (C) (* = $p<0.05$, ** = $p<0.01$, *** = $p<0.001$).

3.1.2 CD47 limits the Clearance of IAV Infection

The first experiments depict a strong expression of CD47 on alveolar immune cells in healthy mice. In combination with the increased expression upon influenza virus infection, the obtained results indicate a role of CD47 in IAV infection. To address its impact on IAV clearance, mice lacking the expression of CD47 (CD47$^{-/-}$) were infected with IAV strain A/PR8/34. The course and severity of infection was monitored and compared to infected WT mice sufficient to express CD47 (Figure 3-3 A). The disease severity was analyzed based on the body weight loss and the viral load in infected tissue, which was determined by qRT-PCR as well as plaque assay. Upon IAV infection, no differences in the loss of body weight were observed between WT and KO mice (Figure 3-3 B). Interestingly, the analyses of the viral load in infected lungs revealed a significantly lower amount of infectious virus in CD47$^{-/-}$ mice compared to the WT 7 dpi (Figure 3-3 C). However, the differences between WT and KO mice manifested late during infection since the virus titer increased similarly in both mouse strains from day three until day five post infection (Figure 3-3 D).

To exclude a direct impact of CD47 on IAV entry or replication within target cells, the *in vitro* infection of *MDCK* cells pre-treated with a CD47-blocking antibody (mAbCD47) was performed. The viral titer of IAV was assessed by qRT-PCR and compared to untreated MDCK cells (Ø) or cells treated with an isotype control (mAbIso). Here, the differently treated cells exhibited no changes in the viral load (Figure 3-4 A). Additionally, AEC II as primary targets of influenza virus were isolated from the lungs of naïve WT and CD47$^{-/-}$ mice and *ex vivo* infected with different doses of IAV. After two days the viral load of WT and KO AEC II was determined via qRT-PCR. At low doses of IAV, similar amounts of viral RNA were detected in WT AEC II and those deficient for CD47. However, at high doses CD47 deficient AEC II were unable to control virus replication whereas virus titers were limited in WT epithelial cells (Figure 3-4 B). Hence, CD47 neither contributes to viral entry nor replication of IAV in host cells. Taken together, the first experiments indicate a negative impact of CD47 on viral clearance.

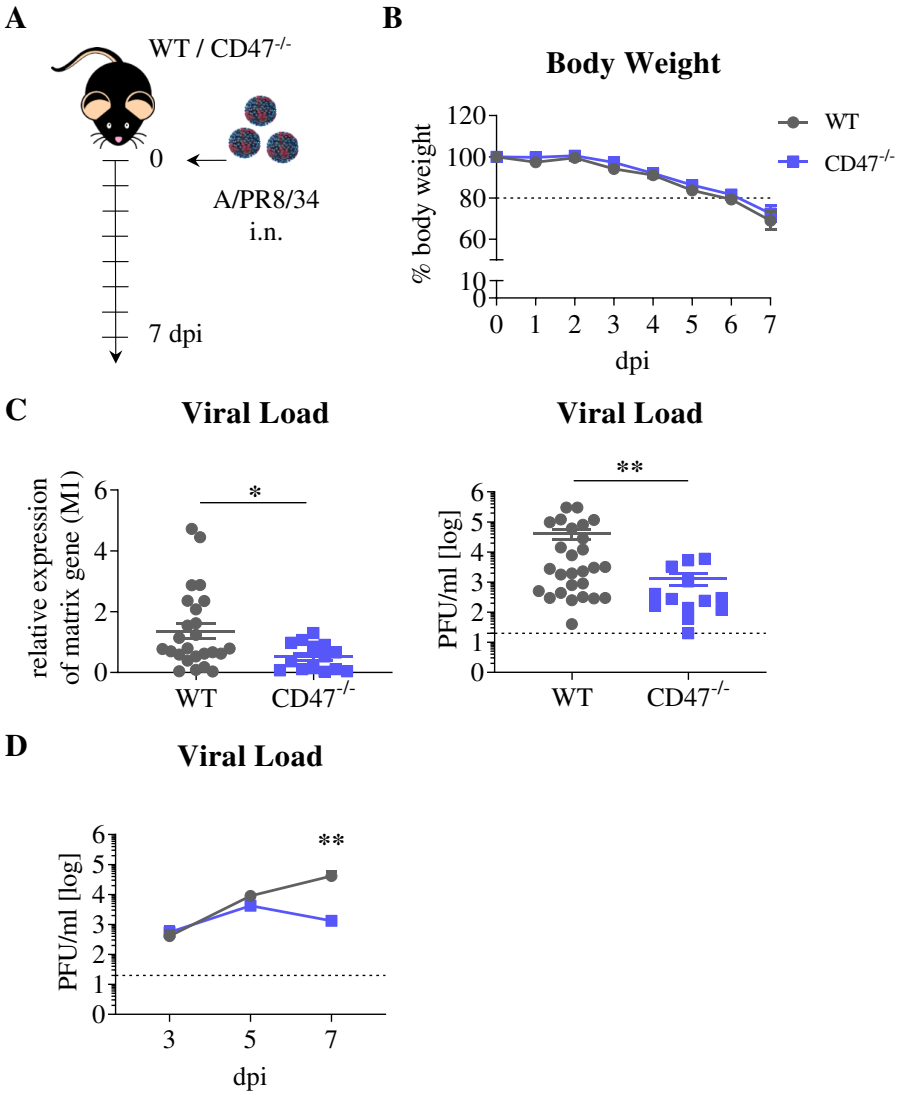

Figure 3-3: Reduced viral load in CD47$^{-/-}$ mice compared to wildtype mice during influenza A virus infection. (A) C57BL/6 as well as mice deficient for CD47 were infected with influenza strain A/PR8/34 via intranasal (i.n.) instillation. (B) The course of infection was monitored by daily weighing. (C) Moreover, the lungs of infected mice were collected seven days post infection (dpi) to assess the viral load by quantitative real-time PCR of the matrix protein M1 as well as the concentration of plaque forming units (PFU) via plaque assay. (D) In addition to this, the progression of viral replication was monitored by plaque assay of infected tissue 3, 5 and 7 dpi. The graphs illustrate the results of up to ten independent experiments (n = 8-34). Statistical analyses were done based on a Two-way ANOVA with Sidak's multiple comparisons test (B) and an unpaired Mann-Whitney U test (C-D) (* = p<0.05, ** = p<0.01).

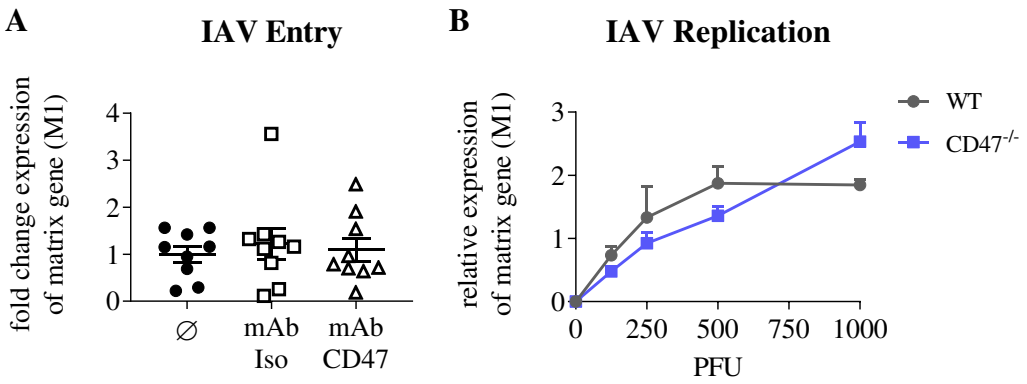

Figure 3-4: Influenza A virus entry and replication are not restricted in absence of CD47. (A) *MDCK* cells were infected with 500 PFU of influenza strain A/PR8/34 after pre-treatment with a CD47-blocking antibody

(mAbCD47), an isotype control (mAbIso) or medium (Ø). Three days later the virus titer in the infected *MDCK* cell was examined by quantitative real-time PCR (qRT-PCR) of the viral matrix protein M1. The expression of M1 was normalized to the untreated control. (B) Moreover, alveolar type II epithelial cells (AECII) were isolated from the lungs of naïve C57BL/6 as well as CD47$^{-/-}$ mice. Subsequently, the cells were infected *ex vivo* with different doses of IAV. After two days the viral load in the WT and KO cells was determined by qRT-PCR. Shown is the relative expression of M1 in relation to the housekeeping gene RPS9. The results of two independent experiments are depicted and for statistical analyses a nonparametric Kruskal Wallis test together with a Dunn's test for multiple comparisons (A) as well as Two-way ANOVA with post hoc Sidak's test (B) were performed (** = $p<0.01$).

3.2 Improved Viral Clearance is Independent of Adaptive Immunity

Clearance of influenza virus infection is a multifactorial process dependent on various immune cells. Especially, adaptive immune responses mediated by CD8$^+$ T cells (Bender et al., 1992; Mcmichael et al., 1983; Yap et al., 1978) as well as B cells (Gerhard et al., 1997; Iwasaki and Nozima, 1977) are described to be essential for efficient viral clearance. Although the initial experiments showed MΦ to express the highest amounts of CD47 under homeostasis, CD8$^+$ T cells as well as T_{reg} massively upregulated the protein of interest upon IAV infection. Moreover, CD47 has been described to be involved in the activation of T cells as well as B cells (1.2.2). Thus, the focus of the following experiments was on the role of CD47 on adaptive immune responses during IAV infection. To this end, WT and CD47$^{-/-}$ mice were infected with IAV as described (Figure 3-3 A) and sacrificed for analyses 7 dpi.

3.2.1 CD47 does not limit Antiviral T cell Responses against IAV Infection

The T cell responses of WT and CD47$^{-/-}$ mice were determined by flow cytometry. In general, immune cells were initially identified during flow cytometric analyses based on their size and granularity by the forward scatter (FSC) and sideward scatter (SSC), respectively. In the next step, the expression of cell surface markers was used to identify the cells of interest. Here, CD4$^+$ and CD8$^+$ T cells were selected and further classified as CD11a$^+$ CD49d$^+$ CD4$^+$ effector T cells (T_{eff}), CD25$^+$ Foxp3$^+$ T_{regs} as well as CD11a$^+$ CD8$^+$ T_{eff} cells (Figure 3-5). As expected, CD4$^+$ and CD8$^+$ T cells accumulated in the lung upon influenza virus infection. However, mice lacking CD47 displayed lower numbers of CD4$^+$ T cells compared to WT mice. In line with this, the frequency of CD4$^+$ T_{eff} cells was reduced whereas the frequency of T_{reg} was augmented in absence of CD47 (Figure 3-5 A). Within the CD8$^+$ T cell compartment no differences were observed between WT and KO animals regarding their magnitude in response to IAV infection(Figure 3-5 B).

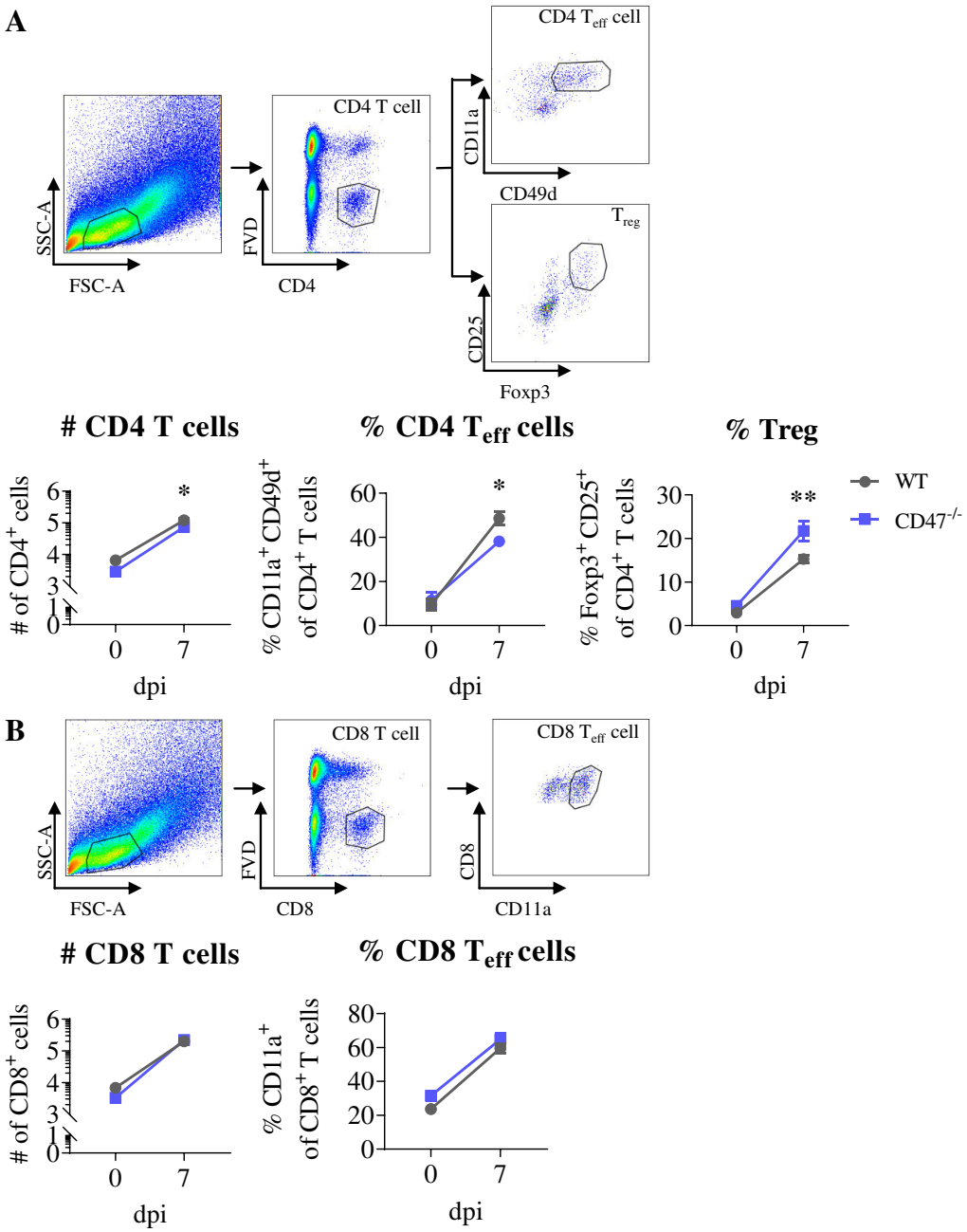

Figure 3-5: Frequencies of T cells are not improved in CD47$^{-/-}$ mice compared to wildtype mice during influenza A virus infection. Leukocytes were isolated from the lung of naïve as well as IAV-infected mice seven days post infection (dpi) and stained with fluorochrome linked antibodies for flow cytometric analyses. The cells of interest were initially identified by their characteristics in the forward scatter (FSC) and sideward scatter (SSC). (A) Subsequently, the number of CD4$^+$ T lymphocytes were determined which were further divided into CD11a$^+$ CD49d$^+$ CD4$^+$ effector T cells (T_{eff}) and CD25$^+$ Foxp3$^+$ regulatory T cell ($T_{regs.}$). (B) Moreover, CD8$^+$ T cell numbers as well as the frequencies of CD11a$^+$ CD8$^+$ T_{eff} cells were examined. The graphs show the results of three independent experiments (n = 9-12) as well as representative dotplots of the utilized gating strategy. Statistical analyses were performed based on a Two-way ANOVA with a post hoc Sidak's test (* = $p<0.05$, ** = $p<0.01$).

Apart from the number, the functionality of T cells is essential for pathogen clearance. On the one hand, the functionality can be characterized by the ability of T cells to secret multiple cytokines. Thus, the expression of the pro-inflammatory cytokines IL-2, IFN-γ, and TNF-α was analyzed after restimulation of T cells from IAV-infected WT and KO mice by flow

cytometry (Figure 3-6 A). Regarding the $CD4^+$ T cells no alternations were detected whereas the functionality of $CD8^+$ T cells was impaired in CD47 deficient compared to WT mice. In absence of CD47, the frequency of single and double cytokine producers among the $CD8^+$ T cells was significantly reduced. These changes were based on significantly lower frequencies of IL-2 and IFN-γ secreting $CD8^+$ T cells as well as double producers of IL-2/IFN-γ and TNFα/IFN-γ (Figure 3-6 B-C).

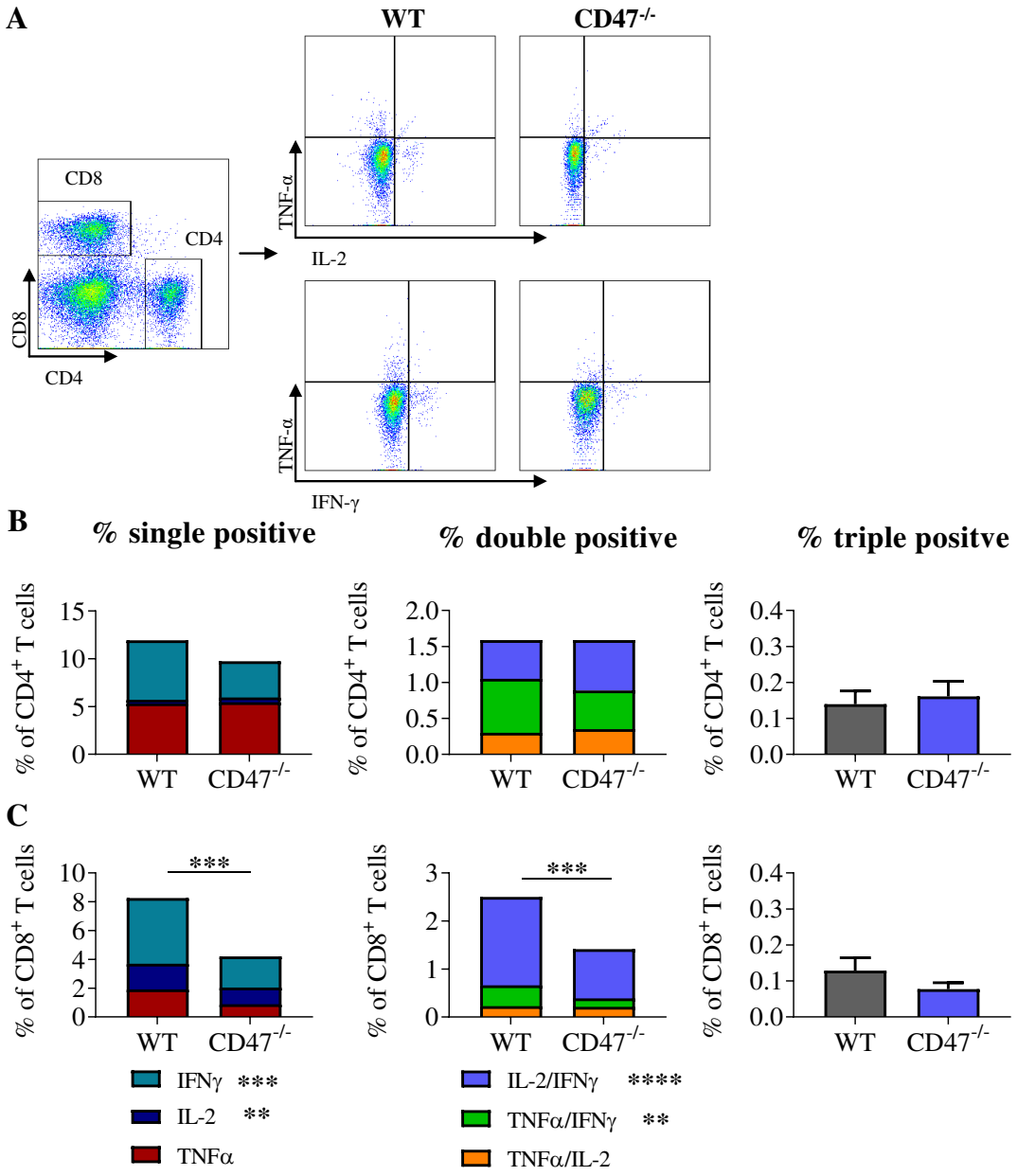

Figure 3-6: $CD47^{-/-}$ mice display reduced of $CD8^+$ T cell functionality compared to wildtype mice. On day seven post infection leukocytes were isolated from the lung of influenza virus-infected mice and stimulated with ionomycin and PMA in the presence of brefeldin A. Subsequently, the cells were stained with fluorochrome linked antibodies for flow cytometric analyses. The expression of the pro-inflammatory cytokines interleukin-2 (IL-2), interferon-γ (IFN-γ) and tumor necrosis factor-α (TNF-α) was analyzed via flow cytometry and among the viable $CD4^+$ (B) and $CD8^+$ (C) T cells single, double, and triple producers were identified. Depicted are representative graphs of the used gating strategy (A) and the results of two independent experiments (n = 8). For statistical analyses, an unpaired t-test or Mann-Whitney U test was used (** = $p<0.01$, *** = $p<0.001$).

On the other hand, the functionality of T cells can also be defined by the expression of effector molecules. For this purpose, cytotoxic effector molecules, such as GzmB or CD107a, were analyzed in $CD4^+$ and $CD8^+$ T cells upon influenza virus infection by flow cytometry. The expression of none of the analyzed effector molecules was increased in $CD4^+$ T cells of CD47 KO mice. Within the $CD8^+$ T cell population the frequencies of $GzmB^+$ and $CD107a^+$ cells were reduced in absence of CD47 despite an augmented expression of eomesodermin (EOMES) (Figure 3-7). Thus, CD47 did not improve the number or the function of T_{eff} cell immunity against IAV.

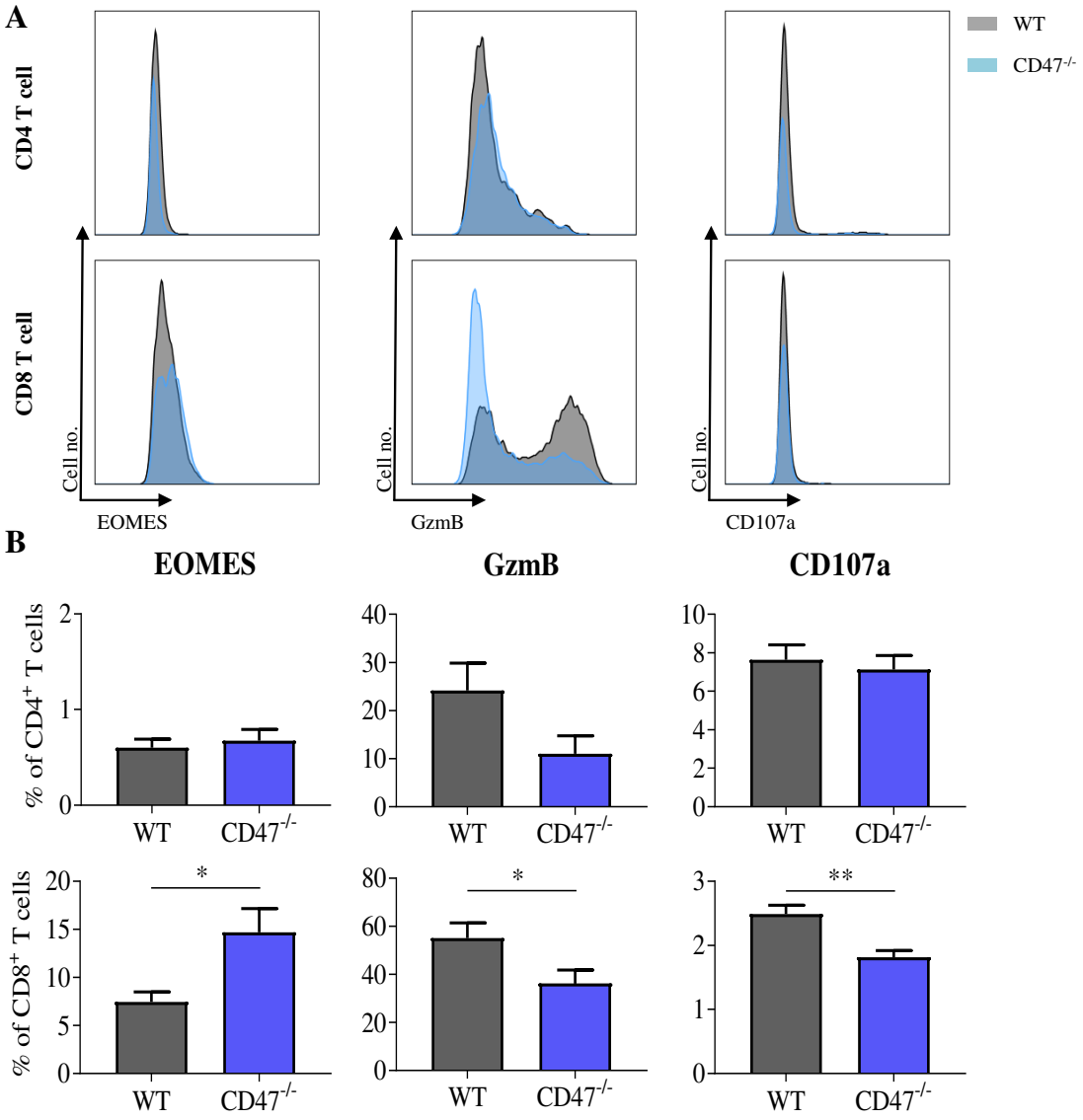

Figure 3-7: Reduced level of cytotoxic effector molecules in $CD4^+$ and $CD8^+$ T cells from $CD47^{-/-}$ mice compared to wildtype mice. Lymphocytes were isolated from the lung of WT and CD47 deficient mice on day seven post infection. In order to analyze the cytotoxic potential of $CD4^+$ and $CD8^+$ T cells, the lymphocytes were stimulated with ionomycin and PMA in the presence of brefeldin A and the frequency of granzyme B (GzmB), CD107a, and eomesodermin (EOMES) producing cells was examined via flow cytometry. Depicted are representative histograms of the analyzed effector molecules (A) as well as the results of two independent experiments (B) (n = 8). For statistical analyses, either an unpaired t-test or Mann-Whitney U test was performed.

3.2.2 Humoral Immune Responses against IAV are not restrained by CD47

Besides cellular immunity mediated by T cells, the humoral immune response of infected WT and CD47$^{-/-}$ mice was analyzed. To this end, the quantity of IAV-specific antibodies in the broncho-alveolar lavage fluid (BALF) was determined via ELISA. Most influenza virus-specific antibodies in the BALF of WT and KO mice belonged to the class of IgA, which are associated with mucosal immunity. Only low amounts of IgM and IgG were detected upon infection. Interestingly, the magnitude of antibody responses was not altered in absence of CD47 compared to WT mice (Figure 3-8). Hence, the augmented clearance of IAV in absence of CD47 seems to be independent from humoral immune responses. Together with the results from the T cell analyses, this suggests a minor influence of CD47 on the adaptive immune responses during IAV infection.

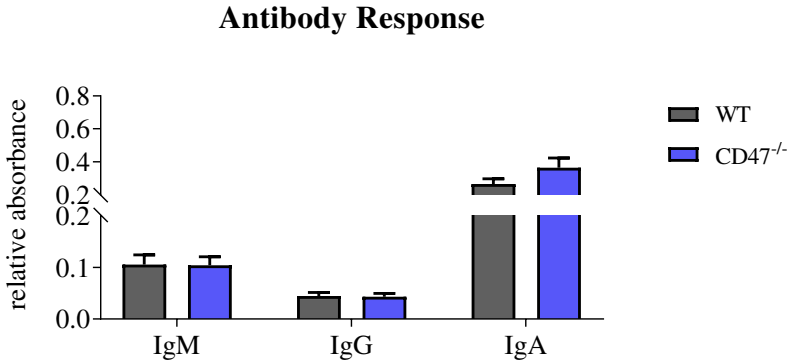

Figure 3-8: CD47 does not interfere with antibody responses during IAV infection. On day seven post infection the broncho-alveolar lavage fluid (BALF) of WT and CD47$^{-/-}$ mice was collected and used for an enzyme linked immunosorbent assay (ELISA) to detect the amount of IAV-specific antibodies. For this purpose, ELISA plates were pre-coated with heat-inactivated influenza virus strain A/PR8/34 and IAV-specific antibodies were detected by horseradish peroxidase (HRP) linked secondary antibodies. Depicted are the results of three independent experiments (n = 9-10). For statistical analyses, an unpaired t-test or Mann-Whitney U test was used.

3.3 Enhanced aMΦ Responses in Absence of CD47

In addition to adaptive immune responses, innate immune cells such as MΦ and neutrophils were shown to participate in the clearance of influenza virus infection (Fujimoto et al., 2000; Tate et al., 2009; Tumpey et al., 2005). Therefore, the following part of the project deals with the impact of CD47 on antiviral innate immunity against IAV infection. In line with previous experiments, WT as well as CD47$^{-/-}$ mice were infected with IAV (Figure 3-3 A) and the magnitude of innate immune responses was assessed early during infection (3 dpi) as well as at the peak of infection (7 dpi) via flow cytometry.

3.3.1 Neutrophil Responses against IAV remain Unchanged in Absence of CD47

CD47 has been shown to contribute to neutrophil recruitment to the side of infection and thus aggravates bacterial infection of the respiratory system (Su et al., 2008). Hence, first the effect

of CD47 on neutrophil responses during influenza virus infection was assessed. Neutrophils were identified among the CD45$^+$ hematopoietic cells based on their high expression of Ly6G and CD11b. Upon influenza virus infection the number of neutrophils was increased to the same extend in WT mice and those deficient of CD47 (Figure 3-9 A). Similarly, the activation of neutrophils that correlates with the expression level of CD11b (Kinhult et al., 2003; Simon et al., 1995) was the same in WT and KO mice early during infection (Figure 3-9 B). Additionally, the concentration of neutrophil-related cytokines in the BALF of naïve as well as influenza virus-infected mice was determined. However, IAV-infected WT and CD47 deficient mice showed similarly increased levels of granulocyte colony-stimulating factor (G-CSF) within the BALF, which is involved in the recruitment as well as the function of neutrophils, (Figure 3-9 C). Hence, improved clearance of IAV in CD47$^{-/-}$ mice was obviously not based on changes in the neutrophil response.

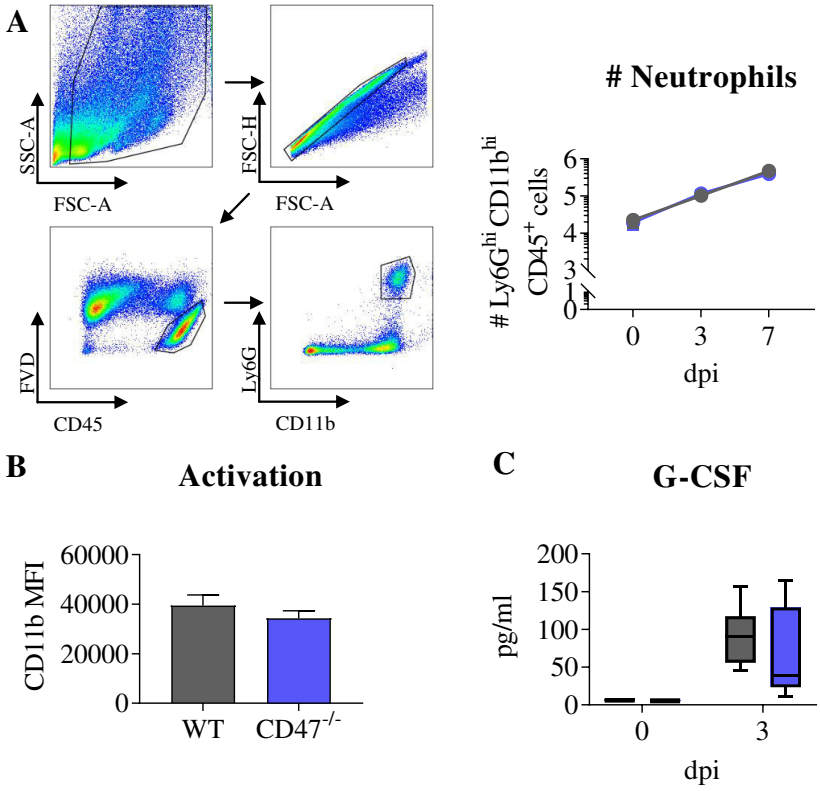

Figure 3-9: CD47 does not limit antiviral neutrophil responses during influenza A virus infection. Leukocytes were isolated from the lung of naïve as well as IAV-infected mice and stained with fluorochrome linked antibodies for flow cytometric analyses. (A) The number of Ly6G^{high} CD11b^{high} CD45$^+$ neutrophils within the lung was determined three and seven days post infection (dpi). (B) The mean fluorescence intensity (MFI) of CD11b on neutrophils was assessed at day three post infection. (C) Moreover, the concentration of granulocyte colony-stimulating factor (G-CSF) in the broncho-alveolar lavage fluid (BALF) of WT and CD47 deficient mice was assessed on day three after influenza virus infection via Luminex® Assay. Depicted are representative dotplots of the used gating strategy and the results of three independent experiments (n = 6-10). For statistical analyses, a Two-way ANOVA with a post hoc Sidak's test (A) as well as an unpaired t-test was performed (B-C).

3.3.2 Enhanced Viral Clearance in CD47$^{-/-}$ Mice is Independent of Monocytes

Apart from its impact on neutrophil recruitment, CD47 has been described to facilitate the migration of monocytes to the inflamed tissue (Rosseau et al., 2000; de Vries et al., 2002). However, monocytes have a dual role during influenza virus infection both aggravating and attenuating the disease. Therefore, the focus of the next experiments was on the effect of CD47 on monocyte responses during IAV infection. In addition to flow cytometric analyses, the concentration of the monocyte attracting cytokine CCL2 in the BALF of infected mice was examined. Monocytes were identified by a strong expression of CD11b as well as a lack of NK1.1 and CD11c. Among the monocytes two subpopulations with distinct functional properties can be distinguished. Ly6C^{hi} CCR2^{+} inflammatory monocytes are recruited upon infection in a CCL2-dependent manner. At the site of infection, they differentiate into pro-inflammatory DCs as well as MΦ (Lin et al., 2008; Rosseau et al., 2000). In contrast to this, Ly6C^{low} CX3CR1^{+} peripheral monocytes constantly patrol the peripheral tissue. Upon activation they differentiate into alternatively activated MΦ contributing to tissue repair (Shi and Pamer, 2011) (Figure 3-10 A). Upon IAV infection the level of CCL2 was increased in the BALF independently from the presence or absence of CD47 (Figure 3-10 B). In line with this, the absolute number of monocytes in the lung of WT and KO mice raised equally and showed a steady expansion until the peak of infection (Figure 3-10 C). Inflammatory monocytes are rapidly recruited to the site of infection. However, decreased frequencies of inflammatory monocytes were detected early during infection approximately due to the differentiation into DCs and MΦ. In contrast to this, the frequency of peripheral monocytes was diminished at the peak of infection reflecting their potential role in tissue regeneration. The genetic ablation of CD47 did not change the course of inflammatory monocyte immunity, whereas the frequency of peripheral monocytes already decreased early during infection. Thus, CD47 deficient mice displayed significantly lower levels of peripheral monocytes at day three post infection compared to WT mice (Figure 3-10 D).

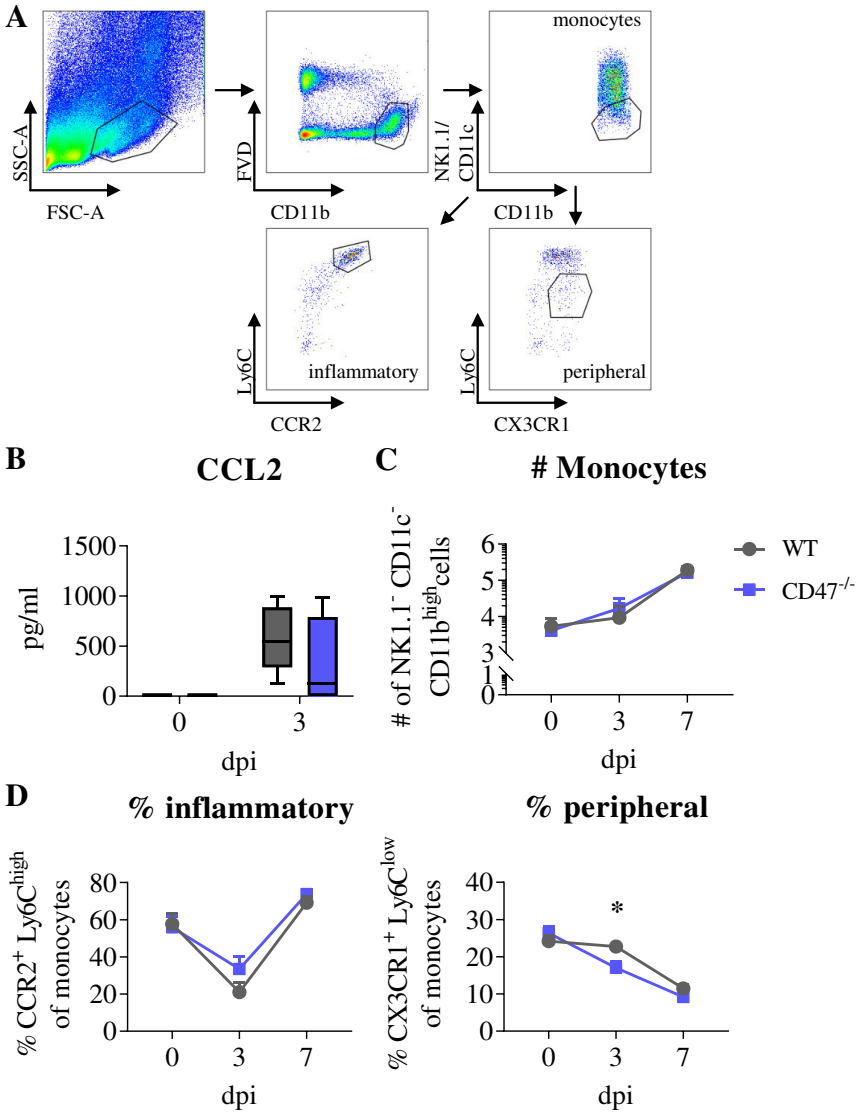

Figure 3-10: Monocyte responses are not enhanced in CD47$^{-/-}$ mice compared to wildtype mice. CD47 deficient mice as well as WT ones were infected intranasally with influenza virus strain A/PR8/34. Leukocytes were isolated from the lung on days three and seven after influenza virus infection and monocyte responses were analyzed by flow cytometry. (A) Monocytes were identified via the forward scatter (FCS) and sideward scatter (SSC) as well as the markers CD11b^{hi}, NK1.1^{-}, and CD11c^{-}. Next, two subpopulations of circulating monocytes were distinguished: Ly6G^{hi} CCR2^{+} inflammatory monocytes and Ly6G^{low} CX3CR1^{+} peripheral monocytes. The number of monocytes (C) as well as the frequencies of inflammatory and peripheral monocyte subpopulations(D) were determined. (B) Moreover, the concentration of the monocyte-attractant protein CCL2 was assessed in the broncho-alveolar lavage fluid (BALF) via Luminex® Assay. The graphs show the results of three independent experiments (n = 6-10). For statistical analyses, a Two-way ANOVA together with a Sidak's test for multiple comparisons was used (* = $p<0.05$).

As mentioned above, peripheral monocytes are thought to contribute to tissue repair during infection. Thus, an early differentiation of these monocytes might limit the pathology during influenza virus infection. Hence, the pathology in WT and KO mice upon intranasal infection with IAV (Figure 3-3 A) was assessed. On the one hand, the pathology was determined by the number of cells recruited to the lung tissue as well as the alveolar lumen. On the other hand, the pathology was assessed by histological analyses. During influenza virus infection WT and CD47$^{-/-}$ mice displayed an equal recruitment of cells to the lung tissue and the alveoli

(Figure 3-11 A). In line with this, histopathological analyses of the infected tissue revealed no differences between WT mice and mice deficient of CD47. The tissue sections were scored for different parameters including inflammation, hyperplasia, histiocytosis, neutrophils and necrosis. However, none of them was significantly decreased in absence of CD47 (Figure 3-11 B). Thus, altered monocyte responses did not protect $CD47^{-/-}$ mice from influenza virus-related immuno-pathology.

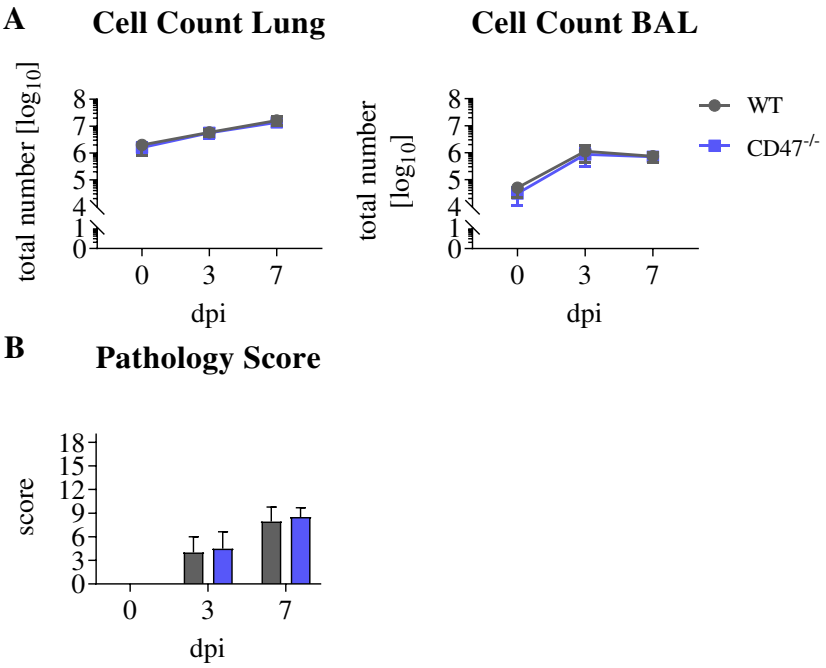

Figure 3-11: $CD47^{-/-}$ mice have no lowered pathology compared to wildtype mice during influenza A virus infection. WT as well as CD47 deficient mice were infected by single intranasal instillation of influenza virus strain A/PR8/34. Three and seven days post infection (dpi) the broncho-alveolar lavage fluid (BALF) as well as the lung tissue were collected and the pathological changes were analyzed. (A) On the one hand, the pathology was determined via the overall number of cells within the pulmonary tissue as well as the alveolar lumen. (B) On the other hand, histological analyses were performed to score the pathology of infected WT and KO mice. The pathology score is made up of single evaluations of the inflammation, hyperplasia, histiocytosis, neutrophils and necrosis with a maximum score of 19. Depicted are the results of four (B) to eight (A) independent experiments (n = 3-40). For statistical analyses, a Two-way ANOVA together with a Sidak's test for multiple comparisons was used.

3.3.3 CD47 does not limit DC Responses during IAV Infection

In addition of neutrophil and monocyte responses CD47 has been described to control the migration as well as the activation of DCs (1.2.2). Thus, the role of CD47 in DC responses during IAV infection was analyzed in more detail. DCs were identified via the expression of CD11c and the distinct subpopulations of DCs were distinguished based on the expression of Ly6C. Among the $Ly6C^-$ DCs, $CD11b^+$ $CD103^-$ cDCs as well as $CD11b^-$ $CD103^+$ cDCs were identified. Furthermore, $Ly6C^+$ DCs were divided into $CD11b^+$ moDCs / tipDCs and $CD11b^-$ pDCs (Figure 3-12 A). Upon influenza virus infection the number of DCs in the lung of WT and CD47 deficient mice steadily increased. Due to the recruitment of moDCs / tipDCs, the frequencies of lung resident $CD11b^+$ as well as $CD103^+$ DCs were

decreased early upon infection. Moreover, the tissue resident cDCs are described to migrate to the draining LN. Contrary to this, the frequency of pDCs was steadily augmented upon influenza virus infection. However, the composition as well as the magnitude of WT and KO DC immunity did not differ except for an initial higher frequency of CD103^{+} cDCs in the lung of naïve CD47$^{-/-}$ mice (Figure 3-12 B). Thus, boosted viral clearance of IAV in CD47$^{-/-}$ mice seems to be independent of DCs.

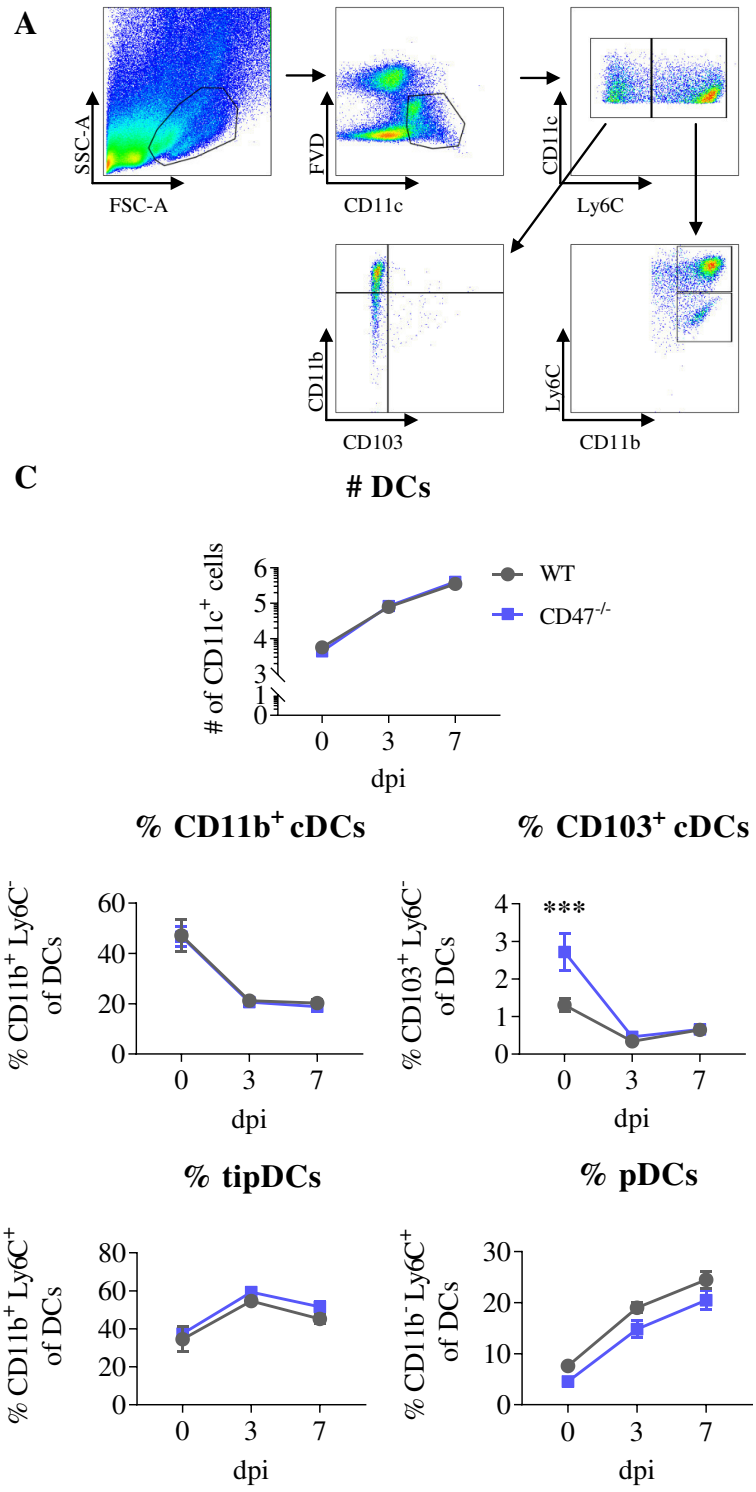

Figure 3-12: CD47 does not impede antiviral immune responses mediated by dendritic cells. WT and CD47$^{-/-}$ mice were infected with A/PR8/34 influenza virus. On days three and seven post infection DCs in the lungs of naïve and infected mice were stained with fluorochrome linked antibodies for flow cytometric analyses.

(A) Dendritic cells (DCs) were identified via the forward scatter (FSC) and sideward scatter (SSC) as well as the expression of CD11c. Moreover, different DC-subsets were classified based on the expression of Ly6C. Ly6C$^-$ cells were divided into CD11b$^+$ CD103$^-$ DCs and CD11b$^-$ CD103$^+$ DCs whereas Ly6C$^+$ cells were separated into CD11b$^+$ monocyte derived DCs (moDCs) and CD11b$^-$ plasmacytoid DCs (pDCs). (B) The total number of DCs as well as the frequencies of different subpopulation were assessed. Depicted are the results of three independent experiments (n = 6-10). For statistical analyses, a Two-way ANOVA and a post-hoc Sidak's test were performed (*** = p<0.001).

3.3.4 CD47$^{-/-}$ Mice have a Shift of MΦ Responses during IAV Infection

The initial experiments suggested no contribution of neutrophils, monocytes as well as DCs to the enhanced clearance of IAV in absence of CD47. Thus, in the next step the MΦ responses of CD47$^{-/-}$ mice during influenza virus infection were analyzed, as CD47 is known to control the activation and function of MΦ (Oldenborg et al., 2000; Stein et al., 2016). During flow cytometric analyses MΦ were identified via the FSC and SSC with a subsequent exclusion of doublets. The cell surface marker F4/80 was used to specifically select the MΦ which were further divided into CD11b$^+$ iMΦ and CD11b$^-$ aMΦ (Misharin et al., 2013) (Figure 3-13).

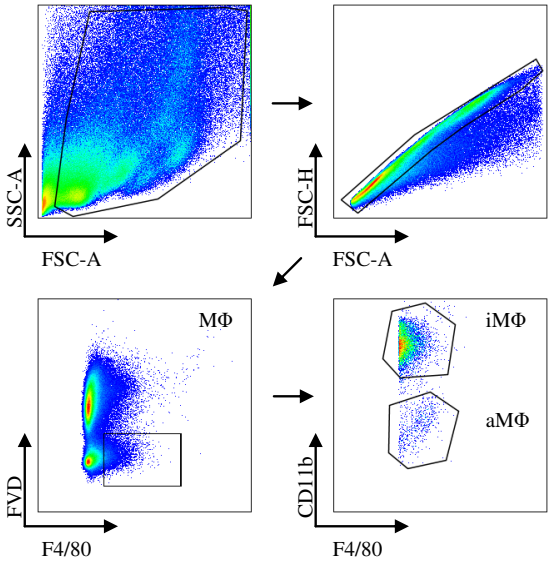

Figure 3-13: Gating strategy of pulmonary macrophage populations. Leukocytes were isolated from the lung of naïve and influenza virus-infected mice and stained with fluorochrome linked antibodies for flow cytometric analyses. Macrophages (MΦ) were identified via the forward scatter (FSC) as well as sideward scatter (SSC) and doublets were excluded based their height (FSC-H) and area (FSC-A) in the FSC. Moreover, the MΦ-specific marker F4/80 was utilized to select MΦ, which were further classified as CD11b$^-$ alveolar MΦ and CD11b$^+$ interstitial MΦ.

Upon IAV infection MΦ steadily accumulated in the lung with no differences between WT and KO mice (Figure 3-14 A). Regarding the two subpopulations, the percentage of aMΦ was reduced upon influenza virus infection due to the recruitment of iMΦ. Interestingly, the accumulation of iMΦ was less strong within CD47 deficient mice early during infection. Thus, CD47$^{-/-}$ mice displayed higher frequencies of aMΦ on day three after influenza virus infection compared to WT mice. However, the effect of CD47 on MΦ responses was only

transient as the frequencies of aMΦ and iMΦ were the same in WT and KO mice at the peak of infection (7 dpi) (Figure 3-14 B).

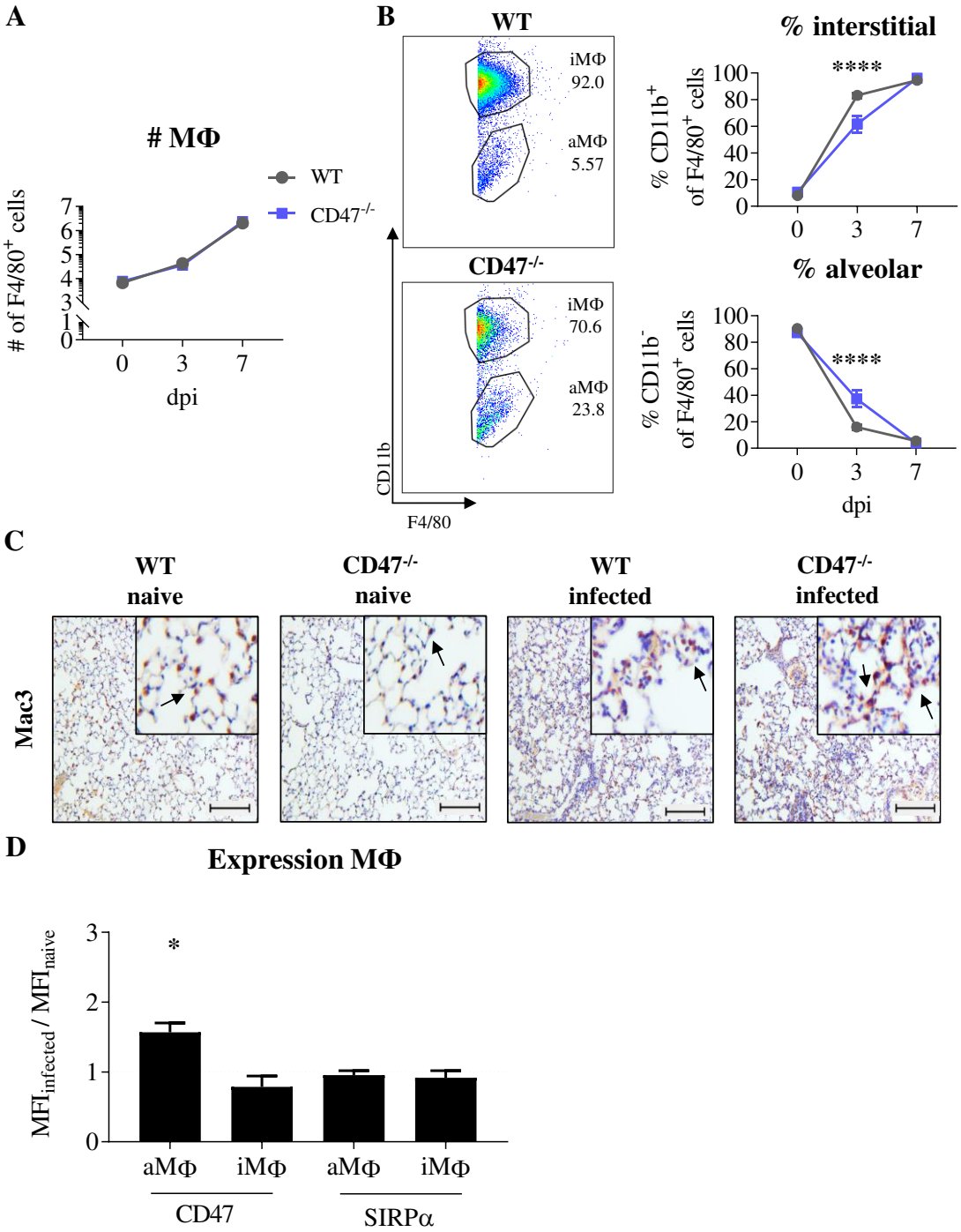

Figure 3-14: Augmented alveolar macrophage responses in CD47$^{-/-}$ mice during influenza virus infection compared to wildtype mice. WT and CD47 deficient mice were infected with influenza virus strain A/PR8/34. Three and seven days post infection (dpi) leukocytes were isolated from the lung and the number of macrophages (MΦ) (A) as well as the frequencies of the two subsets (alveolar = aMΦ, interstitial = iMΦ) (B) were examined by flow cytometry. Representative dotplots of the flow cytometric analyses of infected WT and CD47 deficient mice at day three post infection are depicted. (C) Moreover, immuno-histochemical analyses of the lung were performed to determine the MΦ response based on the MΦ-marker Mac3. Depicted are representative images of lungs-sections (brown = Mac3^{+} cells; blue = nuclei) of WT and KO mice from one experiment (scale bar = 100 µm). The arrows mark aMΦ in the lumen of the alveoli. (D) Finally, the expression of CD47 and its ligand signal-regulatory protein-α (SIRPα) on aMΦ and iMΦ was assessed via flow cytometry. Shown is the mean fluorescence intensity (MFI) of infected cells normalized to the naïve MFI. The graphs show the results of three (A-B) to seven (D) independent experiments (n = 9-27). For statistical analyses, a Two-way

ANOVA with Sidak's multiple comparisons test (A-B) as well as an unpaired t-test and Mann-Whitney U test (D) were performed (* = $p<0.05$, **** = $p<0.0001$).

To support these findings, the number of MΦ within the lung was assessed by immunohistochemical analyses based on the expression of the MΦ marker Mac3 3 dpi. Uninfected WT and CD47 deficient mice displayed similar amounts of MΦ in the lung which mainly resided within the alveolar lumen and were evenly distributed. Upon IAV infection, MΦ in the alveoli of WT mice remained the same in number but were found to group into clusters. In contrast to this, increased numbers of MΦ were observed in infected CD47$^{-/-}$ mice (Figure 3-14 C). The initial experiments demonstrated an upregulation of CD47 on MΦ in the lung of influenza virus-infected mice. In order to assess whether the altered aMΦ responses correlated with an enhanced expression of CD47 the level of the protein of interest was detected 3 dpi via flow cytometry. Moreover, the expression of its ligand SIRPα was examined since it has been described to be an important regulator of myeloid cells. CD47 expression was significantly increased on aMΦ but not on iMΦ upon IAV infection whereas SIRPα was not enhanced on any of the cells (Figure 3-14 D). Taken together, the obtained results depict an enhanced aMΦ response in absence of CD47, which might correlate with the improved clearance of IAV in CD47$^{-/-}$ mice.

3.4 CD47 impedes Antiviral aMΦ Responses during IAV Infection

3.4.1 Enhanced Clearance of IAV in CD47$^{-/-}$ Mice is mediated by aMΦ

The previous experiments demonstrated a negative impact of CD47 on the elimination of IAV, which was not due to a limitation of adaptive immune responses. Instead, an increased aMΦ response was observed in CD47$^{-/-}$ mice. To address the link between the clearance of IAV and the improved aMΦ responses, those cells were depleted in WT and KO mice prior to influenza virus infection. However, the augmented aMΦ frequencies might result from a reduced recruitment of iMΦ. Thus, the impact of iMΦ on the elimination of IAV from infected lungs was similarly defined by a depletion in the lungs prior to infection. Systemic application of clodronate containing liposomes efficiently depleted the invading iMΦ population from the lung (Figure 3-15 A). However, the depletion of iMΦ in WT mice did not enhance the viral clearance nor did iMΦ-depleted CD47 KO mice display reduced virus titers (Figure 3-15 C). On the other hand, intranasal application of liposomes specifically reduced aMΦ percentages by ~60 % (Figure 3-15 A). Importantly, concerning their role in viral clearance, the phenotype of CD47 deficient mice was reversed upon aMΦ depletion whereas no changes were detectable in aMΦ-depleted WT mice (Figure 3-15 B). Thus, aMΦ directly enhance the elimination of IAV in absence of CD47 independent of recruited iMΦ.

To investigate whether the CD47 deficiency in MΦ is important to induce virus clearance WT or CD47$^{-/-}$ aMΦ were isolated and adoptively transferred into WT recipient mice prior to influenza virus infection. Importantly, the transfer of CD47$^{-/-}$ aMΦ into WT mice that were depleted for aMΦ before reduced the viral load in the lung compared to the transfer of WT MΦ (Figure 3-16).

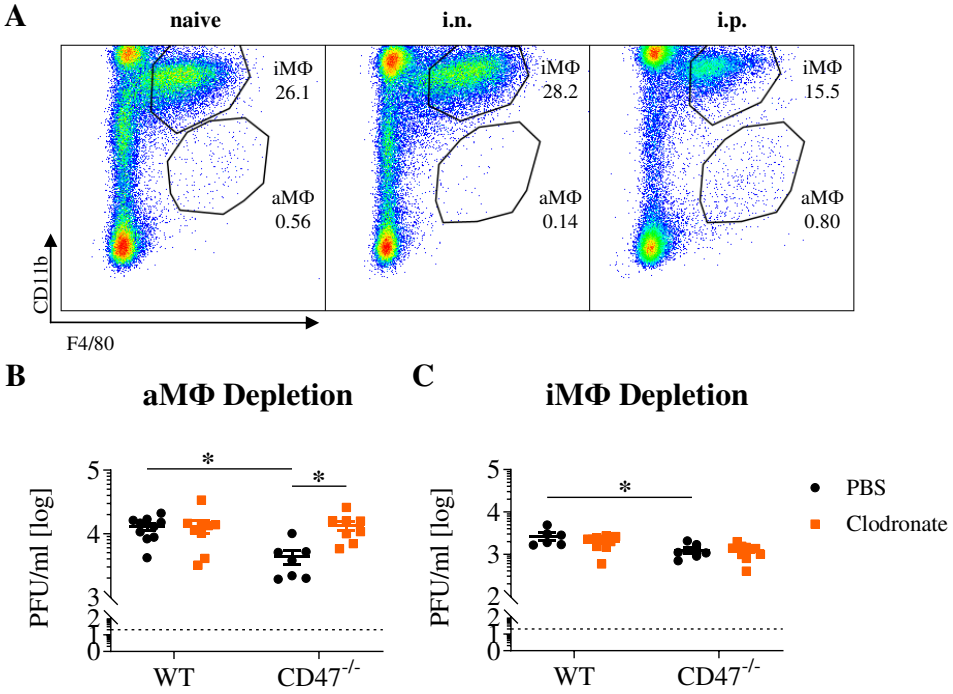

Figure 3-15: Alveolar macrophage depletion reversed the phenotype of CD47$^{-/-}$ mice. WT and CD47 deficient mice were treated with clodronate containing liposomes to deplete MΦ from the lung. aMΦ were depleted by a single intranasal (i.n.) installation of clodronate-liposomes three days prior to infection whereas iMΦ were eliminated by a repeated intraperitoneal (i.p.) application on days three and one prior to infection. (A) The efficiency and specificity of MΦ-depletion was determined by flow cytometry on day three post infection and the pulmonary MΦ subsets were distinguished based on the expression of F4/80 and CD11b. The impact of aMΦ (B) and iMΦ (C) depletion on the clearance of influenza virus infection was defined based on the viral load in infected tissues five days post infection by plaque assay. Depicted are the results of three independent experiments (n = 9-10). Statistical analyses were performed based on a Two-way ANOVA with post-hoc Sidak's test (* = p<0.05).

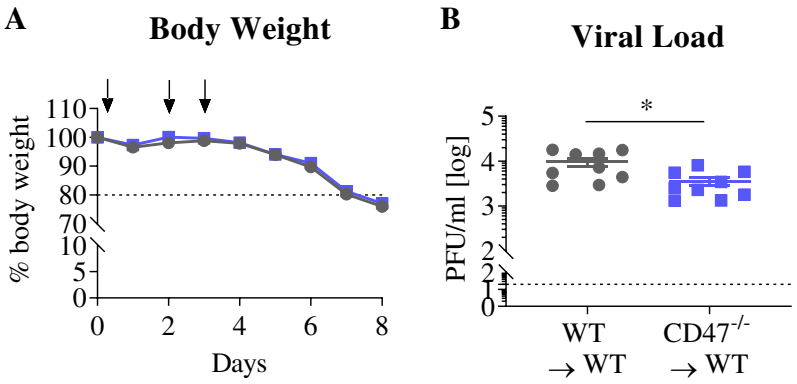

Figure 3-16: Enhanced viral clearance in CD47$^{-/-}$ mice is mediated by alveolar macrophages. Endogenous alveolar macrophages (aMΦ) of WT recipient mice were depleted by a single intranasal administration of clodronate containing liposomes three days prior to infection. After 48 h aMΦ of naïve WT and CD47$^{-/-}$ mice were isolated by fluorescence activated cell sorting and transferred into WT recipient mice. On the next day, recipient mice were infected with influenza virus strain A/PR8/34. (A) The course of disease was monitored by

daily weighing and (B) five days post infection (dpi) the viral load in the infected lungs was examined by plaque assay. Depicted are the results of three independent experiments (n = 9). For statistical analyses, an unpaired t-test was used (* = $p<0.05$)

3.4.2 The Phenotype of aMΦ is not altered in Absence of CD47

To gain a better insight into the mechanisms mediating the antiviral function of aMΦ in absence of CD47, the functionality of WT and $CD47^{-/-}$ aMΦ upon influenza virus infection was examined. Depending on the activating signal MΦ acquire different phenotypes with distinct functional properties. Classically activated, pro-inflammatory M1 MΦ drive the clearance of invading pathogens whereas alternatively activated, anti-inflammatory M2 MΦ are involved in tissue repair. In order to assess the impact of CD47 on the phenotype of pulmonary MΦ during influenza virus infection, the MΦ of WT and KO mice were analyzed via flow cytometry 3 dpi. M1 MΦ were identified by the expression of iNOS whereas M2 MΦ were selected based on the expression of arginase (Arg). In absence of CD47 the frequency of M1 and M2 aMΦ was not altered whereas both phenotypes were reduced within the iMΦ population indicating a higher proportion of inactivated MΦ (Figure 3-17 A). Besides the phenotype, secretion of pro- and anti-inflammatory cytokines such as IL-1β and IL-10 was assessed in the BALF of infected WT and KO mice. In line with the reduced activation of iMΦ, the level of the pro-inflammatory cytokines IL-1β and IFN-γ as well as anti-inflammatory IL-10 was lowered in the BALF of CD47 deficient compared to WT ones early during infection. Interestingly, the concentration of IFN-α, which is mainly associated with aMΦ, was also reduced 3 dpi despite an unaltered phenotype of these MΦ. Unexpectedly, the amount of IL-6 and TNF-α in the BALF of CD47 KO mice was strongly enhanced at later phases exceeding even the amount of cytokines in WT mice at day seven post infection (Figure 3-17 B).

Finally, the expression of different activation markers on pulmonary MΦ was examined via flow cytometric analyses. Upon activation MΦ induce the expression of different markers such as MHC class II as well as the co-stimulatory molecules CD80 and CD86. According to the previous results, the expression of MHC class II and CD86 were reduced in iMΦ of CD47 deficient mice compared to WT MΦ. Interestingly, $CD47^{-/-}$ aMΦ displayed a similar reduced expression of these activation markers (Figure 3-18). Taken together, $CD47^{-/-}$ aMΦ exhibit a reduced activation compared to WT MΦ. Thus, the enhanced clearance of IAV did not correlate with a generally strengthened aMΦ-activation.

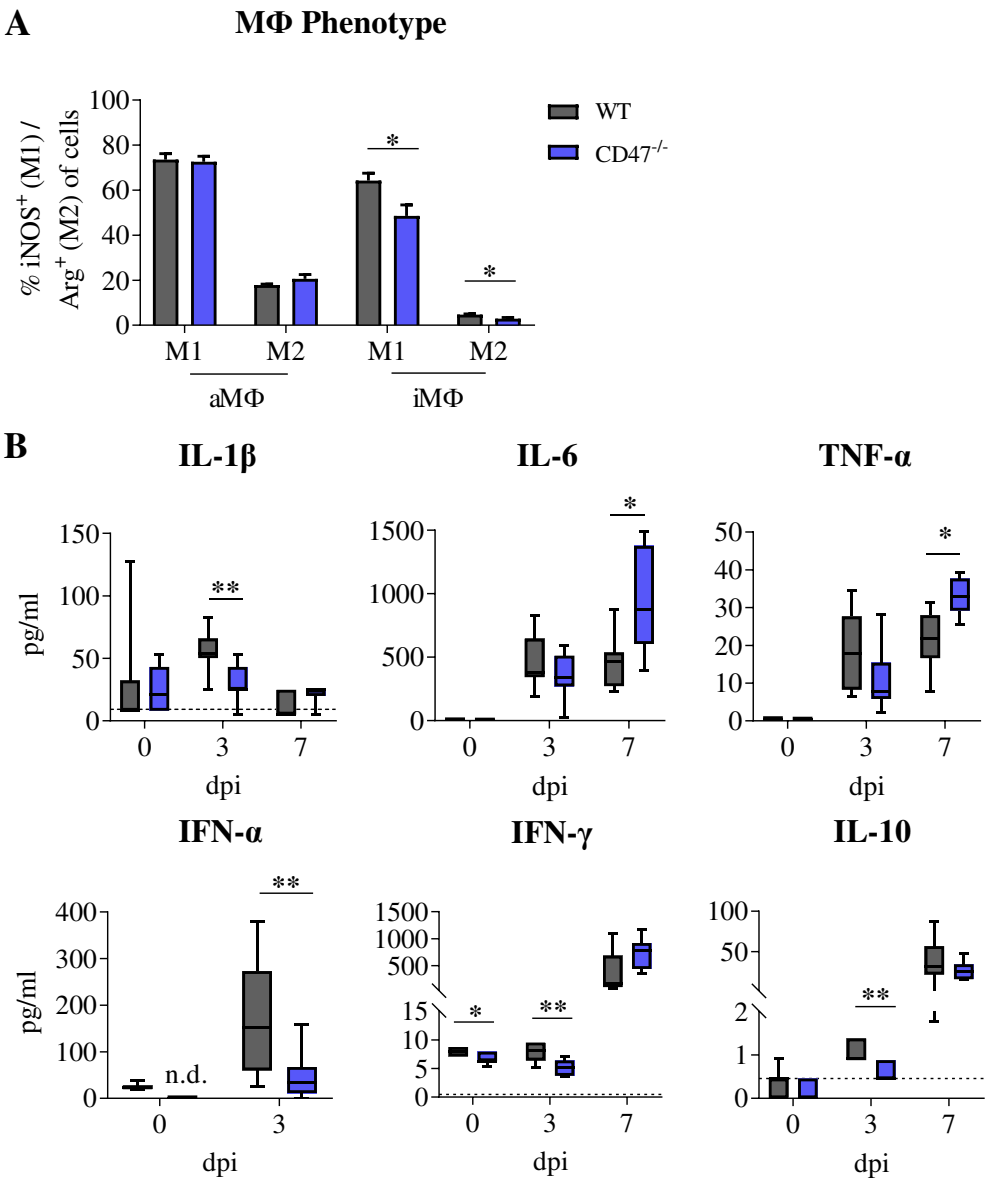

Figure 3-17: The phenotype of aMΦ is not altered in absence of CD47. (A) Leukocytes were isolated from the lung of influenza virus-infected mice on day three post infection (dpi) and the phenotype of alveolar (aMΦ) and interstitial macrophages (iMΦ) was defined by flow cytometry. Pro-inflammatory M1 MΦ were identified via the inducible nitric oxide synthase (iNOS) whereas anti-inflammatory M2 MΦ were classified based on arginase expression (Arg). (B) Moreover, cytokine responses related to aMΦ and iMΦ were analyzed in naïve and infected mice 3 and 7 dpi by broncho-alveolar lavage and Luminex Assay® of the resulting fluid. Depicted are the results of three independent experiments (n = 5-12). For statistical analyses, an unpaired t-test and Mann-Whitney U test were utilized (* = $p<0.05$, ** = $p<0.01$).

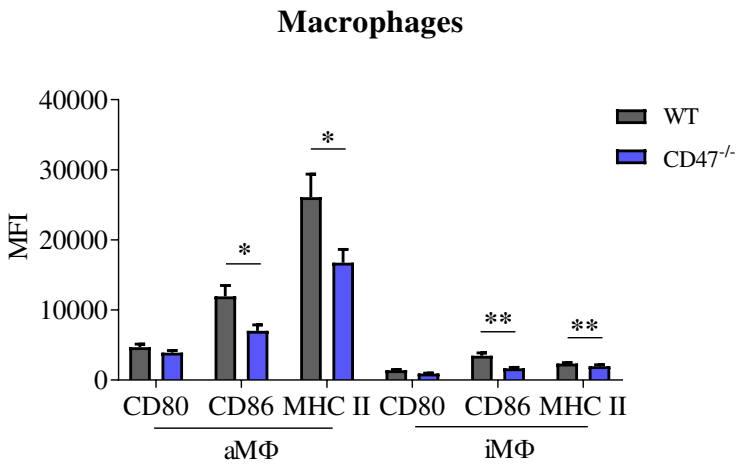

Figure 3-18: Reduced expression of co-stimulatory molecules on CD47$^{-/-}$ compared to wildtype macrophages. Leukocytes were isolated from the lung of influenza virus-infected mice on day three post infection (dpi) and the expression of different activation markers involved in antigen-presentation was assessed by flow cytometry. The graph shows the results of three independent experiments (n = 9) and statistical analyses were based on an unpaired t-test (* = $p<0.05$, ** = $p<0.01$).

3.4.3 CD47$^{-/-}$ aMΦ express High Amounts of Hemoglobin in Response to IAV Infection

During IAV infection aMΦ play an important role in the clearance of aggregated viral particles. Since CD47-SIRPα interaction is known to limit the phagocytic activity of MΦ, the ability of aMΦ to engulf foreign particles was examined. To this end, an *in vivo* phagocytosis assay was performed. Here, pHrodo™ Green *E. coli* BioParticles™ were intranasally applied to naïve or IAV-infected mice on day three post infection. The phagocytic activity of aMΦ or iMΦ was determined by flow cytometry based on the specific fluorescence of the pHrodo™ dye in the acidic environment of the lysosomes. In absence of CD47 aMΦ did not display an enhanced phagocytic activity towards the fluorescent particles neither in naïve nor in infected mice. However, in line with the literature the phagocytic uptake of foreign particles by aMΦ was significantly reduced upon influenza virus infection in WT as well as CD47$^{-/-}$ mice (Astry and Jakab, 1984). The same effect of IAV was observed in iMΦ. Interestingly, the phagocytic activity of naïve CD47$^{-/-}$ iMΦ was significantly reduced compared to naïve WT MΦ which was no longer the case during IAV infection (Figure 3-19).

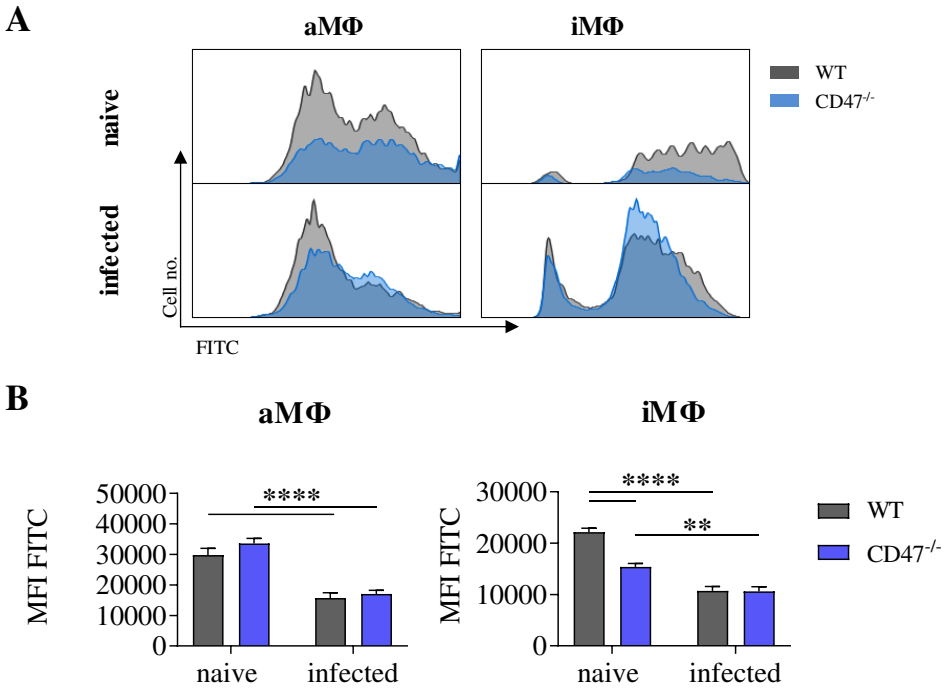

Figure 3-19: The phagocytic activity of alveolar macrophages was not augmented in CD47$^{-/-}$ mice. Naïve and influenza virus-infected WT and CD47$^{-/-}$ mice were intranasally treated with pHrodo^{TM} Green *E. coli* BioParticles^{TM} three days post infection (dpi). After 1 h the phagocytic uptake of fluorescent particles was determined by flow cytometry. (A) Representative histograms of the phagocytic activity are depicted and (B) the uptake of fluorescent particles was correlated to the mean fluorescence intensity (MFI). The graph shows the results of three independent experiments (n = 9-10). For statistical analyses, a Two-way ANOVA and post-hoc Sidak's test were performed (** = p<0.01, **** = p<0.0001)

Apart from the clearance of viral aggregates, aMΦ contribute to the clearance of IAV via the phagocytosis of dying or dead infected cells (Fujimoto et al., 2000). Since different receptors mediate the efferocytosis than the phagocytic uptake of foreign particles, an *in vivo* efferocytosis assay was performed to determine the ability of WT and CD47 deficient aMΦ to clear dead cells from the alveolar lumen. For this purpose, AEC II of naïve WT and CD47 KO mice were isolated, *ex vivo* infected with IAV and labeled with a fluorescent dye. After intranasal application of these cells into naïve as well as infected WT and KO mice the uptake of AEC II by aMΦ was determined by flow cytometry. In line with the uptake of foreign particles, the efferocytosis of dying or dead infected cells was not restrained by CD47. AEC II of WT and CD47$^{-/-}$ mice were equally phagocytosed in both mouse strains although clearance of CD47$^{-/-}$ AEC II from the alveolar lumen was in tendency more efficient. On the contrary, infection of recipient mice prior to the transfer of AEC II resulted in a significantly reduced uptake of AEC II lacking the expression of CD47. However, the phagocytosis of WT epithelial cells was not altered in IAV-infected mice. Thus, the efficiency of ACE II-efferocytosis was not determined by the expression of CD47 on aMΦ of recipient mice, but was dependent on the genotype of the transferred cells (Figure 3-20). Taken together, no enhanced phagocytic clearance of foreign particles or dying infected cells was

detected in mice deficient of CD47 compared to WT animals. Therefore, the reduced viral load of IAV-infected CD47$^{-/-}$ mice was not due to an enhanced phagocytic activity of aMΦ.

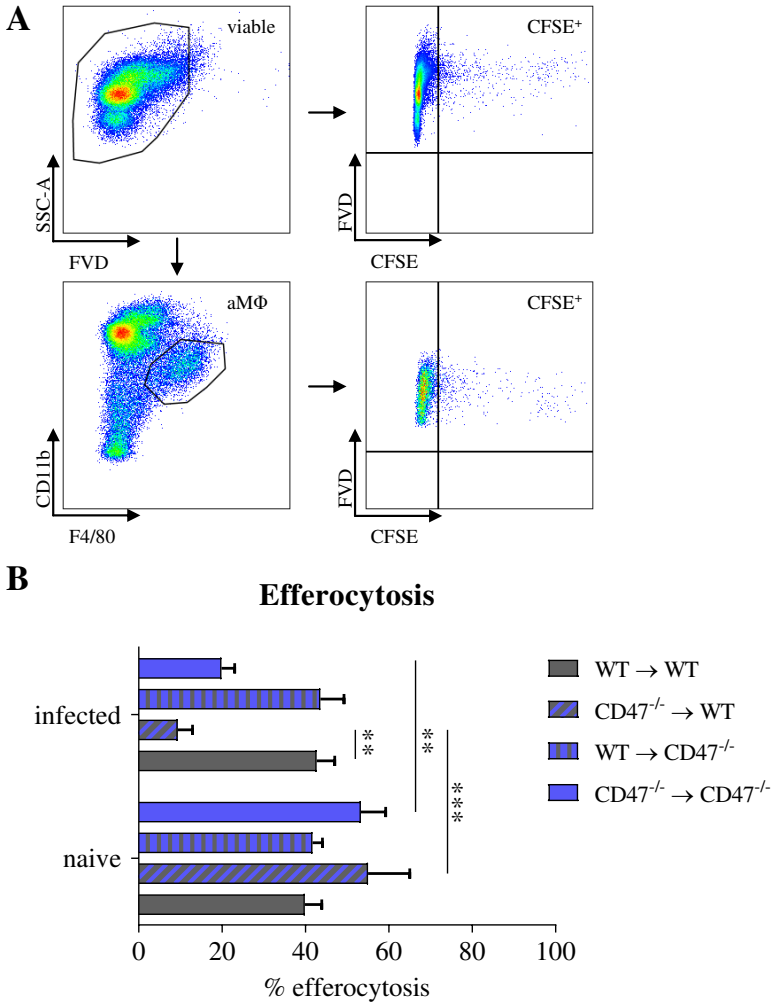

Figure 3-20: CD47$^{-/-}$ alveolar macrophages do not exhibit enhanced efferocytosis of infected epithelial cells. Alveolar type II epithelial cells (AEC II) were isolated from naïve WT and CD47$^{-/-}$ mice and stained with CFSE 48 h after *ex vivo* infection with 500 PFU A/PR8/34. Subsequently, the cells were transferred into naïve or influenza virus-infected WT and CD47$^{-/-}$ mice at day three post infection. After 1 h, the efferocytosis of infected AEC II was examined by flow cytometry. The efficiency of efferocytosis (% Efferocytosis) was calculated as follows: % CFSE^{+} of viable cells / % CFSE^{+} alveolar macrophages (aMΦ) of viable cells. Depicted are the results of one experiment (n = 4). For statistical analyses, a Two-way ANOVA and post-hoc Sidak's test were performed (** = p<0.01, *** = p<0.001).

To get further insight into the functional differences of WT and KO aMΦ, transcriptome analyses of naïve and infected aMΦ were performed via an Affymetrix MircoArray. Already at steady state, the expression of different genes was up- or downregulated in aMΦ deficient of CD47. Upregulated genes were mainly involved in cell adhesion (e.g. SELP = selectin platelet), chemotaxis (e.g. EDNRB = endothelin receptor type B), and inflammation (e.g. C4a = complement component 4a) whereas downregulated genes trigger adaptive immune responses (e.g. H2-Ab1 = histocompatibility 2, class II antigen A, beta 1) as well as apoptosis (e.g. ACVR1C = activin A receptor, type IC). Interestingly, an increased expression of hemoglobin-β (HBB) was found in naïve CD47 deficient aMΦ compared to WT MΦ. Upon

influenza virus infection the augmented expression of hemoglobin was even more prominent as four out of the eight upregulated genes encode for hemoglobin (HBA = hemoglobin-α). Moreover, CD47 KO aMΦ exhibit a reduced expression of krüppel-like factor 3 (KLF3), which is a negative regulator of hemoglobin expression in erythrocytes (Funnell et al., 2012, 2013) (Figure 3-21).

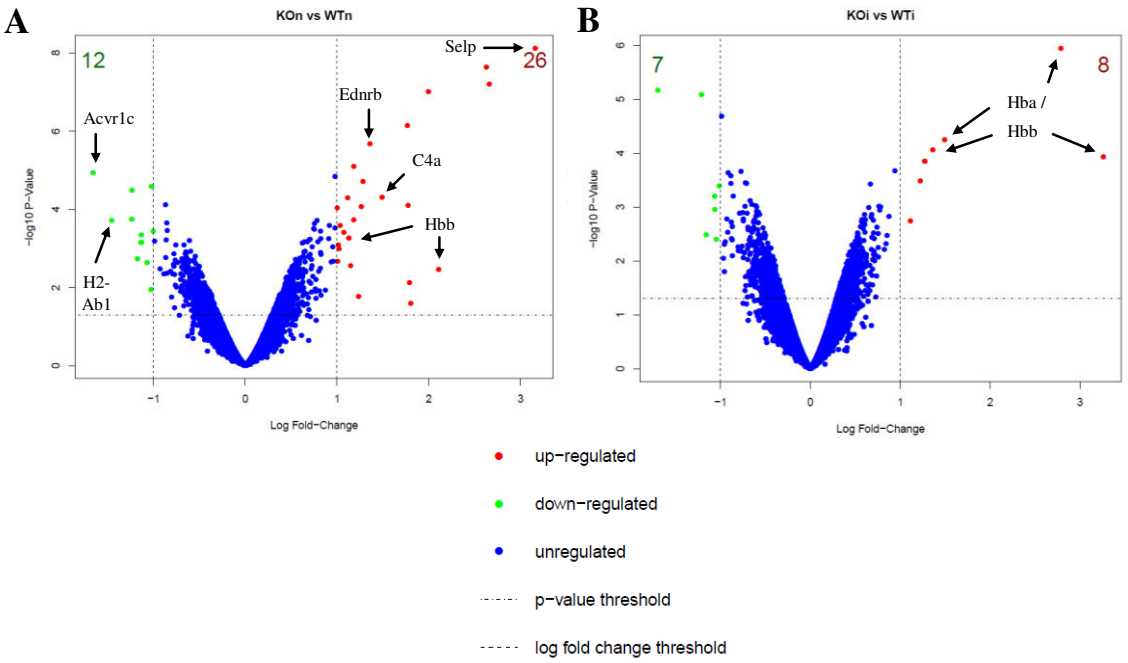

Figure 3-21: CD47$^{-/-}$ alveolar macrophages upregulate the expression of hemoglobin. Alveolar Macrophages (aMΦ) of naïve as well as infected WT and CD47 deficient mice were isolated via fluorescence-activated cell sorting (FACS) at day three post infection. Total RNA was isolated from the sorted cells and processed for Affymetrix MicroArray analyses of the transcriptome. Global gene expression of WT and KO aMΦ was compared and the differences in the transcriptome were illustrated by volcano plots. The threshold to define significantly up- or downregulated gene was set as follows: $\log_2$(fold-change) > ± 1, p-value < 0.05. Depicted are the results of one experiment (n = 2).

The expression of non-erythroid hemoglobin by MΦ has been first described by Liu, Zeng, and Stamler in 1999. Although hemoglobin is mainly known for its role in oxygen transport, additional functions of hemoglobin have been described. For example, C-terminal fragments of hemoglobin-β limit the growth of different bacteria including *E. coli* and *S. aureus* (A. Parish et al., 2001; Hobson and Hirsch, 1958; Liepke et al., 2003; Mak et al., 2000) as well as the infectivity of Herpes-Simplex-Virus 2 (HSV-2) (Groß et al., 2020). In order to define the impact of hemoglobin on influenza virus infection, the BALF of WT and CD47 deficient mice were analyzed 3 and 7 dpi in regard to their antiviral activity *in vitro*. Interestingly, treatment of *MDCK* cells with the BALF of infected CD47 KO mice prior to influenza virus infection restrained the viral replication contrary to WT BALF indicated by a decreased suppressive activity (Figure 3-22). Thus, the reduced viral load of CD47$^{-/-}$ mice seems to rely in part on soluble mediators which might also include hemoglobin fragments. Nevertheless,

further studies are necessary, to define the role of hemoglobin during IAV infection in more detail.

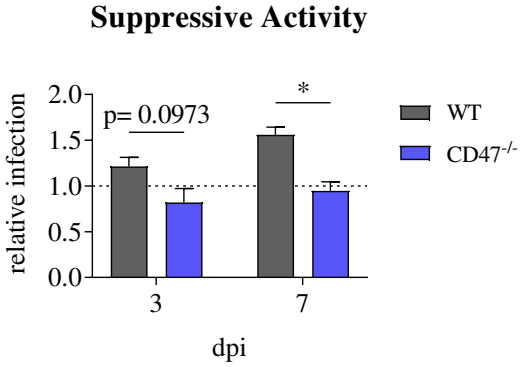

Figure 3-22: Pulmonary fluid of CD47$^{-/-}$ mice suppresses the replication of IAV *in vitro*. Wildtype (WT) and CD47$^{-/-}$ mice were infected with influenza virus strain A/PR8/34 via intranasal instillation. On days three and seven post infection the broncho-alveolar lavage fluid (BALF) of infected mice was collected and applied to MDCK cells prior to IAV infection. Three days post infection (dpi) viral plaques within the cell layer were determined and normalized to a control solely infected with IAV to assess the suppressive activity of the BALF samples. Depicted are the results of a single experiments (n = 2-3). Statistical analyses were based on a Mann-Whitney U test (* = $p<0.05$).

3.5 Enhanced MΦ Responses are Independent of CD47-SIRPα Signaling

In the first part of this study, the impact of CD47 on immune responses against influenza virus infection was defined. However, the immuno-regulatory function of CD47 is mainly mediated by the interaction with its ligands SIRPα and TSP-1. Thus, in the next part of the study the signaling mechanisms underlying the phenotype of CD47 deficient mice were addressed in more detail. While TSP-1 has mainly been described to control adaptive immune responses, SIRPα has been found to regulate myeloid cells. Since the improved viral clearance in mice deficient of CD47 was associated with aMΦ responses, the role of CD47-SIRPα signaling was examined. At first, the expression of SIRPα on naïve pulmonary MΦ and splenic MΦ was assessed by flow cytometry. Similar to CD47, SIRPα showed the highest expression on aMΦ compared to the other MΦ subsets. However, CD47 deficient mice displayed significantly reduced levels of SIRPα on aMΦ compared to WT mice. In contrast to this the expression of SIRPα on splenic MΦ was significantly augmented. Nevertheless, SIRPα was most abundantly expressed on aMΦ in mice lacking CD47 (Figure 3-23 A). Next, the impact of the alveolar environment on the expression of SIRPα was assessed. To this end, splenic MΦ were isolated and incubated with TGF-β or IL-10. Again, TGF-β exhibited a minor potential to induce the protein of interest whereas IL-10 significantly augmented the expression of SIRPα on WT as well as KO MΦ compared to the untreated controls (Figure 3-23 B).

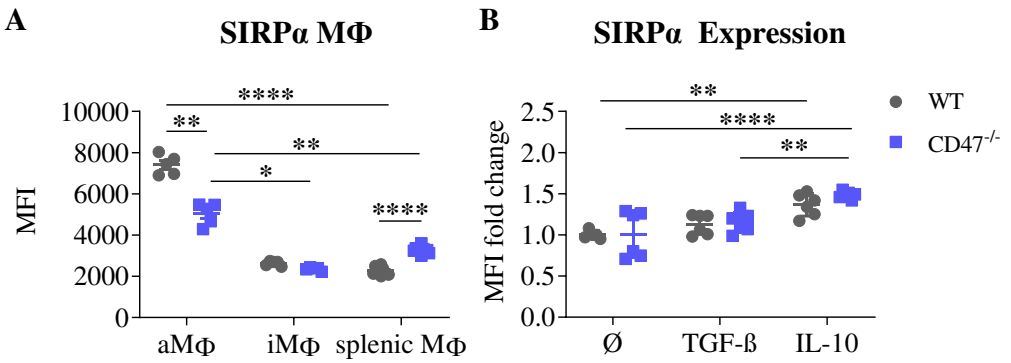

Figure 3-23: Alveolar macrophages exhibit a specifically high expression of SIRPα. (A) Leukocytes were isolated from the lung and the spleen of naïve WT and CD47$^{-/-}$mice. Subsequently, pulmonary alveolar (aMΦ) and interstitial macrophages (iMΦ) as well as on splenic MΦ were analyzed by flow cytometry regarding the expression of SIRPα on the surface based on the mean fluorescence intensity (MFI). (B) Splenic MΦ were isolated from naïve WT and KO mice via magnetic-activated cell sorting based on the surface marker F4/80. Subsequently, isolated macrophages were incubated at 37 °C with either transforming growth factor-β (TGF-β) or interleukin-10 (IL-10). After 4 h the expression of SIRPα on the cell surface was determined by flow cytometry as the relative MFI normalized to the untreated WT control. Depicted are the results of two independent experiments (n = 5-6). Statistical analyses were performed based on a Kruskal-Wallis test and a post-hoc Dunn's test (* = p<0.05, ** = p<0.01, *** = p<0.001, **** = p<0.0001).

To further assess the regulatory effect of SIRPα during influenza virus infection, SIRPα$^{-/-}$ mice were infected with influenza virus strain A/PR8/34. The course of infection was monitored by daily weighing and at the peak of infection (7 dpi) the viral load in infected lungs was determined. During influenza virus infection the body weight loss of WT and SIRPα deficient mice did not differ. In line with this, the number of infectious particles was similar in both mouse strains (Figure 3-24). In contrast to CD47$^{-/-}$ mice, which have been described to have no phenotypic alternations under homeostasis, SIRPα$^{-/-}$ mice exhibit mild thrombocytopenia as well as reduced CD4^{+} and CD8^{+} T cell numbers in the spleen of naïve mice (Yamao et al., 2002). To exclude an influence of these phenotypic changes on the outcome of influenza virus infection, the experiments were repeated in WT mice treated with a monoclonal SIRPα-blocking antibody.

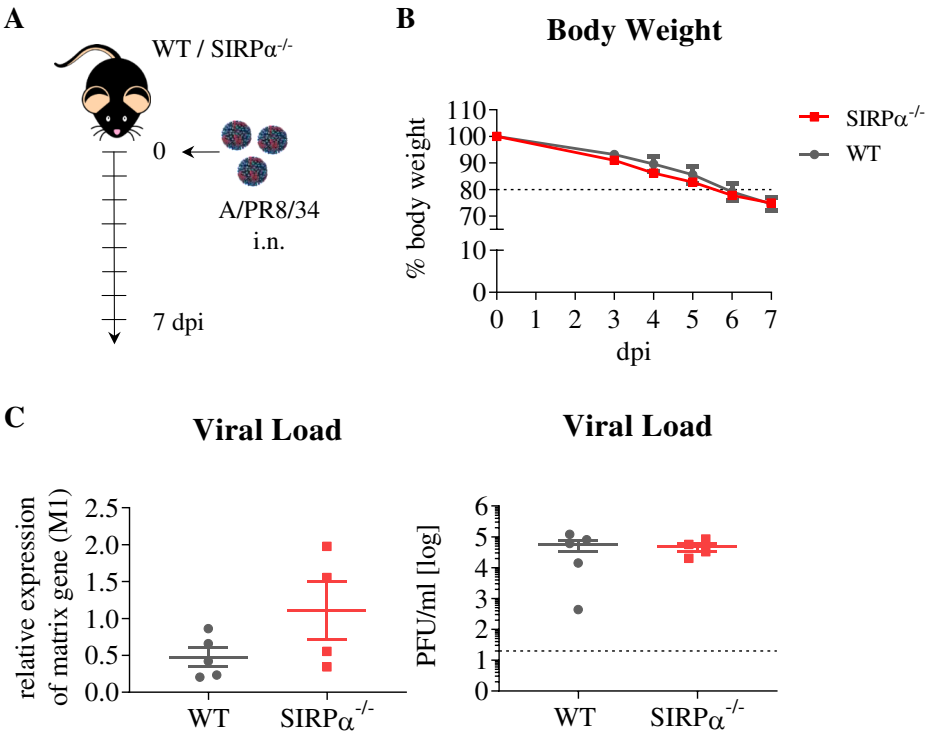

Figure 3-24: Clearance of IAV is not boosted in SIRPα$^{-/-}$ mice compared to wildtype mice. (A) C57BL/6 (WT) and SIRPα$^{-/-}$ mice were infected with influenza strain A/PR8/34 by intranasal (i.n.) instillation and the course of disease was monitored till day seven post infection. (B) The disease severity was assessed via the daily loss of body weight as well as (C) the viral load in the lungs at the peak of disease 7 days post infection (dpi). qRT-PCR as well as plaque assays were performed to determine the viral titer. The shown data was obtained in a single experiment (n = 4-5). For statistical analyses, an unpaired Mann-Whitney U test was performed.

The blockade of SIRPα in IAV-infected WT mice was achieved by a single intravenous application of a monoclonal SIRPα-blocking antibody (mAbSIRPα) or an isotype control (mAbIso) (Figure 3-25 A). After influenza virus infection the course of disease was monitored by the loss of body weight. In addition, the pathology in infected tissues was assessed by histological analyses at the peak of infection. Similar to SIRPα mutant mice, no changes in the body weight loss was observed upon SIRPα-blockade (Figure 3-25 B). Moreover, disruption of CD47-SIRPα signaling did not improve the viral clearance of IAV. On the contrary, the pathological lesions upon IAV infection were even enhanced in tendency in mice treated with a SIRPα-blocking antibody compared to isotype control treated mice (Figure 3-25 C-D).

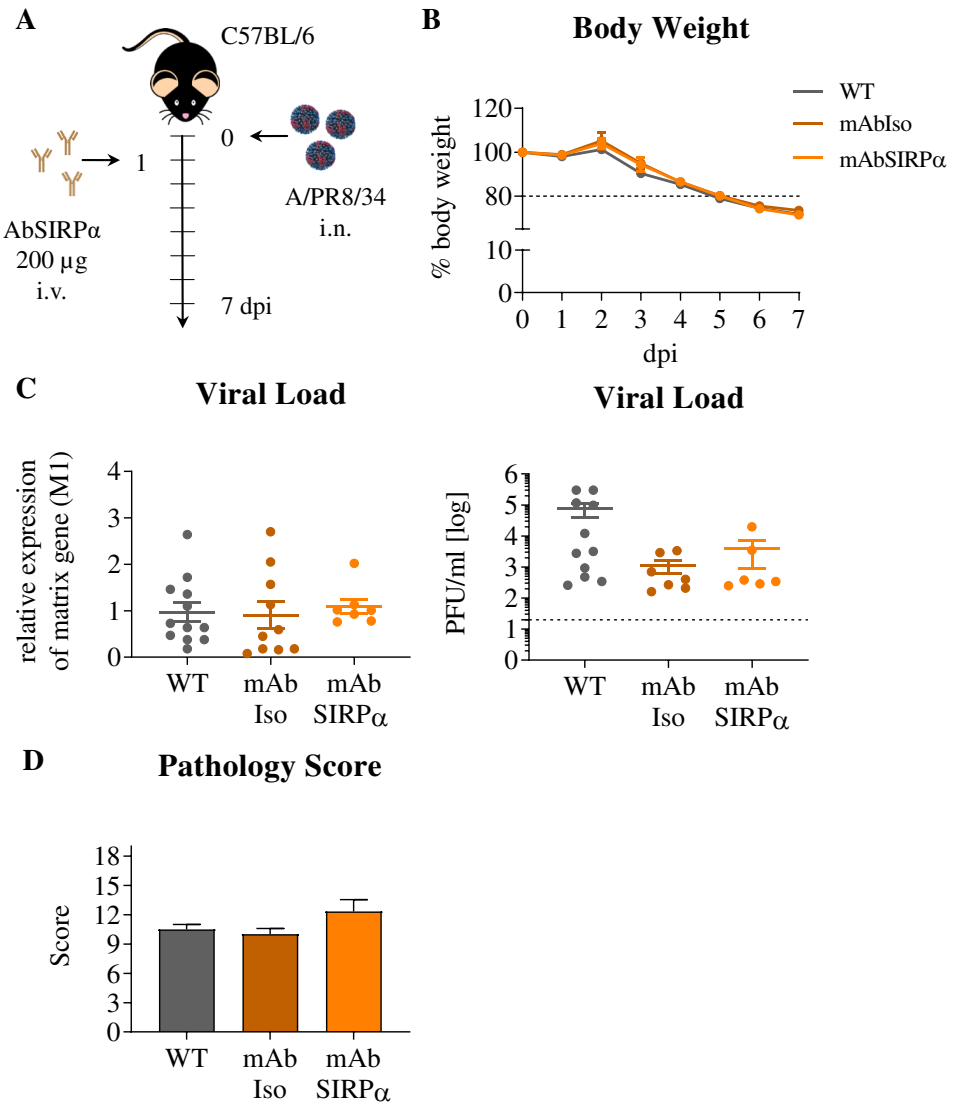

Figure 3-25: Blockade of SIRPα does not improve the clearance of influenza A virus infection. (A) C57BL/6 (WT) mice were intranasally (i.n.) infected with the influenza virus strain A/PR8/34. One day post infection (dpi) mice were treated with 200µg of a SIRPα-blocking monoclonal antibody (mAbSIRPα) or an isotype control (mAbIso) by intravenous (i.v.) injection. The disease severity was defined based on the daily body weight loss (B), the viral load at the peak of infection (C) as well as the pathological lesions within the infected lungs (D). The viral load was determined by qRT-PCR and plaque assays whereas the pathology was examined by histological analyses. The pathology score is composed of single evaluations of the lungs regarding the inflammation, hyperplasia, histiocytosis, neutrophils and necrosis with a maximum total score of 19. Depicted are the results of one (D) to three (B-C) independent experiments (n = 4-12). Statistical analyses were based on a Kruskal-Wallis test and a post-hoc Dunn's test for multiple comparison.

Although blockade of SIRPα had no effect on the disease severity during influenza virus infection, the MΦ responses in treated WT mice were analyzed. The mice were treated as described before and the number of MΦ was examined via flow cytometry early during infection. During flow cytometric analyses MΦ were identified as depicted previously (Figure 3-13). Mice treated with a SIRPα-blocking antibody displayed a significantly reduced number of MΦ when compared to untreated mice. Within the MΦ compartment the frequency of aMΦ was increased in tendency upon SIRPα blockade compared to untreated mice whereas the proportion of iMΦ was significantly decreased. However, the effects in

mAbSIRPα-treated mice were not specific to SIRPα as mice treated with an isotype control had in tendency the same phenotype (Figure 3-26). Thus, the restriction of aMΦ responses during IAV infection by CD47 is not mediated through the interaction with MΦ-expressed SIRPα.

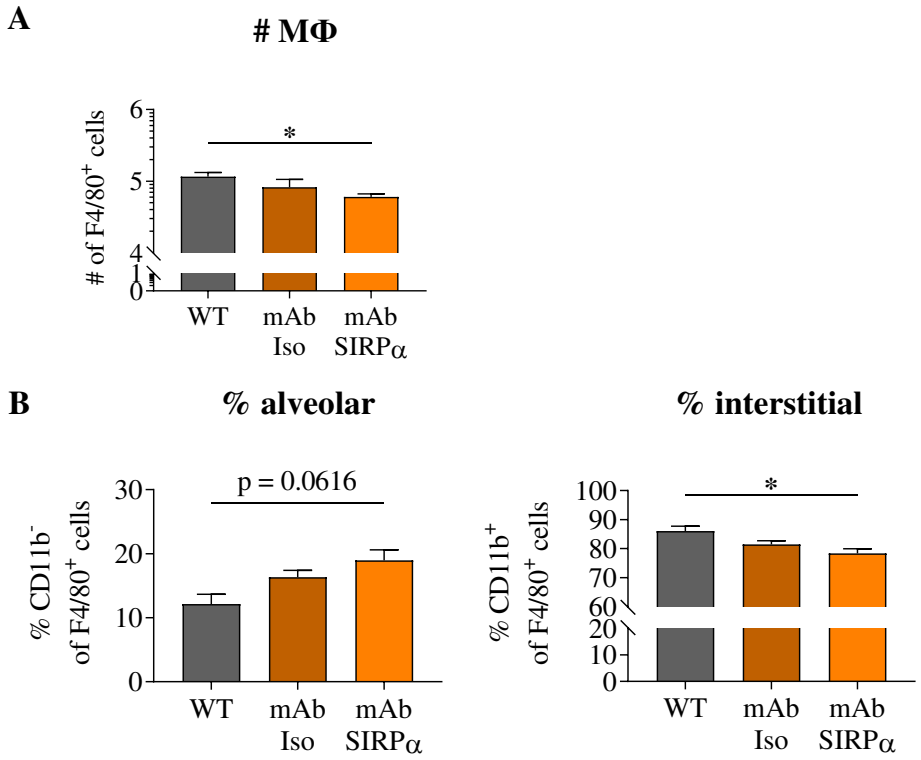

Figure 3-26: Blockade of SIRPα does not augment alveolar macrophage responses during influenza A virus infection. WT mice were infected with influenza strain A/PR8/34 and treated with 200 µg of a SIRPα-blocking antibody (mAbSIRPα) or an isotype control (mAbIso) one day post infection. At day three post infection leukocytes were isolated from the lung of infected mice and stained for flow cytometric analyses. The number of macrophages (MΦ) as well as the frequencies of the two pulmonary subsets (alveolar = aMΦ, interstitial = iMΦ) were determined. Depicted are the results of two independent experiments (n = 6). For statistical analyses, a Kruskal-Wallis test and a post-hoc Dunn's test for multiple comparison were performed (* = $p<0.05$).

3.6 Therapeutic Application of CD47

In the final part of this project, the therapeutic potential of CD47 was specified more closely. To this end, WT mice were infected as described previously with IAV and treated at daily intervals with a CD47-blocking antibody (mAbCD47) by intraperitoneal application. The experimental setup was adapted to a previous study of Cham et al. in 2020, who addressed the role of CD47 during systemic LCMV infection (Figure 3-27 A). On day seven post infection, the virus titer in the infected lungs was determined by qRT-PCR as well as plaque assay. No differences between the mAbCD47 or isotype control treated mice were observed (Figure 3-27 B). Thus, further studies are needed to define the potential of CD47 blockade as a treatment option during influenza virus infection.

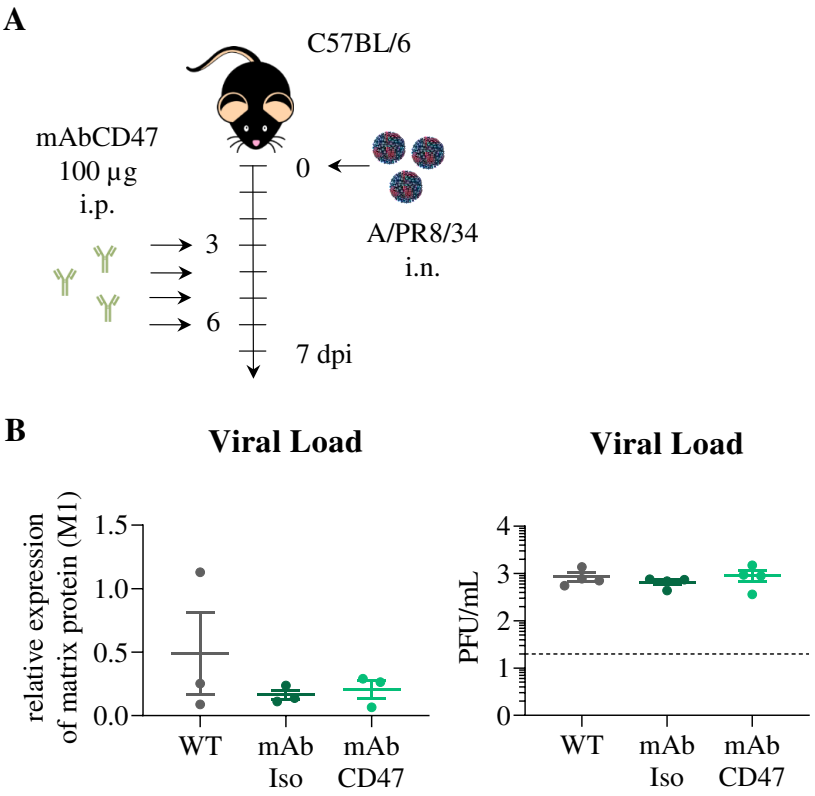

Figure 3-27: Therapeutic blockade of CD47 during severe influenza A virus infection. (A) C57BL/6 (WT) mice were infected with influenza virus strain A/PR8/34 by intranasal (i.n.) instillation. From day three till day six post infection mice were treated daily with a monoclonal CD47-blocking antibody (mAbCD47) or an isotype control (mAbIso). At the peak of infection, the lungs were collected and the virus titer was assessed by qRT-PCR and plaque assay. The depicted results were obtained in a single experiment (n = 4) and statistical analyses were based on a Kruskal-Wallis test and a post-hoc Dunn's test.

4 Discussion

Despite our increasing knowledge of many pathogens and their related immune responses, infectious diseases are still a severe threat to human health. Especially lower respiratory infections, which are commonly associated with influenza viruses, account for many deaths worldwide each year. Although, vaccines and antivirals against influenza virus infections are available, therapeutic as well as prophylactic treatment is still limited due to the high mutation rate of the virus. Thus, novel treatment strategies do not only focus on the virus itself but also on related immune responses, which have been shown to contribute to disease severity. One currently well-known protein with immuno-regulatory function is CD47. CD47 is mainly noted for its function as a "don't eat me signal" regulating the phagocytosis of CD47 expressing cells. In this regard, it is at the moment an interesting target for cancer therapy (Veillette and Chen, 2018; Willingham et al., 2012). However, it has also been shown to regulate different aspects of innate and adaptive immune responses, such as the migration and activation of immune cells, and thereby contributes to the clearance of different pathogens. Interestingly, the impact of CD47 on protective immune responses during bacterial or fungal infection is controversial depending on the pathogen and the site of infection (Banerjee et al., 2015; Gresham et al., 2000; Lindberg et al., 1996; Su et al., 2008). Recent studies also linked CD47 to influenza vaccination related immunity (Lee et al., 2016), but its role during acute influenza virus infection is still poorly understood.

Hence, this study dissects the impact of CD47 on innate and adaptive immune responses during IAV infection and the resulting consequences for viral clearance. To this end, mice lacking the expression of CD47 were infected with influenza virus (strain A/PR8/34). The severity of disease as well as the antiviral immune responses were examined and compared to infected WT mice. For the first time, this study identified CD47 as a negative regulator of antiviral immunity during primary influenza virus infection impeding antiviral aMΦ responses. Interestingly, this mechanism did not rely on the interaction with the myeloid inhibitory receptor SIRPα but was directly based on CD47 on aMΦ. Hence, these results contribute to a better understanding of the immuno-regulatory function of CD47 during severe influenza virus infection and thereby might open new treatment strategies.

Interestingly, the non-specific nature of CD47 targeting therapies, might even enable the treatment of a wide range of other respiratory infections. Besides influenza viruses the emerging severe acute respiratory syndrome coronavirus type 2 (SARS-CoV-2) is currently a serious challenge for the human health. Since SARS-CoV-2 also infects epithelial cells of the respiratory system, infection of the lower airways can culminate in a severe ARDS similar to IAV infection (Howley and Knipe, 2020). The newly uncovered CD47-mediated limitation of

aMΦ response against IAV infection might therefore also apply for the immune response during the SARS-CoV-2 induced COVID-19. Interestingly, recent studies by Tal *et al.* depicted an upregulation of CD47 on human pulmonary tumor cell line A549 upon *in vitro* SARS-CoV-2 infection. Thus, targeting the CD47 pathway might also have implications for other viral respiratory infections besides IAV.

4.1 CD47 and its Impact on Antiviral Immune Responses

Recent attempts to study the influence of CD47 on immune responses have mainly relied on tumor models and thus focused on its anti-phagocytic function. Only few studies have addressed the role of CD47 during infectious diseases and the results obtained have been controversial. Several infections have been shown to upregulate the expression of CD47 on infected as well as immune cells mediated by pro-inflammatory stimuli such as PRR- or cytokine-signaling (Betancur et al., 2017; Kojima et al., 2016; Tal et al., 2020). Likewise, the present study showed an upregulation of CD47 on different immune cells upon IAV infection *in vivo* including MΦ, neutrophils and $CD8^+$ T cells. In line with tumor cells, which exploit the immuno-suppressive function of CD47 to evade anti-tumor immune responses, pathogens are supposed to trigger CD47 expression on infected as well as immune cells to limit their clearance from the host (Majeti et al., 2009; Tal et al., 2020; Willingham et al., 2012). In this context, poxviruses have been shown to encode a CD47 mimic limiting antiviral immune response by the interaction with SIRPα (Cameron et al., 2005; Parkinson et al., 1995). Similarly, within this study a reduced viral load of IAV was found in the lung of $CD47^{-/-}$ mice during acute infection compared to WT mice. An *ex vivo* infection of CD47 KO and WT AEC II revealed that the decrease in viral loads was not affiliated to an impeded viral replication cycle as a similar accumulation of viral RNA was observed in both types of AEC II. Likewise, the blockade of CD47 on *MDCK* cells prior to infection did not change the subsequent replication of IAV. In this regard, bone marrow chimeric mice would be a common solution to further analyze whether the expression of CD47 by tissue cells has an impact on the viral life cycle of IAV. However, since CD47 is also regulating the phagocytosis of cells this approach is difficult to implement since a stable transfer of CD47 deficient cells into WT mice has not been achieved so far (Wang et al., 2007). Yet, the obtained results depicted, that the reduced viral titers were not based on a lessened susceptibility of CD47 deficient pulmonary epithelial cells but rather dependent on viral clearance of IAV.

The clearance of IAV is a multifactorial process dependent on various immune cells. Typically, the elimination of IAV is attributed to adaptive immune responses mediated by

B cells and $CD8^+$ T cells. Here, neutralizing antibodies secreted by B cells mediate the protection against viral particles whereas $CD8^+$ T cells are responsible for the clearance of virus-producing cells. Although CD47 has been described to limit the humoral immune response during influenza vaccination, the secretion of antibodies in the BALF of unvaccinated CD47 KO mice has not been affected upon acute influenza virus infection (Lee et al., 2016). Likewise, the amount of IgA, IgM and IgG antibodies was not enhanced in $CD47^{-/-}$ mice 7 dpi within the present study. Interestingly, $CD8^+$ T cell responses seemed also to be not influenced by CD47 during IAV infection, since the frequencies in the lung were similar compared to infected WT mice. Moreover, the activation of $CD8^+$ T cells was even decreased due to CD47 deficiency as indicated by the reduced expression of cytokines and cytotoxic effector molecules such as IFN-γ and GzmB. However, previous studies by Cham *et al.* claimed a restrictive role of CD47 for $CD8^+$ T cell responses during LCMV infection. In more detail, antibody-mediated blockade of CD47 has been shown to increase the CTL-mediated clearance of the virus. The differences between both studies might arise from the disturbed $CD4^+$ T helper cell response which was observed in CD47 KO mice during IAV infection in the present study and has also been described before (Lee et al., 2016; Lindberg et al., 1996). Moreover, CD47 is not solely immuno-suppressive but has been shown to contribute to T cell activation (Reinhold et al., 1997; Ticchioni et al., 1997). Additionally, Cham *et al.* have identified APCs such as DCs to be the base of beneficial effects of CD47 blockade on $CD8^+$ T cell responses. However, an enhanced DC response was not observed during IAV infection of $CD47^{-/-}$ mice in the current study. Thus, the differences between both studies might also rely on the timing of CD47 blockade as the receptor has not only been shown to limit the activation of DCs but also facilitates their migration to the draining LN (Van et al., 2006). Hence, blockade of CD47 signaling early during infection might support the APC function of DCs in the LN whereas immediate inhibition due to genetic ablation might impede the initial recruitment of DCs limiting their function.

Besides DC responses, neutrophils and monocytes have been shown to contribute to influenza virus clearance. However, these pro-inflammatory immune responses always come at the risk of immune-induced pathology. CD47 has been shown to contribute to the recruitment of neutrophils and monocytes supporting the clearance of systemic bacterial or fungal infection (Lindberg et al., 1996; Navarathna et al., 2015). On the contrary, CD47-mediated recruitment of neutrophils aggravates bacterial infection of the respiratory system (Su et al., 2008). Thus, limiting the recruitment of neutrophils or monocytes during influenza virus infection might be beneficial due to a reduced immunopathology (Coates et al., 2018; Lin et al., 2008; Tate et al., 2009). However, in the present study the responses of neutrophils as well as monocytes were

not impeded three or seven days after IAV infection in mice lacking the expression of CD47. Importantly, the absence of CD47 has been shown to induce a delayed migration of these innate immune cells to the site of infection but does not abolish the neutrophil and monocyte responses completely (Liu et al., 2001; Rosseau et al., 2000). As these innate immune cells are recruited to the site of infection within the first days, a delayed recruitment might not be visible anymore at day three post infection. However, in line with the observed neutrophil and monocyte immunity, the pathology of CD47 deficient mice was not altered during infection. Interestingly, besides its immuno-suppressive function different studies have shown, that CD47 regulates the contraction of T cell responses through the induction of apoptosis (Lamy et al., 2007; Van et al., 2012). In line with this, the present study revealed the increase of pro-inflammatory cytokines such as IL-6 and TNF-α in CD47 KO compared to WT mice at day seven post infection supporting an additional role of CD47 in terminating the immune responses at the close of infection (Belisle et al., 2010; DeBerge et al., 2014; Paquette et al., 2012; Tisoncik et al., 2012).

Another cell type known to be involved in influenza virus clearance and to be regulated by CD47 are MΦ. Interaction of CD47 and MΦ-expressed SIRPα inhibits the phagocytic activity of myeloid cells and limits their function (Oldenborg et al., 2000; Zhang et al., 2016). Yet, the number of total MΦ was not altered in influenza virus-infected $CD47^{-/-}$ mice compared to WT animals in this study. However, within the lung two distinct subsets of MΦ have been described, which carry out specific features upon influenza virus infection. The impact of CD47 on the different MΦ subpopulations have not been addressed so far.

4.2 Enhanced Viral Clearance in $CD47^{-/-}$ Mice is mediated by aMΦ

The current study demonstrated for the first time, that CD47 limits aMΦ responses in the lung during IAV infection since $CD47^{-/-}$ mice display higher frequencies of aMΦ early during infection whereas the iMΦ response was reduced compared to WT mice 3 dpi. Upon influenza virus infection, iMΦ actually derive from inflammatory monocytes, which are recruited to the site of infection, and thus aggravate the severity of disease (Lin et al., 2008). However, depletion of iMΦ did neither affect the viral clearance in WT nor in CD47 KO mice in the present work. Thus, the reduced response of iMΦ in absence of CD47 does not improve the clearance of IAV. In contrast to this, the depletion of aMΦ with the lung reversed the enhanced viral clearance of influenza virus-infected CD47 deficient mice, whereas the viral load in WT mice was not affected (Reading et al., 2010; Tate et al., 2010). CD47 deficiency seems to be directly important for aMΦ since an adoptive transfer of CD47 deficient aMΦ into aMΦ-depleted WT mice led to reduced virus titers comparable to the viral

clearance observed in CD47$^{-/-}$ mice. Thus, this study showed for the first time a boosted antiviral aMΦ immunity during influenza virus infection in absence of CD47.

Upon activation MΦ can adopt distinct phenotypes, which differ greatly in function. While pro-inflammatory M1 MΦ are described to clear pathogens, anti-inflammatory M2 MΦ drive the tissue repair during infection. Interestingly, the genetic ablation of CD47 did neither affect the M1 nor M2 phenotype of aMΦ in IAV-infected mice. Regarding the pro-inflammatory phenotype, these results are consistent with the unaltered pathology of CD47$^{-/-}$ mice as iNOS the utilized marker of M1 MΦ was shown to contribute to the clearance of IAV but also to the pathology of severe IAV infection (Burggraaf et al., 2011; Perrone et al., 2013; Rimmelzwaan et al., 2001). Contrary to the phenotype of MΦ, the expression of different activation markers, namely the co-stimulatory molecules CD86 and MHC class II, was diminished on aMΦ of influenza virus-infected CD47 KO mice compared to WT. Likewise, the amount of IFN-α, which mainly derives from aMΦ during influenza virus infection, was reduced in the BALF of CD47 deficient mice. Interestingly, a decreased expression of genes involved in type I and type II IFN signaling was already demonstrated in NK cells of CD47$^{-/-}$ mice upon chronic LCMV infection (Nath et al., 2019). However, the mechanisms involved in reduced IFN responses in absence of CD47 need further investigation. Taken together, the obtained results revealed, that the increased viral clearance of IAV in CD47 KO mice did not correlate with an overall enhanced aMΦ-activation.

The clearance of IAV mediated by aMΦ has been described to rely mainly on the phagocytosis of viral aggregates as well as dying or dead infected epithelial cells (Fujimoto et al., 2000; He et al., 2017; Huber et al., 2001). Interestingly, CD47 is best known for its inhibition of phagocytosis mediated by the binding to SIRPα on the phagocyte. Here, CD47-SIRPα signaling on the same cell as well as *trans*-interactions have been shown to play an important role (Hayes et al., 2020). Thus, CD47 deficient aMΦ might display an enhanced phagocytic activity. Unexpectedly, CD47 KO aMΦ did neither exhibit an enhanced uptake of foreign particles nor improved efferocytosis of influenza virus-infected AEC II. Interestingly, additional transcriptome analyses of WT and CD47$^{-/-}$ aMΦ, which should give further insight into the mechanisms involved in the enhanced aMΦ-mediated clearance of IAV in CD47 KO mice, revealed an enhanced expression of hemoglobin-α and -β subunits upon influenza virus infection in absence of CD47.

Liu, Zeng and Stamler first described the expression of non-erythroid hemoglobin by MΦ upon stimulation with LPS or IFN-γ in 1999. Since then various cells including AEC II and neuronal cells have been shown to express hemoglobin (Bhaskaran et al., 2005; Biagioli et al., 2009). Classically, hemoglobin is known to facilitate the oxygen transport by interaction with

heme co-factors. However, additional functions of hemoglobin in antimicrobial and antiviral defense have been described. Here, C-terminal fragments of hemoglobin-β limit the growth of different bacteria including *E. coli* and *S. aureus* (A. Parish et al., 2001; Hobson and Hirsch, 1958; Liepke et al., 2003; Mak et al., 2000). Moreover, an antiviral activity against HSV-2 has been recently attributed to the hemoglobin-β fragment (Groß et al., 2020). Interestingly, extracted lung fluid from IAV-infected CD47$^{-/-}$ mice was able to diminish the *in vitro* infection of *MDCK* cells by IAV. Since other antiviral factors such as IFN-α and IFN-γ were reduced in the BALF, this suggests that other antiviral agents, including hemoglobin, must be secreted in case of CD47 deficiency. Additionally, the study of Groß *et al.* demonstrated a pH sensitivity regarding the generation as well as the antimicrobial function of the analyzed hemoglobin-β fragment. Thus, an optimal antimicrobial activity of hemoglobin has been observed in an acidic environment. Of note, various infections including IAV have been shown to trigger an extracellular acidification *in vitro* (Liu et al., 2016). Hence, the dynamics of acidification in the lung of IAV-infected CD47 deficient mice might lead to the time delay between the improved viral clearance and the altered MΦ responses. Taken together, CD47$^{-/-}$ aMΦ-mediated clearance of influenza virus might rely on the augmented expression as well as an antiviral activity of hemoglobin.

The expression of hemoglobin is regulated by different KLFs, which represent a group of transcription factors involved in the regulation of various cellular processes such as proliferation, differentiation, or apoptosis (Pearson et al., 2008). Within erythroid cells KLF1 induces the expression of hemoglobin-β while KLF2 and KLF4 have been described to induce hemoglobin-α expression in endothelial cells (Miller and Bieker, 1993; Parkins et al., 1995; Sangwung et al., 2017). In contrast to this, KLF3 is described to counteract the activating signal mediated by KLF1 (Funnell et al., 2012; Ilsley et al., 2017). Interestingly, the present study revealed a reduced expression of KLF3 in infected aMΦ of CD47 deficient mice compared to WT MΦ. Thus, CD47 might suppress the expression of antiviral hemoglobin in aMΦ via KLF3. However, further studies are needed to define the regulating and functional mechanisms in detail.

4.3 Enhanced MΦ Responses are Independent of CD47-SIRPα Signaling

Within the present study the obtained results revealed an enhanced viral clearance in CD47$^{-/-}$ mice, which was based on an altered aMΦ response. In regard to the underlying mechanism, the control of myeloid cell activation by CD47 is mainly described to be indirectly mediated by its interaction with SIRPα. SIRPα is an inhibitor receptor of the SIRP family of paired receptors and is mainly expressed on myeloid cells. Upon binding to CD47, SIRPα has been

described to suppress the activation of different myeloid cells including DCs and MΦ (Braun et al., 2006; Latour et al., 2001; Oldenborg et al., 2000). Thus, the enhanced aMΦ immunity in CD47 deficient mice might be based on an interrupted CD47-SIRPα signaling. In line with this, an increased expression of SIRPα in the lung of infected WT mice was found in the present study. Moreover, the experiments revealed, that aMΦ express higher amounts of SIRPα on the surface compared to iMΦ. Interestingly, the expression of the inhibitory receptor is in part induced by the anti-inflammatory cytokine IL-10, which represents a part of the immuno-suppressive milieu in the lung. Since the lung is one of the main interfaces of the human body that gets in touch with the environment, the immuno-suppressive conditions in the lung facilitate a hyporesponsiveness of resident immune cells to avoid undesirable immune responses. For this purpose, the milieu regulates the activation of different inhibitory receptors such as CD200 (Snelgrove et al., 2008). Despite the high expression of SIRPα on aMΦ, the viral clearance of IAV was neither enhanced in SIRPα KO mice nor in WT mice treated with a SIRPα-blocking antibody. Interestingly, the alternative ligands of SIRPα, SPA and SPD, can only be found in the lung and have been shown to regulate the activation of aMΦ (Janssen et al., 2008). Thus, SPA and SPD might compensate for the disrupted CD47-SIRPα signaling within the respiratory system of CD47 deficient mice. Hence, the phenotype of IAV-infected $CD47^{-/-}$ mice seems to be independent of CD47-SIRPα signaling.

Another known ligand of CD47 is TSP-l a homotrimeric glycoprotein, which is part of the extracellular matrix and can be secreted by various cells (Jaffe et al., 1985; Raugi et al., 1982). TSP-1 has been mainly described to be involved in the regulation of T cell responses (Lamy et al., 2003; Rodríguez-Jiménez et al., 2019). In line with this, the expression of TSP-1 was found to be increased in WT mice at the peak of adaptive immune responses 7 dpi in the present study. However, binding of TSP-1 to CD47 has also been described to regulate the activation of myeloid cells (Doyen et al., 2003; Xing et al., 2017). In this context, besides SIRPα, aMΦ display a significantly high expression of CD47 compared to iMΦ, which was again inducible by the anti-inflammatory cytokine IL-10. Thus, this study is the first to show, that besides pro-inflammatory signals anti-inflammatory cytokines can trigger the expression of CD47. Moreover, aMΦ upregulate CD47 but not SIRPα upon influenza virus infection indicating a direct role of CD47 for the regulation of those cells. In this context, again bone marrow chimeric mice would be an ideal way to define the role of aMΦ-expressed CD47 in more detail. Yet, as mentioned before the anti-phagocytic activity of CD47 impedes the use of this technique. Nevertheless, the essential role of CD47 expressed on aMΦ is further supported by the adoptive transfer of CD47 KO aMΦ, which are sufficient to reduce the viral load in WT recipient mice during IAV infection compared to transferred WT MΦ.

Additionally, the transcriptome analysis of aMΦ from infected WT and CD47 deficient mice imply an underlying regulatory mechanism mediated by TSP-1 as the binding of TSP-1 to CD47 was shown to regulate the expression of different transcription factors including KLF4 (Kaur et al., 2013). Interestingly, a reduced expression of KLF3 was observed in the aMΦ of IAV-infected CD47 deficient mice. Thus, CD47-TSP-1 signaling might regulate the expression of KLF3 and thereby antiviral immune responses of aMΦ during IAV infection.

4.4 Therapeutic Targeting of CD47

As the obtained results of the present study depict CD47 as a negative regulator of antiviral immune responses against influenza virus infection, CD47 might be a potential target for therapeutic treatment. The blockade of CD47 by monoclonal antibodies has been shown to be an effective therapy against various cancers (Veillette and Chen, 2018; Willingham et al., 2012) and was also introduced by Cham *et al.* as a treatment during infectious diseases although the immunological mechanisms are rather different. Interestingly, different monoclonal antibodies targeting CD47 are already in phase I clinical trials for the treatment of different cancers making them a compelling target for the treatment of severe influenza virus infection. However, the initial study was not able to show a beneficial role of CD47 blockade for the clearance of IAV. The utilized experimental setup was based on the study of Cham *et al.* in 2020 however another type of antibody was applied. Two types of monoclonal antibodies binding to murine CD47 are commercially available to date, Miap301 and Miap410. Importantly, both clones differ in their ability to disrupt CD47-SIRPα interaction as well as their ability to activate Fc-receptor-mediated phagocytosis. Miap301 has been shown to strongly interfere with CD47-SIRPα signaling but reveals a minor activation of Fc-receptors. In contrast, *vice versa* biological activities have been reported for Miap410 (Veillette and Chen, 2018). As a consequence of this, effects mediated by Miap410 might not solely rely on a disrupted CD47-SIRPα signaling but also on Fc-receptor mediated phagocytosis of CD47 expressing cells such as infected cells. In order to avoid such adverse effects, the clone Miap301 was used in the present study. Thus, differences in the antiviral activity of CD47 blockade in both studies might be related to the used antibody. Moreover, the previous study by Cham *et al.* used the WE strain of LCMV as a model for viral infection, which results in a systemic distribution of the virus. In contrast to this, the influenza virus infection utilized in the present study is locally restricted to the lung. Interestingly, human infections mainly display a localized rather than systemic propagation of the virus. Due to the distinct infection sites in both models, the accessibility of the CD47 antibody to the involved immune cells might vary. Thus, within future experiments the route of application needs to be

optimized to target the local immune responses in the lung more efficiently. Furthermore, the previous results of the present study depicted a reduced viral load in CD47 deficient mice mediated by aMΦ. These tissue resident MΦ are the first cells responding to an influenza virus infection of the respiratory system orchestrating the recruitment of the subsequent immune cells. Blockade of CD47 after the initial aMΦ responses might not be able to elicit the enhanced aMΦ phenotype of $CD47^{-/-}$ mice but rather affects the recruited cells. Thus, a treatment at earlier times of infection might be of interest to address the aMΦ responses. Asides from the location and timing of CD47 blockade, the duration of treatment might also affect the outcome of IAV infection as CD47 has not only been shown to limit the induction but is also involved in the contraction of immune responses (Van et al., 2012). Thus, prolonged blockade of CD47 might even aggravate the severity of influenza virus infection. Interestingly, contrary to the SIRPα based mechanisms described by Cham *et al.* the impact of CD47 blockade on SIRPα signaling during respiratory infections might be limited due to the unique expression of the surfactant proteins within the lung which are alternative ligands of SIRPα. Instead, the experiments of the present study implied a negative impact of CD47 on viral clearance during influenza virus infection, which was mediated by TSP-1. Although TSP-1 and SIRPα compete for the binding to CD47 (Isenberg et al., 2009), the exact binding sites of both ligands seem to differ (Kaur et al., 2011). Hence, the efficiency of CD47-blocking antibodies to interfere with TSP-1 induced signaling cascades is controversial. For example, Bauer *et al.* have suggested an agonistic function of CD47-blocking antibodies regarding signaling pathways activated via TSP-1. On the contrary, Csányi *et al.* have demonstrated an inhibitor effect of Miap301 on the TSP-1 mediated activation of CD47. Nevertheless, CD47-blocking antibodies might be a potential target to treat severe influenza virus infections.

Taken together, the present study revealed a detrimental role of CD47 during IAV infection, which was independent of adaptive immune responses. Instead, CD47 was shown to obstruct aMΦ-related antiviral immune responses. Interestingly, the inhibition of aMΦ antiviral activity via CD47 was not dependent on SIRPα but might to rely on the ligation of TSP-1. Moreover, the expression of non-erythroid hemoglobin in aMΦ seems to contribute to the enhanced clearance of IAV in absence of CD47. Despite the promising results in CD47 deficient mice, no enhanced viral clearance could be induced by the application of CD47-blocking antibodies so far. However, due to the localized infection of IAV as well as the specifically targeted cells the experimental setup to define the therapeutic potential of CD47-blocking antibodies during influenza virus infection needs to be optimized within further studies.

5 Summary

Our knowledge of many pathogens and their related immune responses extends continually. Nevertheless, despite existing antivirals or vaccines 290.000 - 650.000 people die of respiratory diseases linked to seasonal flu annually. Hence, in addition to intrinsic viral factors novel treatment strategies focus on influenza-related immune responses. CD47 is a currently well-known immuno-regulatory protein and a promising target for cancer therapy due to its function as “don’t eat me signal”. However, it has also been shown to contribute to the clearance of different pathogens whereas its impact on antiviral immunity is still poorly understood. Thus, the present study defines the role of CD47 for innate and adaptive immune responses during acute influenza A virus (IAV) infection. To this end, mice lacking the expression of CD47 were infected with IAV (strain A/PR8/34) and the disease severity as well as the antiviral immune responses were analyzed.

The present study demonstrated for the first time a detrimental role of CD47 in antiviral immune responses during IAV infection as reduced viral titers were found in $CD47^{-/-}$ mice. Interestingly, this effect was neither based on an inhibition of humoral immune responses nor on a restriction of T cell-mediated clearance of IAV. Instead, CD47 was shown to trigger reduced alveolar macrophage (aMΦ) frequencies during acute influenza virus infection. Moreover, depletion of aMΦ identified this specialized cell type to be mainly responsible for the enhanced elimination of IAV in absence of CD47. Unexpectedly, the obstructive function of CD47 on aMΦ was not mediated by its interaction with the myeloid inhibitory receptor SIRPα demonstrated by the blockade of SIRPα during IAV infection. Accordantly, no augmented phagocytic or efferocytic activity of CD47 KO aMΦ was observed in this study. On the contrary, the immuno-regulatory function of CD47 during acute IAV infection rather seemed to be related to TSP-1 signaling controlling the expression of antiviral hemoglobin in aMΦ. Hence, future studies will address the possible use of CD47-blocking antibodies during severe influenza virus infection as well as the specific mechanisms associated with the reduced viral load of IAV-infected $CD47^{-/-}$ mice more closely. Interestingly, the unspecific nature of CD47 signaling might enable the treatment of various respiratory viruses. Hence, the obtained results depict CD47 as negative regulator of antiviral immunity and imply CD47 as a potential target to treat severe pulmonary infections, such as influenza or Covid-19.

6 Zusammenfassung

Obwohl unser Wissen zu Krankheitserregern und den damit verbundenen Immunantworten stetig erweitert wird, sterben jährlich bis zu 650.000 Menschen an Infektionen der unteren Atemwege, hervorgerufen durch saisonal auftretende Influenzaviren. Aufgrund der limitierten Wirksamkeit vorhandener Virostatika, sowie Impfstoffe befassen sich neue Strategien zur Behandlung von schweren Influenzavirus-Infektionen, mit der Manipulation antiviraler Immunantworten. Ein, aufgrund seiner Funktion als „*don't eat me signal*" derzeit bekanntes, immunregulatorisches Protein ist CD47. Neben vielversprechender Einsatzmöglichkeiten in der Krebstherapie konnte gezeigt werden, dass CD47 zur Eliminierung verschiedener Krankheitserreger beiträgt. Sein Einfluss auf die antivirale Immunantwort ist jedoch bislang noch ungeklärt. Daher ist das Ziel der vorliegenden Arbeit, die Charakterisierung von CD47 hinsichtlich seiner Bedeutung für die Immunreaktion während einer akuten Influenza A-Virus (IAV) Infektion. Hierzu wurden $CD47^{-/-}$ Mäuse mit dem IAV-Stamm A/PR8/34 infiziert und bezüglich des Krankheitsverlaufs, sowie der einhergehenden Immunantwort untersucht.

Die vorliegende Studie konnte erstmals anhand von verringerten Viruskonzentrationen in $CD47^{-/-}$ Mäusen zeigen, dass CD47 die Klärung des Influenzavirus durch das Immunsystem nachteilig beeinflusst. Dieser Vorgang basierte weder auf einer inhibierten humoralen Immunantwort noch auf einer eingeschränkten Klärung des Virus durch T-Zellen. Stattdessen konnte herausgestellt werden, dass CD47 während der akuten Influenzavirus-Infektion eine Reduktion der Anzahl an Alveolar-Makrophagen (aMΦ) bewirkt. Des Weiteren konnten mittels spezifischer Depletion die aMΦ als Ursache für die verstärkte Klärung von IAV in Abwesenheit von CD47 identifiziert werden. Die Blockade von SIRPα während der IAV-Infektion zeigte, dass die inhibierende Funktion von CD47 auf aMΦ nicht durch eine Interaktion mit dem myeloiden Rezeptor SIRPα vermittelt wurde. Ebenso konnte keine verstärkte Phagozytose oder Efferozytose durch $CD47^{-/-}$ aMΦ beobachtet werden. Im Gegensatz dazu weisen die Ergebnisse auf eine TSP-1-induzierte regulatorische Funktion von CD47 hin, welche die Expression von antiviralem Hämoglobin in aMΦ kontrolliert. Zukünftige Studien werden daher die mögliche Verwendung von CD47-blockierenden Antikörpern zur Behandlung einer schweren IAV-Infektion genauer untersuchen, sowie die spezifischen Mechanismen, welche mit der reduzierten Viruslast von IAV-infizierten $CD47^{-/-}$ Mäusen zusammenhängen. Die unspezifische Natur der CD47-Signalübertragung könnte hierbei die Behandlung einer Vielzahl von respiratorischen Infektion ermöglichen. Zusammenfassend stellen die gewonnenen Ergebnisse CD47 als negativen Regulator von antiviralen Immunantworten dar und weisen CD47 als potenzielles Ziel für die Behandlung schwerer Lungeninfektionen, wie Influenza oder womöglich auch COVID-19, aus.

7 Literature

A. Parish, C., Jiang, H., Tokiwa, Y., Berova, N., Nakanishi, K., McCabe, D., Zuckerman, W., Ming Xia, M., and E. Gabay, J. (2001). Broad-spectrum antimicrobial activity of hemoglobin. Bioorg. Med. Chem. *9*, 377–382.

Adams, S., van der Laan, L.J., Vernon-Wilson, E., Renardel de Lavalette, C., Döpp, E.A., Dijkstra, C.D., Simmons, D.L., and van den Berg, T.K. (1998). Signal-regulatory protein is selectively expressed by myeloid and neuronal cells. J. Immunol.

Alberts, B., Johnson, A., Lewis, J., Morgan, D., Raff, M., Roberts, K., Walter, P., Wilson, J., and Hunt, T. (2014). Molecular Biology of the Cell (New York: Garland Science, Taylor & Francis Group, LLC, an informa business).

Aldridge, J.R., Moseley, C.E., Boltz, D.A., Negovetich, N.J., Reynolds, C., Franks, J., Brown, S.A., Doherty, P.C., Webster, R.G., and Thomas, P.G. (2009). TNF/iNOS-producing dendritic cells are the necessary evil of lethal influenza virus infection. Proc. Natl. Acad. Sci. *106*, 5306–5311.

Allen, I.C., Scull, M.A., Moore, C.B., Holl, E.K., McElvania-TeKippe, E., Taxman, D.J., Guthrie, E.H., Pickles, R.J., and Ting, J.P.Y. (2009). The NLRP3 Inflammasome Mediates In Vivo Innate Immunity to Influenza A Virus through Recognition of Viral RNA. Immunity.

Altorki, N.K., Markowitz, G.J., Gao, D., Port, J.L., Saxena, A., Stiles, B., McGraw, T., and Mittal, V. (2019). The lung microenvironment: an important regulator of tumour growth and metastasis. Nat. Rev. Cancer *19*, 9–31.

Antunes, I., and Kassiotis, G. (2010). Suppression of Innate Immune Pathology by Regulatory T Cells during Influenza A Virus Infection of Immunodeficient Mice. J. Virol.

Arya, M., Shergill, I.S., Williamson, M., Gommersall, L., Arya, N., and Patel, H.R.H. (2005). Basic principles of real-time quantitative PCR. Expert Rev. Mol. Diagn. *5*, 209–219.

Ashkenazi, S., Vertruyen, A., Arístegui, J., Esposito, S., McKeith, D.D., Klemola, T., Biolek, J., Kühr, J., Bujnowski, T., Desgrandchamps, D., et al. (2006). Superior relative efficacy of live attenuated influenza vaccine compared with inactivated influenza vaccine in young children with recurrent respiratory tract infections. Pediatr. Infect. Dis. J.

Astry, C.L., and Jakab, G.J. (1984). Influenza virus-induced immune complexes suppress alveolar macrophage phagocytosis. J. Virol. *50*, 287–292.

Avice, M.-N., Rubio, M., Sergerie, M., Delespesse, G., and Sarfati, M. (2000). CD47 Ligation Selectively Inhibits the Development of Human Naive T Cells into Th1 Effectors. J. Immunol. *165*, 4624–4631.

Ayi, K., Lu, Z., Serghides, L., Ho, J.M., Finney, C., Wang, J.C.Y., Conrad Liles, W., and Kain, K.C. (2016). CD47-SIRPα interactions regulate macrophage uptake of Plasmodium falciparum-infected erythrocytes and clearance of malaria in vivo. Infect. Immun. *84*, 2002–2011.

Baccam, P., Beauchemin, C., Macken, C.A., Hayden, F.G., and Perelson, A.S. (2006). Kinetics of Influenza A Virus Infection in Humans. J. Virol.

Baenziger, N.L., Brodie, G.N., and Majerus, P.W. (1971). A thrombin-sensitive protein of human platelet membranes. Proc. Natl. Acad. Sci. U. S. A.

Banerjee, R., Khandelwal, S., Kozakai, Y., Sahu, B., and Kumar, S. (2015). CD47 regulates the phagocytic clearance and replication of the Plasmodium yoelii malaria parasite. Proc. Natl. Acad. Sci. U. S. A.

Barclay, A.N., and van den Berg, T.K. (2014). The Interaction Between Signal Regulatory Protein Alpha (SIRP α) and CD47: Structure, Function, and Therapeutic Target . Annu. Rev. Immunol. *32*, 25–50.

Barlow, P.G., Svoboda, P., Mackellar, A., Nash, A.A., York, I.A., Pohl, J., Davidson, D.J., and Donis, R.O. (2011). Antiviral Activity and Increased Host Defense against Influenza Infection Elicited by the Human Cathelicidin LL-37. PLoS One *6*, e25333.

Baumgarth, N., Herman, O.C., Jager, G.C., Brown, L., Herzenberg, L.A., and Herzenberg, L.A. (1999). Innate and acquired humoral immunities to influenza virus are mediated by distinct arms of the immune system. Proc. Natl. Acad. Sci. U. S. A. *96*, 2250–2255.

Beare, A.S., Schild, G.C., and Craig, J.W. (1975). Trials in Man with live recombinants made from A/PR/8/34 (H0N1) and wild H3N2 Influenza Viruses. Lancet.

van Beek, E.M., Zarate, J.A., van Bruggen, R., Schornagel, K., Tool, A.T.J., Matozaki, T., Kraal, G., Roos, D., and van den Berg, T.K. (2012). SIRPα Controls the Activity of the Phagocyte NADPH Oxidase by Restricting the Expression of gp91phox. Cell Rep. *2*, 748–755.

Belisle, S.E., Tisoncik, J.R., Korth, M.J., Carter, V.S., Proll, S.C., Swayne, D.E., Pantin-Jackwood, M., Tumpey, T.M., and Katze, M.G. (2010). Genomic Profiling of Tumor Necrosis Factor Alpha (TNF-α) Receptor and Interleukin-1 Receptor Knockout Mice Reveals a Link between TNF-α Signaling and Increased Severity of 1918 Pandemic Influenza Virus Infection. J. Virol.

Belshe, R.B., Edwards, K.M., Vesikari, T., Black, S. V., Walker, R.E., Hultquist, M., Kemble, G., and Connor, E.M. (2007). Live attenuated versus inactivated influenza vaccine in infants and young children. N. Engl. J. Med. *356*, 685–696.

Bender, B.S., Croghan, T., Zhang, L., and Small, P.A. (1992). Transgenic mice lacking class i major histocompatibility complex-restricted t cells have delayed viral clearance and increased mortality after influenza virus challenge. J. Exp. Med.

Benne, C.A., Benaissa-Trouw, B., Van Strijp, J.A.G., Kraaijeveld, C.A., and Van Iwaarden, J.F.F. (1997). Surfactant protein A, but not surfactant protein D, is an opsonin for influenza A virus phagocytosis by rat alveolar macrophages. Eur. J. Immunol. *27*, 886–890.

Betancur, P.A., Abraham, B.J., Yiu, Y.Y., Willingham, S.B., Khameneh, F., Zarnegar, M., Kuo, A.H., McKenna, K., Kojima, Y., Leeper, N.J., et al. (2017). A CD47-associated super-enhancer links pro-inflammatory signalling to CD47 upregulation in breast cancer. Nat. Commun. *8*.

Bhaskaran, M., Chen, H., Chen, Z., and Liu, L. (2005). Hemoglobin is expressed in alveolar epithelial type II cells. Biochem. Biophys. Res. Commun. *333*, 1348–1352.

Biagioli, M., Pinto, M., Cesselli, D., Zaninello, M., Lazarevic, D., Roncaglia, P., Simone, R., Vlachouli, C., Plessy, C., Bertin, N., et al. (2009). Unexpected expression of α- and β-globin in mesencephalic dopaminergic neurons and glial cells. Proc. Natl. Acad. Sci. *106*, 15454 LP – 15459.

Bouguermouh, S., Van, V.Q., Martel, J., Gautier, P., Rubio, M., and Sarfati, M. (2008). CD47 Expression on T Cell Is a Self-Control Negative Regulator of Type 1 Immune Response. J. Immunol. *180*, 8073–8082.

Brandes, M., Klauschen, F., Kuchen, S., and Germain, R.N. (2013). A systems analysis identifies a feedforward inflammatory circuit leading to lethal influenza infection. Cell *154*, 197.

Braun, D., Galibert, L., Nakajima, T., Saito, H., Quang, V.V., Rubio, M., and Sarfati, M. (2006). Semimature Stage: A Checkpoint in a Dendritic Cell Maturation Program That Allows for Functional Reversion after Signal-Regulatory Protein-α Ligation and Maturation Signals. J. Immunol. *177*, 8550–8559.

Bright, R.A., Shay, D.K., Shu, B., Cox, N.J., and Klimov, A.I. (2006). Adamantane Resistance Among Influenza A Viruses Isolated Early During the 2005-2006 Influenza Season in the United States. JAMA *295*, 891–894.

Brincks, E.L., Katewa, A., Kucaba, T.A., Griffith, T.S., and Legge, K.L. (2008). CD8 T Cells Utilize TRAIL to Control Influenza Virus Infection. J. Immunol.

Brooke, G., Holbrook, J.D., Brown, M.H., and Barclay, A.N. (2004). Human Lymphocytes Interact Directly with CD47 through a Novel Member of the Signal Regulatory Protein (SIRP) Family. J. Immunol. *173*, 2562 LP – 2570.

Brown, E.J., and Frazier, W.A. (2001). Integrin-associated protein (CD47) and its ligands. Trends Cell Biol. *11*, 130–135.

Brown, E., Hooper, L., Ho, T., and Gresham, H. (1990). Integrin-associated protein: A 50-kD plasma membrane antigen physically and functionally associated with integrins. J. Cell Biol. *111*, 2785–2794.

Bui, M., Whittaker, G., and Helenius, A. (1996). Effect of M1 protein and low pH on nuclear transport of influenza virus ribonucleoproteins. J. Virol.

Bullough, P.A., Hughson, F.M., Skehel, J.J., and Wiley, D.C. (1994). Structure of influenza haemagglutinin at the pH of membrane fusion. Nature.

Burggraaf, S., Bingham, J., Payne, J., Kimpton, W.G., Lowenthal, J.W., and Bean, A.G.D. (2011). Increased inducible nitric oxide synthase expression in organs is associated with a higher severity of H5N1 influenza virus infection. PLoS One *6*, e14561–e14561.

Burnet, F.M. (1951). Mucoproteins in Relation to Virus Action. Physiol. Rev. *31*, 131–150.

Burnet, M., Fraser, K.B., and Lind, P.E. (1953). Genetic Interaction Between Influenza Viruses. Nature *171*, 163–165.

Cameron, C.M., Barrett, J.W., Mann, M., Lucas, A., and McFadden, G. (2005). Myxoma virus M128L is expressed as a cell surface CD47-like virulence factor that contributes to the downregulation of macrophage activation in vivo. Virology.

Campbell, I.G., Freemont, P.S., Foulkes, W., and Trowsdale, J. (1992). An Ovarian Tumor Marker with Homology to Vaccinia Virus Contains an IgV-like Region and Multiple Transmembrane Domains. Cancer Res. *52*, 5416 LP – 5420.

Carlin, L.E., Hemann, E.A., Zacharias, Z.R., Heusel, J.W., and Legge, K.L. (2018). Natural killer cell recruitment to the lung during influenza A virus infection is dependent on CXCR3, CCR5, and virus exposure dose. Front. Immunol.

Centers for Disease Control and Prevention (2019). Types of Influenza Viruses.

Chakrabarti, A., Jha, B.K., and Silverman, R.H. (2011). New insights into the role of RNase L in innate immunity. J. Interferon Cytokine Res. *31*, 49–57.

Cham, L.B., Torrez Dulgeroff, L.B., Tal, M.C., Adomati, T., Li, F., Bhat, H., Huang, A., Lang, P.A., Moreno, M.E., Rivera, J.M., et al. (2020). Immunotherapeutic Blockade of CD47 Inhibitory Signaling Enhances Innate and Adaptive Immune Responses to Viral Infection. Cell Rep. *31*, 107494.

Chen, W., Calvo, P.A., Malide, D., Gibbs, J., Schubert, U., Bacik, I., Basta, S., O'Neill, R., Schickli, J., Palese, P., et al. (2001). A novel influenza A virus mitochondrial protein that induces cell death. Nat. Med. *7*, 1306–1312.

Chu, C.M., Dawson, I.M., and Elford, W.J. (1949). Filamentous Forms associated with newly isolated Influenza Virus. Lancet *253*.

Coates, B.M., Staricha, K.L., Koch, C.M., Cheng, Y., Shumaker, D.K., Budinger, G.R.S., Perlman, H., Misharin, A. V., and Ridge, K.M. (2018). Inflammatory Monocytes Drive Influenza A Virus–Mediated Lung Injury in Juvenile Mice. J. Immunol. *200*, 2391–2404.

Coker, R.K., Laurent, G.J., Shahzeidi, S., Hernández-Rodríguez, N.A., Pantelidis, P., Du Bois, R.M., Jeffery, P.K., and McAnulty, R.J. (1996). Diverse cellular TGF-β1 and TGF-β3 gene expression in normal human and murine lung. Eur. Respir. J.

Connor, R.J., Kawaoka, Y., Webster, R.G., and Paulson, J.C. (1994). Receptor Specificity in Human, Avian and Equine H2 and H3 Influenza Virus Isolates. Virology *205*, 17–23.

Crapo, J.D., Barry, B.E., Gehr, P., Bachofen, M., and Weibel, E.R. (1982). Cell Number and Cell Characteristics of the Normal Human Lung. Am. Rev. Respir. Dis. *126*, 332–337.

Csányi, G., Yao, M., Rodríguez, A.I., Al Ghouleh, I., Sharifi-Sanjani, M., Frazziano, G., Huang, X., Kelley, E.E., Isenberg, J.S., and Pagano, P.J. (2012). Thrombospondin-1 regulates blood flow via CD47 receptor-mediated activation of NADPH oxidase 1. Arterioscler. Thromb. Vasc. Biol. *32*, 2966–2973.

Danto, S.I., Shannon, J.M., Borok, Z., Zabski, S.M., and Crandall, E.D. (1995). Reversible transdifferentiation of alveolar epithelial cells. Am. J. Respir. Cell Mol. Biol. *12*, 497–502.

Davies, P., and Barry, R.D. (1966). Nucleic Acid of Influenza Virus. Nature *211*, 384–387.

DeBerge, M.P., Ely, K.H., and Enelow, R.I. (2014). Soluble, but Not Transmembrane, TNF-α Is Required during Influenza Infection To Limit the Magnitude of Immune Responses and the Extent of Immunopathology. J. Immunol. *192*, 5839 LP – 5851.

Demeure, C.E., Tanaka, H., Mateo, V., Rubio, M., Delespesse, G., and Sarfati, M. (2000). CD47 Engagement Inhibits Cytokine Production and Maturation of Human Dendritic Cells. J. Immunol. *164*, 2193–2199.

Dias, A., Bouvier, D., Crépin, T., McCarthy, A.A., Hart, D.J., Baudin, F., Cusack, S., and Ruigrok, R.W.H. (2009). The cap-snatching endonuclease of influenza virus polymerase resides in the PA subunit. Nature *458*, 914–918.

Dietrich, J., Cella, M., Seiffert, M., Bühring, H.-J., and Colonna, M. (2000). Cutting Edge: Signal-Regulatory Protein β1 Is a DAP12-Associated Activating Receptor Expressed in Myeloid Cells. J. Immunol.

DiLillo, D.J., Palese, P., Wilson, P.C., and Ravetch, J. V. (2016). Broadly neutralizing anti-influenza antibodies require Fc receptor engagement for in vivo protection. J. Clin. Invest.

Divangahi, M., King, I.L., and Pernet, E. (2015). Alveolar macrophages and type I IFN in airway homeostasis and immunity. Trends Immunol. *36*, 307–314.

Dou, D., Revol, R., Östbye, H., Wang, H., and Daniels, R. (2018). Influenza A virus cell entry, replication, virion assembly and movement. Front. Immunol. *9*, 1–17.

Downey, J., Pernet, E., Coulombe, F., and Divangahi, M. (2018). Dissecting host cell death programs in the pathogenesis of influenza. Microbes Infect.

Doyen, V., Rubio, M., Braun, D., Nakajima, T., Abe, J., Saito, H., Delespesse, G., and Sarfati, M. (2003). Thrombospondin 1 Is an Autocrine Negative Regulator of Human Dendritic Cell Activation. J. Exp. Med. *198*, 1277–1283.

Drbal, K., Cern, J., Angelisová, P., Hilgert, I., Cebecauer, M., Inkora, J., and Horejí, V. (2000). CDw149 antibodies recognize a clustered subset of CD47 molecules associated with cytoplasmic signaling molecules. Tissue Antigens.

Ehre, C., Worthington, E.N., Liesman, R.M., Grubb, B.R., Barbier, D., O'Neal, W.K., Sallenave, J.M., Pickles, R.J., and Boucher, R.C. (2012). Overexpressing mouse model demonstrates the protective role of Muc5ac in the lungs. Proc. Natl. Acad. Sci. U. S. A.

Engvall, E., and Perlmann, P. (1972). Enzyme-linked immunosorbent assay, Elisa. 3. Quantitation of specific antibodies by enzyme-labeled anti-immunoglobulin in antigen-coated tubes. J. Immunol. *109*, 129–135.

Francis, T. (1934). Transmission of influenza by a filterable virus. Science (80-.). *80*, 457–459.

Francis, T., Salk, J.E., Pearson, H.E., and Brown, P.N. (1944). Protective Effect of Vaccination Against Induced Influenza A. Proc. Soc. Exp. Biol. Med. *55*, 104–105.

Frazier, W.A., Gao, A.G., Dimitry, J., Chung, J., Brown, E.J., Lindberg, F.P., and Linder, M.E. (1999). The thrombospondin receptor integrin-associated protein (CD47) functionally couples to heterotrimeric G(i). J. Biol. Chem. *274*, 8554–8560.

Fuchs, S., Hollins, A., Laue, M., Schaefer, U., Roemer, K., Gumbleton, M., and Lehr, C.-M. (2003). Differentiation of human alveolar epithelial cells in primary culture: morphological characterization and synthesis of caveolin-1 and surfactant protein-C. Cell Tissue Res. *311*, 31–45.

Fujimoto, I., Pan, J., Takizawa, T., and Nakanishi, Y. (2000). Virus Clearance through Apoptosis-Dependent Phagocytosis of Influenza A Virus-Infected Cells by Macrophages. J. Virol. *74*, 3399–3403.

Fujimoto, T.-T., Katsutani, S., Shimomura, T., and Fujimura, K. (2003). Thrombospondin-bound Integrin-associated Protein (CD47) Physically and Functionally Modifies Integrin αIIbβ3 by Its Extracellular Domain. J. Biol. Chem. *278*, 26655–26665.

Fujioka, Y., Matozaki, T., Noguchi, T., Iwamatsu, A., Yamao, T., Takahashi, N., Tsuda, M., Takada, T., and Kasuga, M. (1996). A novel membrane glycoprotein, SHPS-1, that binds the SH2-domain-containing protein tyrosine phosphatase SHP-2 in response to mitogens and cell adhesion. Mol. Cell. Biol.

Funnell, A.P.W., Norton, L.J., Mak, K.S., Burdach, J., Artuz, C.M., Twine, N.A., Wilkins, M.R., Power, C.A., Hung, T.-T., Perdomo, J., et al. (2012). The CACCC-binding protein KLF3/BKLF represses a subset of KLF1/EKLF target genes and is required for proper erythroid maturation in vivo. Mol. Cell. Biol. *32*, 3281–3292.

Funnell, A.P.W., Mak, K.S., Twine, N.A., Pelka, G.J., Norton, L.J., Radziewic, T., Power, M., Wilkins, M.R., Bell-Anderson, K.S., Fraser, S.T., et al. (2013). Generation of mice deficient in both KLF3/BKLF and KLF8 reveals a genetic interaction and a role for these factors in embryonic globin gene silencing. Mol. Cell. Biol. *33*, 2976–2987.

Gao, A.G., and Frazier, W.A. (1994). Identification of a receptor candidate for the carboxyl-terminal cell binding domain of thrombospondins. J. Biol. Chem.

Gao, A.G., Lindberg, F.P., Dimitry, J.M., Brown, E.J., and Frazier, W.A. (1996). Thrombospondin modulates alpha v beta 3 function through integrin-associated protein. J. Cell Biol. *135*, 533–544.

Gardai, S.J., Xiao, Y.Q., Dickinson, M., Nick, J.A., Voelker, D.R., Greene, K.E., and Henson, P.M. (2003). By binding SIRPα or calreticulin/CD91, lung collectins act as dual function surveillance molecules to suppress or enhance inflammation. Cell.

Gaush, C.R., and Smith, T.F. (1968). Replication and plaque assay of influenza virus in an established line of canine kidney cells. Appl. Microbiol. *16*, 588–594.

Gaush, C.R., Hard, W.L., and Smith, T.F. (1966). Characterization of an Established Line of Canine Kidney Cells (MDCK). Proc. Soc. Exp. Biol. Med. *122*, 931–935.

Gazit, R., Gruda, R., Elboim, M., Arnon, T.I., Katz, G., Achdout, H., Hanna, J., Qimron, U., Landau, G., Greenbaum, E., et al. (2006). Lethal influenza infection in the absence of the natural killer cell receptor gene Ncr1. Nat. Immunol.

Ge, M.Q., Ho, A.W.S., Tang, Y., Wong, K.H.S., Chua, B.Y.L., Gasser, S., and Kemeny, D.M. (2012). NK Cells Regulate CD8 + T Cell Priming and Dendritic Cell Migration during Influenza A Infection by IFN-γ and Perforin-Dependent Mechanisms . J. Immunol.

Gereke, M., Autengruber, A., Gröbe, L., Jeron, A., Bruder, D., and Stegemann-Koniszewski, S. (2012). Flow cytometric isolation of primary murine type II alveolar epithelial cells for functional and molecular studies. J. Vis. Exp. 1–7.

Gerhard, W., Mozdzanowska, K., Furchner, M., Washko, G., and Maiese, K. (1997). Role of the B-cell response in recovery of mice from primary influenza virus infection. Immunol. Rev.

GeurtsvanKessel, C.H., Willart, M.A.M., Van Rijt, L.S., Muskens, F., Kool, M., Baas, C., Thielemans, K., Bennett, C., Clausen, B.E., Hoogsteden, H.C., et al. (2008). Clearance of influenza virus from the lung depends on migratory langerin+CD11b- but not plasmacytoid dendritic cells. J. Exp. Med. *205*, 1621–1634.

Goffic, R. Le, Balloy, V., Lagranderie, M., Alexopoulou, L., Escriou, N., Flavell, R., Chignard, M., and Si-Tahar, M. (2006). Detrimental Contribution of the Toll-Like Receptor (TLR)3 to Influenza A Virus–Induced Acute Pneumonia. PLOS Pathog. *2*, e53.

Grabiec, A.M., and Hussell, T. (2016). The role of airway macrophages in apoptotic cell clearance following acute and chronic lung inflammation. Semin. Immunopathol. *38*, 409–423.

Green, T. (2013). Membrane protein complexes involved in thrombospondin-1 regulation of nitric oxide signaling.

Gresham, H.D., Lowrance, J.H., Caver, T.E., Wilson, B.S., Cheung, A.L., and Lindberg, F.P. (2000). Survival of Staphylococcus aureus Inside Neutrophils Contributes to Infection. J. Immunol.

Grimbert, P., Bouguermouh, S., Baba, N., Nakajima, T., Allakhverdi, Z., Braun, D., Saito, H., Rubio, M., Delespesse, G., and Sarfati, M. (2006). Thrombospondin/CD47 Interaction: A Pathway to Generate Regulatory T Cells from Human CD4 + CD25 − T Cells in Response to Inflammation . J. Immunol. *177*, 3534–3541.

Grohskopf, L.A., Alyanak, E., Broder, K.R., Walter, E.B., Fry, A.M., and Jernigan, D.B. (2019). Prevention and Control of Seasonal Influenza with Vaccines: Recommendations of the Advisory Committee on Immunization Practices - United States, 2019-20 Influenza Season. MMWR. Recomm. Reports Morb. Mortal. Wkly. Report. Recomm. Reports *68*, 1–21.

Groß, R., Bauer, R., Krüger, F., Rücker-Braun, E., Olari, L.R., Ständker, L., Preising, N., Rodríguez, A.A., Conzelmann, C., Gerbl, F., et al. (2020). A Placenta Derived C-Terminal Fragment of β-Hemoglobin With Combined Antibacterial and Antiviral Activity. Front. Microbiol.

Guilliams, M., De Kleer, I., Henri, S., Post, S., Vanhoutte, L., De Prijck, S., Deswarte, K., Malissen, B., Hammad, H., and Lambrecht, B.N. (2013). Alveolar macrophages develop from fetal monocytes that differentiate into long-lived cells in the first week of life via GM-CSF. J. Exp. Med.

Guillot, L., Le Goffic, R., Bloch, S., Escriou, N., Akira, S., Chignard, M., and Si-Tahar, M. (2005). Involvement of Toll-like Receptor 3 in the Immune Response of Lung Epithelial Cells to Double-stranded RNA and Influenza A Virus. J. Biol. Chem. *280*, 5571–5580.

Guillot, L., Nathan, N., Tabary, O., Thouvenin, G., Le Rouzic, P., Corvol, H., Amselem, S., and Clement, A. (2013). Alveolar epithelial cells: Master regulators of lung homeostasis. Int. J. Biochem. Cell Biol. *45*, 2568–2573.

Hamada, H., Bassity, E., Flies, A., Strutt, T.M., Garcia-Hernandez, M. de L., McKinstry, K.K., Zou, T., Swain, S.L., and Dutton, R.W. (2013). Multiple Redundant Effector Mechanisms of CD8 + T Cells Protect against Influenza Infection. J. Immunol. *190*, 296–306.

Harris, A., Cardone, G., Winkler, D.C., Heymann, J.B., Brecher, M., White, J.M., and Steven, A.C. (2006). Influenza virus pleiomorphy characterized by cryoelectron tomography. Proc. Natl. Acad. Sci. U. S. A. *103*, 19123–19127.

Hartshorn, K.L., Crouch, E.C., White, M.R., Eggleton, P., Tauber, A.I., Chang, D., and Sastry, K. (1994). Evidence for a protective role of pulmonary surfactant protein D (SP-D) against influenza A viruses. J. Clin. Invest.

Hartshorn, K.L., White, M.R., Shepherd, V., Reid, K., Jensenius, J.G., and Crouch, E.C. (1997). Mechanisms of anti-influenza activity of surfactant proteins A and D: Comparison with serum collectins. Am. J. Physiol. - Lung Cell. Mol. Physiol.

Hashimoto, D., Chow, A., Noizat, C., Teo, P., Beasley, M.B., Leboeuf, M., Becker, C.D., See, P., Price, J., Lucas, D., et al. (2013). Tissue-resident macrophages self-maintain locally throughout adult life with minimal contribution from circulating monocytes. Immunity *38*, 792–804.

Hashimoto, Y., Moki, T., Takizawa, T., Shiratsuchi, A., and Nakanishi, Y. (2007). Evidence for Phagocytosis of Influenza Virus-Infected, Apoptotic Cells by Neutrophils and Macrophages in Mice. J. Immunol.

Hatherley, D., Graham, S.C., Turner, J., Harlos, K., Stuart, D.I., and Barclay, A.N. (2008). Paired Receptor Specificity Explained by Structures of Signal Regulatory Proteins Alone and Complexed with CD47. Mol. Cell *31*, 266–277.

Hay, A.J., Lomniczi, B., Bellamy, A.R., and Skehel, J.J. (1977). Transcription of the influenza virus genome. Virology *83*, 337–355.

Hay, A.J., Wolstenholme, A.J., Skehel, J.J., and Smith, M.H. (1985). The molecular basis of the specific anti-influenza action of amantadine. EMBO J. *4*, 3021–3024.

Hayakawa, K., Hardy, R.R., Herzenberg, L.A., and Herzenberg, L.A. (1985). Progenitors for Ly-1 B cells are distinct from progenitors for other B cells. J. Exp. Med. *161*, 1554–1568.

Hayden, F.G., Cote, K.M., and Douglas, R.G. (1980). Plaque inhibition assay for drug susceptibility testing of influenza viruses. Antimicrob. Agents Chemother. *17*, 865 LP – 870.

Hayden, F.G., Fritz, R., Lobo, M.C., Alvord, W., Strober, W., and Straus, S.E. (1998). Local and systemic cytokine responses during experimental human influenza A virus infection. Relation to symptom formation and host defense. J. Clin. Invest. *101*, 643–649.

Hayden, F.G., Sugaya, N., Hirotsu, N., Lee, N., de Jong, M.D., Hurt, A.C., Ishida, T., Sekino, H., Yamada, K., Portsmouth, S., et al. (2018). Baloxavir Marboxil for Uncomplicated Influenza in Adults and Adolescents. N. Engl. J. Med. *379*, 913–923.

Hayes, B.H., Tsai, R.K., Dooling, L.J., Kadu, S., Lee, J.Y., Pantano, D., Rodriguez, P.L., Subramanian, S., Shin, J.W., and Discher, D.E. (2020). Macrophages show higher levels of engulfment after disruption of cis interactions between CD47 and the checkpoint receptor SIRPα. J. Cell Sci. *133*.

He, W., Chen, C.J., Mullarkey, C.E., Hamilton, J.R., Wong, C.K., Leon, P.E., Uccellini, M.B., Chromikova, V., Henry, C., Hoffman, K.W., et al. (2017). Alveolar macrophages are critical for broadly-reactive antibody-mediated protection against influenza A virus in mice. Nat. Commun. *8*, 1–13.

Heider, H., Adamczyk, B., Presber, H.W., Schroeder, C., Feldblum, R., and Indulen, M.K. (1981). Occurrence of amantadine- and rimantadine-resistant influenza. A virus strains during the 1980 epidemic. Acta Virol.

Herold, S., von Wulffen, W., Steinmueller, M., Pleschka, S., Kuziel, W.A., Mack, M., Srivastava, M., Seeger, W., Maus, U.A., and Lohmeyer, J. (2006). Alveolar Epithelial Cells Direct Monocyte Transepithelial Migration upon Influenza Virus Infection: Impact of Chemokines and Adhesion Molecules. J. Immunol. *177*, 1817–1824.

Hers, J.F.P., and Mulder, J. (1961). Broad Aspects of the Pathology and Pathogenesis of Human Influenza. Am. Rev. Respir. Dis. *83*, 84–97.

Hirst, G.K. (1943). Studies of Antigenic Differences among Strains of Influenza A by Means of Red Cell Agglutination. J. Exp. Med. *78*, 407–423.

Hirst, G.K. (1962). Genetic recombination with Newcastle disease virus, polioviruses, and influenza. Cold Spring Harb. Symp. Quant. Biol. *27*, 303–309.

Ho, A.W.S., Prabhu, N., Betts, R.J., Ge, M.Q., Dai, X., Hutchinson, P.E., Lew, F.C., Wong, K.L., Hanson, B.J., Macary, P.A., et al. (2011). Lung CD103 + Dendritic Cells Efficiently Transport Influenza Virus to the Lymph Node and Load Viral Antigen onto MHC Class I for Presentation to CD8 T Cells . J. Immunol.

Hobson, D., and Hirsch, J.G. (1958). The Antibacterial Activity of Hemoglobin. J. Exp. Med. *107*, 167–183.

Holodick, N.E., Rodríguez-Zhurbenko, N., and Hernández, A.M. (2017). Defining Natural Antibodies . Front. Immunol. *8*, 872.

Holt, P.G. (1993). Regulation of antigen-presenting cell function(s) in lung and airway tissues. Eur. Respir. J.

Horisberger, M.A., Staeheli, P., and Haller, O. (1983). Interferon induces a unique protein in mouse cells bearing a gene for resistance to influenza virus. Proc. Natl. Acad. Sci. *80*, 1910–1914.

Hornick, E.E., Zacharias, Z.R., and Legge, K.L. (2019). Kinetics and Phenotype of the CD4 T Cell Response to Influenza Virus Infections . Front. Immunol. *10*, 2351.

Howley, P.M., and Knipe, D.M. (2020). Field's Virology: Emerging Viruses (Wolters Kluwer).

Huber, V.C., Lynch, J.M., Bucher, D.J., Le, J., and Metzger, D.W. (2001). Fc Receptor-Mediated Phagocytosis Makes a Significant Contribution to Clearance of Influenza Virus Infections. J. Immunol.

Hui, K.P.Y., Ching, R.H.H., Chan, S.K.H., Nicholls, J.M., Sachs, N., Clevers, H., Peiris, J.S.M., and Chan, M.C.W. (2018). Tropism, replication competence, and innate immune responses of influenza virus: an analysis of human airway organoids and ex-vivo bronchus cultures. Lancet Respir. Med. *6*, 846–854.

Ichigotani, Y., Matsuda, S., Machida, K., Oshima, K., Iwamoto, T., Yamaki, K., Hayakawa, T., and Hamaguchi, M. (2000). Molecular cloning of a novel human gene (SIRP-B2) which encodes a new member of the SIRP/SHPS-1 protein family. J. Hum. Genet.

Ilsley, M.D., Gillinder, K.R., Magor, G.W., Huang, S., Bailey, T.L., Crossley, M., and Perkins, A.C. (2017). Krüppel-like factors compete for promoters and enhancers to fine-tune transcription. Nucleic Acids Res. *45*, 6572–6588.

Inglis, S.C., Carroll, A.R., Lamb, R.A., and Mahy, B.W.J. (1976). Polypeptides specified by the influenza virus genome. I. Evidence for eight distinct gene products specified by fowl plague virus. Virology *74*, 489–503.

Isenberg, J.S., Ridnour, L.A., Dimitry, J., Frazier, W.A., Wink, D.A., and Roberts, D.D. (2006). CD47 Is Necessary for Inhibition of Nitric Oxide-stimulated Vascular Cell Responses by Thrombospondin-1. J. Biol. Chem. *281*, 26069–26080.

Isenberg, J.S., Annis, D.S., Pendrak, M.L., Ptaszynska, M., Frazier, W.A., Mosher, D.F., and Roberts, D.D. (2009). Differential interactions of thrombospondin-1, -2, and -4 with CD47 and effects on cGMP signaling and ischemic injury responses. J. Biol. Chem.

Iuliano, A.D., Roguski, K.M., Chang, H.H., Muscatello, D.J., Palekar, R., Tempia, S., Cohen, C., Gran, J.M., Schanzer, D., Cowling, B.J., et al. (2018). Estimates of global seasonal influenza-associated respiratory mortality: a modelling study. Lancet.

Iwasaki, T., and Nozima, T. (1977). Defense mechanisms against primary influenza virus infection in mice. I. The roles of interferon and neutralizing antibodies and thymus dependence of interferon and antibody production. J. Immunol.

Jaffe, E.A., Ruggiero, J.T., and Falcone, D.J. (1985). Monocytes and macrophages synthesize and secrete thrombospondin. Blood.

Janssen, E.M., Droin, N.M., Lemmens, E.E., Pinkoski, M.J., Bensinger, S.J., Ehst, B.D., Griffith, T.S., Green, D.R., and Schoenberger, S.P. (2005). CD4+ T-cell help controls CD8+ T-cell memory via TRAIL-mediated activation-induced cell death. Nature *434*, 88–93.

Janssen, W.J., McPhillips, K.A., Dickinson, M.G., Linderman, D.J., Morimoto, K., Xiao, Y.Q., Oldham, K.M., Vandivier, R.W., Henson, P.M., and Gardai, S.J. (2008). Surfactant proteins A and D suppress alveolar macrophage phagocytosis via interaction with SIRPα. Am. J. Respir. Crit. Care Med. *178*, 158–167.

Janssen, W.J., Barthel, L., Muldrow, A., Oberley-Deegan, R.E., Kearns, M.T., Jakubzick, C., and Henson, P.M. (2011). Fas determines differential fates of resident and recruited macrophages during resolution of acute lung injury. Am. J. Respir. Crit. Care Med. *184*, 547–560.

Jayasekera, J.P., Moseman, E.A., and Carroll, M.C. (2007). Natural Antibody and Complement Mediate Neutralization of Influenza Virus in the Absence of Prior Immunity. J. Virol. *81*, 3487 LP – 3494.

Jego, G., Palucka, A.K., Blanck, J.P., Chalouni, C., Pascual, V., and Banchereau, J. (2003). Plasmacytoid dendritic cells induce plasma cell differentiation through type I interferon and interleukin 6. Immunity.

Jiang, Y., Yang, D., Li, W., Wang, B., Jiang, Z., and Li, M. (2012). Antiviral Activity of Recombinant Mouse β-defensin 3 against Influenza a Virus in vitro and in vivo. Antivir. Chem. Chemother. *22*, 255–262.

Johnson, N.P.A.S., and Mueller, J. (2002). Updating the accounts: global mortality of the 1918-1920 "Spanish" influenza pandemic. Bull. Hist. Med.

Kaur, S., Martin-Manso, G., Pendrak, M.L., Garfield, S.H., Isenberg, J.S., and Roberts, D.D. (2010). Thrombospondin-1 inhibits VEGF receptor-2 signaling by disrupting its association with CD47. J. Biol. Chem.

Kaur, S., Kuznetsova, S.A., Pendrak, M.L., Sipes, J.M., Romeo, M.J., Li, Z., Zhang, L., and Roberts, D.D. (2011). Heparan sulfate modification of the transmembrane receptor CD47 is necessary for inhibition of T Cell receptor signaling by thrombospondin-1. J. Biol. Chem. *286*, 14991–15002.

Kaur, S., Soto-Pantoja, D.R., Stein, E. V., Liu, C., Elkahloun, A.G., Pendrak, M.L., Nicolae, A., Singh, S.P., Nie, Z., Levens, D., et al. (2013). Thrombospondin-1 signaling through CD47 inhibits self-renewal by regulating c-Myc and other stem cell transcription factors. Sci. Rep. *3*, 1–12.

Kaur, S., Chang, T., Singh, S.P., Lim, L., Mannan, P., Garfield, S.H., Pendrak, M.L., Soto-Pantoja, D.R., Rosenberg, A.Z., Jin, S., et al. (2014). CD47 Signaling Regulates the Immunosuppressive Activity of VEGF in T Cells. J. Immunol. *193*, 3914 LP – 3924.

Kavaler, J., Caton, A.J., Staudt, L.M., and Gerhard, W. (1991). A B cell population that dominates the primary response to influenza virus hemagglutinin does not participate in the memory response. Eur. J. Immunol.

Kawabe, T., Isobe, K.I., Hasegawa, Y., Nakashima, I., and Shimokata, K. (1992). Immunosuppressive activity induced by nitric oxide in culture supernatant of activated rat alveolar macrophages. Immunology *76*, 72–78.

Kerr, I.M., and Brown, R.E. (1978). pppA2'p5'A2'p5'A: an inhibitor of protein synthesis synthesized with an enzyme fraction from interferon-treated cells. Proc. Natl. Acad. Sci. U. S. A. *75*, 256–260.

Kharitonenkov, A., Chen, Z., Sures, I., Wang, H., Schilling, J., and Ullrich, A. (1997). A family of proteins that inhibit signalling through tyrosine kinase receptors. Nature.

Kim, T.S., and Braciale, T.J. (2009). Respiratory Dendritic Cell Subsets Differ in Their Capacity to Support the Induction of Virus-Specific Cytotoxic CD8+ T Cell Responses. PLoS One *4*, e4204.

Kim, H.M., Kang, Y.M., Ku, K.B., Park, E.H., Yum, J., Kim, J.C., Jin, S.Y., Lee, J.S., Kim, H.S., and Seo, S.H. (2013). The severe pathogenicity of alveolar macrophage-depleted ferrets infected with 2009 pandemic H1N1 influenza virus. Virology.

Kim, M.J., Lee, J.C., Lee, J.J., Kim, S., Lee, S.G., Park, S.W., Sung, M.W., and Heo, D.S. (2008). Association of CD47 with natural killer cell-mediated cytotoxicity of head-and-neck squamous cell carcinoma lines. Tumor Biol. *29*, 28–34.

King, D.P., and Jones, P.P. (1983). Induction of Ia and H-2 antigens on a macrophage cell line by immune interferon. J. Immunol. *131*, 315 LP – 318.

Kinhult, J., Egesten, A., Benson, M., Uddman, R., and Cardell, L.O. (2003). Increased expression of surface activation markers on neutrophils following migration into the nasal lumen. Clin. Exp. Allergy.

Klein, A., Carnoy, C., Wieruszeski, J.M., Strecker, G., Strang, A.M., Van Halbeek, H., Roussel, P., and Lamblin, G. (1992). The broad diversity of neutral and sialylated oligosaccharides derived from human salivary mucins. Biochemistry *31*, 6152–6165.

Kojima, Y., Volkmer, J.-P., McKenna, K., Civelek, M., Lusis, A.J., Miller, C.L., Direnzo, D., Nanda, V., Ye, J., Connolly, A.J., et al. (2016). CD47-blocking antibodies restore phagocytosis and prevent atherosclerosis. Nature *536*, 86–90.

Kon, K., and Rai, M. (2016). The Microbiology of Respiratory System Infections (San Diego: Academic Press).

Kos, F.J., and Engleman, E.G. (1996). Role of natural killer cells in the generation of influenza virus-specific cytotoxic T cells. Cell. Immunol. *173*, 1–6.

Krammer, F., Smith, G.J.D., Fouchier, R.A.M., Peiris, M., Kedzierska, K., Doherty, P.C., Palese, P., Shaw, M.L., Treanor, J., Webster, R.G., et al. (2018). Influenza. Nat. Rev. Dis. Prim. *4*, 1–21.

Kuiken, T., and Taubenberger, J. (2008). Pathology of Human Influenza Revisited. Vaccine *12*, D59–D66.

Kumagai, Y., Takeuchi, O., Kato, H., Kumar, H., Matsui, K., Morii, E., Aozasa, K., Kawai, T., and Akira, S. (2007). Alveolar Macrophages Are the Primary Interferon-α Producer in Pulmonary Infection with RNA Viruses. Immunity *27*, 240–252.

Kundu, A., Avalos, R.T., Sanderson, C.M., and Nayak, D.P. (1996). Transmembrane domain of influenza virus neuraminidase, a type II protein, possesses an apical sorting signal in polarized MDCK cells. J. Virol. *70*, 6508–6515.

Lakadamyali, M., Rust, M.J., Babcock, H.P., and Zhuang, X. (2003). Visualizing infection of individual influenza viruses. Proc. Natl. Acad. Sci. U. S. A. *100*, 9280–9285.

Lam, J.H., and Baumgarth, N. (2019). The Multifaceted B Cell Response to Influenza Virus. J. Immunol. *202*, 351–359.

Lamb, R.A., and Choppin, P.W. (1979). Segment 8 of the influenza virus genome is unique in coding for two polypeptides. Proc. Natl. Acad. Sci. U. S. A. *76*, 4908–4912.

Lamb, R.A., and Choppin, P.W. (1981). Identification of a second protein (M2) encoded by RNA segment 7 of influenza virus. Virology.

Lamy, L., Ticchioni, M., Rouquette-Jazdanian, A.K., Samson, M., Deckert, M., Greenberg, A.H., and Bernard, A. (2003). CD47 and the 19 kDA interacting protein-3 (BNIP3) in T cell apoptosis. J. Biol. Chem.

Lamy, L., Foussat, A., Brown, E.J., Bornstein, P., Ticchioni, M., and Bernard, A. (2007). Interactions between CD47 and Thrombospondin Reduce Inflammation. J. Immunol. *178*, 5930–5939.

Latour, S., Tanaka, H., Demeure, C., Mateo, V., Rubio, M., Brown, E.J., Maliszewski, C., Lindberg, F.P., Oldenborg, A., Ullrich, A., et al. (2001). Bidirectional Negative Regulation of Human T and Dendritic Cells by CD47 and Its Cognate Receptor Signal-Regulator Protein-α: Down-Regulation of IL-12 Responsiveness and Inhibition of Dendritic Cell Activation. J. Immunol. *167*, 2547–2554.

Lawler, J., and Hynes, R.O. (1986). The structure of human thrombospondin, an adhesive glycoprotein with multiple calcium-binding sites and homologies with several different proteins. J. Cell Biol. *103*, 1635–1648.

Lawler, J.W., Slayter, H.S., and Coligan, J.E. (1978). Isolation and characterization of a high molecular weight glycoprotein from human blood platelets. J. Biol. Chem.

Lawrence, C.W., and Braciale, T.J. (2004). Activation, Differentiation, and Migration of Naive Virus-Specific CD8 + T Cells during Pulmonary Influenza Virus Infection . J. Immunol.

Lee, Y., Ko, E., Lee, Y., Lee, Y., Bian, Z., Liu, Y., and Kang, S. (2016). CD47 Plays a Role as a Negative Regulator in Inducing Protective. *90*, 6746–6758.

Lehenkari, P.P., Kellinsalmi, M., Näpänkangas, J.P., Ylitalo, K. V, Mönkkönen, J., Rogers, M.J., Azhayev, A., Väänänen, H.K., and Hassinen, I.E. (2002). Further Insight into Mechanism of Action of Clodronate: Inhibition of Mitochondrial ADP/ATP Translocase by a Nonhydrolyzable, Adenine-Containing Metabolite. Mol. Pharmacol. *61*, 1255 LP – 1262.

LeMessurier, K.S., Lin, Y., McCullers, J.A., and Samarasinghe, A.E. (2016). Antimicrobial peptides alter early immune response to influenza A virus infection in C57BL/6 mice. Antiviral Res. *133*, 208–217.

de Leve, S., Wirsdörfer, F., Cappuccini, F., Schütze, A., Meyer, A. V, Röck, K., Thompson, L.F., Fischer, J.W., Stuschke, M., and Jendrossek, V. (2017). Loss of CD73 prevents accumulation of alternatively activated macrophages and the formation of prefibrotic macrophage clusters in irradiated lungs. FASEB J. *31*, 2869–2880.

LeVine, A.M., Whitsett, J.A., Hartshorn, K.L., Crouch, E.C., and Korfhagen, T.R. (2001). Surfactant Protein D Enhances Clearance of Influenza A Virus from the Lung In Vivo. J. Immunol. *167*, 5868 LP – 5873.

Li, S.S., Ivanoff, A., Bergström, S.E., Sandström, A., Christensson, B., Van Nerven, J., Holgersson, J., Hauzenberger, D., Arencibia, I., and Sundqvist, K.G. (2002). T lymphocyte expression of thrombospondin-1 and adhesion to extracellular matrix components. Eur. J. Immunol.

Li, Z., He, L., Wilson, K.E., and Roberts, D.D. (2001). Thrombospondin-1 Inhibits TCR-Mediated T Lymphocyte Early Activation. J. Immunol. *166*, 2427–2436.

Liepke, C., Baxmann, S., Heine, C., Breithaupt, N., Ständker, L., and Forssmann, W.-G. (2003). Human hemoglobin-derived peptides exhibit antimicrobial activity: a class of host defense peptides. J. Chromatogr. B *791*, 345–356.

Lin, K.L., Suzuki, Y., Nakano, H., Ramsburg, E., and Gunn, M.D. (2008). CCR2 + Monocyte-Derived Dendritic Cells and Exudate Macrophages Produce Influenza-Induced Pulmonary Immune Pathology and Mortality . J. Immunol. *180*, 2562–2572.

Lin, S.J., Lo, M., Kuo, R.L., Shih, S.R., Ojcius, D.M., Lu, J., Lee, C.K., Chen, H.C., Lin, M.Y., Leu, C.M., et al. (2014). The pathological effects of CCR2+ inflammatory monocytes are amplified by an IFNAR1-triggered chemokine feedback loop in highly pathogenic influenza infection. J. Biomed. Sci. *21*, 1–18.

Lindberg, F.P., Gresham, H.D., Schwarz, E., and Brown, E.J. (1993). Molecular cloning of integrin-associated protein: An immunoglobulin family member with multiple membrane-spanning domains implicated in α(v)β3- dependent ligand binding. J. Cell Biol. *123*, 485–496.

Lindberg, F.P., Lublin, D.M., Telen, M.J., Veile, R.A., Miller, Y.E., Donis-Keller, H., and Brown, E.J. (1994). Rh-related antigen CD47 is the signal-transducer integrin-associated protein. J. Biol. Chem.

Lindberg, F.P., Bullard, D.C., Caver, T.E., Gresham, H.D., Beaudet, A.L., and Brown, E.J. (1996). Decreased resistance to bacterial infection and granulocyte defects in IAP-deficient mice. Science (80-.). *274*, 795–798.

Liu, H., Maruyama, H., Masuda, T., Honda, A., and Arai, F. (2016). The Influence of Virus Infection on the Extracellular pH of the Host Cell Detected on Cell Membrane. Front. Microbiol. *7*, 1127.

Liu, L., Zeng, M., and Stamler, J.S. (1999). Hemoglobin induction in mouse macrophages. Proc. Natl. Acad. Sci. *96*, 6643–6647.

Liu, Y., Merlin, D., Burst, S.L., Pochet, M., Madara, J.L., and Parkos, C.A. (2001). The role of CD47 in neutrophil transmigration: Increased rate of migration correlates with increased cell surface expression of CD47. J. Biol. Chem. *276*, 40156–40166.

Lowen, A.C., and Steel, J. (2014). Roles of Humidity and Temperature in Shaping Influenza Seasonality. J. Virol. *88*, 7692 LP – 7695.

Lund, J.M., Alexopoulou, L., Sato, A., Karow, M., Adams, N.C., Gale, N.W., Iwasaki, A., and Flavell, R. a (2004). Recognition of single-stranded RNA viruses by Toll-like receptor 7. Proc Natl Acad Sci U S A *101*, 5598–5603.

MacCallum, W.G. (1921). Pathologic Anatomy of Pneumonia associated with Influenza. Johns Hopkins Hosp. Rep *20*, 149–249.

Majeti, R., Chao, M.P., Alizadeh, A.A., Pang, W.W., Jaiswal, S., Gibbs, K.D., van Rooijen, N., and Weissman, I.L. (2009). CD47 Is an Adverse Prognostic Factor and Therapeutic Antibody Target on Human Acute Myeloid Leukemia Stem Cells. Cell *138*, 286–299.

Mak, P., Wójcik, K., Silberring, J., and Dubin, A. (2000). Antimicrobial peptides derived from heme-containing proteins: Hemocidins. Antonie Van Leeuwenhoek *77*, 197–207.

Mandelboim, O., Lieberman, N., Lev, M., Paul, L., Arnon, T.I., Bushkin, Y., Davis, D.M., Strominger, J.L., Yewdell, J.W., and Porgador, A. (2001). Recognition of haemagglutinins on virus-infected cells by NKp46 activates lysis by human NK cells. Nature.

Manna, P.P., Dimitry, J., Oldenborg, P.A., and Frazier, W.A. (2005). CD47 augments fas/CD95-mediated apoptosis. J. Biol. Chem.

Margossian, S.S., Lawler, J.W., and Slayter, H.S. (1981). Physical characterization of platelet thrombospondin. J. Biol. Chem.

Mateo, V., Lagneaux, L., Bron, D., Biron, G., Armant, M., Delespesse, G., and Sarfati, M. (1999). CD47 ligation induces caspase-independent cell death in chronic lymphocytic leukemia. Nat. Med.

Matsuoka, Y., Matsumae, H., Katoh, M., Eisfeld, A.J., Neumann, G., Hase, T., Ghosh, S., Shoemaker, J.E., Lopes, T.J.S., Watanabe, T., et al. (2013). A comprehensive map of the influenza A virus replication cycle. BMC Syst. Biol. *7*, 97.

Mawby, W.J., Holmes, C.H., Anstee, D.J., Spring, F.A., and Tanner, M.J.A. (1994). Isolation and characterization of CD47 glycoprotein: A multispanning membrane protein which is the same as integrin-associated protein (IAP) and the ovarian tumour marker OA3. Biochem. J. *304*, 525–530.

Mayer, A.K., Bartz, H., Fey, F., Schmidt, L.M., and Dalpke, A.H. (2008). Airway epithelial cells modify immune responses by inducing an anti-inflammatory microenvironment. Eur. J. Immunol.

McAuley, J.L., Corcilius, L., Tan, H.-X., Payne, R.J., McGuckin, M.A., and Brown, L.E. (2017). The cell surface mucin MUC1 limits the severity of influenza A virus infection. Mucosal Immunol. *10*, 1581–1593.

McGeoch, D., Fellner, P., and Newton, C. (1976). Influenza virus genome consists of eight distinct RNA species. Proc. Natl. Acad. Sci. U. S. A. *73*, 3045–3049.

Mcmichael, A.J., Gotch, F.M., Noble, G.R., and Beare, P.A.S. (1983). Cytotoxic T-Cell Immunity to Influenza. N. Engl. J. Med.

Meliopoulos, V.A., Van de Velde, L.-A., Van de Velde, N.C., Karlsson, E.A., Neale, G., Vogel, P., Guy, C., Sharma, S., Duan, S., Surman, S.L., et al. (2016). An Epithelial Integrin Regulates the Amplitude of Protective Lung Interferon Responses against Multiple Respiratory Pathogens. PLOS Pathog. *12*, e1005804.

Mendel, D.B., Tai, C.Y., Escarpe, P.A., Li, W., Sidwell, R.W., Huffman, J.H., Sweet, C., Jakeman, K.J., Merson, J., Lacy, S.A., et al. (1998). Oral Administration of a Prodrug of the Influenza Virus Neuraminidase Inhibitor GS 4071 Protects Mice and Ferrets against Influenza Infection. Antimicrob. Agents Chemother. *42*, 640 LP – 646.

Mibayashi, M., Martinez-Sobrido, L., Loo, Y.-M., Cardenas, W.B., Gale, M., and Garcia-Sastre, A. (2007). Inhibition of Retinoic Acid-Inducible Gene I-Mediated Induction of Beta Interferon by the NS1 Protein of Influenza A Virus. J. Virol. *81*, 514–524.

Miller, I.J., and Bieker, J.J. (1993). A novel, erythroid cell-specific murine transcription factor that binds to the CACCC element and is related to the Krüppel family of nuclear proteins. Mol. Cell. Biol. *13*, 2776 LP – 2786.

Mir, F.A., Contreras-Ruiz, L., and Masli, S. (2015). Thrombospondin-1-dependent immune regulation by transforming growth factor-β2-exposed antigen-presenting cells. Immunology *146*, 547–556.

Misharin, A. V., Morales-Nebreda, L., Mutlu, G.M., Budinger, G.R.S., and Perlman, H. (2013). Flow cytometric analysis of macrophages and dendritic cell subsets in the mouse lung. Am. J. Respir. Cell Mol. Biol. *49*, 503–510.

Mittal, R., Gonzalez-Gomez, I., and Prasadarao, N. V. (2010). Escherichia coli K1 Promotes the Ligation of CD47 with Thrombospondin-1 To Prevent the Maturation of Dendritic Cells in the Pathogenesis of Neonatal Meningitis . J. Immunol. *185*, 2998–3006.

Moltedo, B., Li, W., Yount, J.S., and Moran, T.M. (2011). Unique type I interferon responses determine the functional fate of migratory lung dendritic cells during influenza virus infection. PLoS Pathog.

Montoya, M., Schiavoni, G., Mattei, F., Gresser, I., Belardelli, F., Borrow, P., and Tough, D.F. (2002). Type I interferons produced by dendritic cells promote their phenotypic and functional activation. Blood *99*, 3263–3271.

Moskophidis, D., and Kioussis, D. (1998). Contribution of virus-specific CD8+ cytotoxic T cells to virus clearance or pathologic manifestations of influenza virus infection in a T cell receptor transgenic mouse model. J. Exp. Med. *188*, 223–232.

Mosley, V.M., and Wyckoff, R.W.G. (1946). Electron Micrography of the Virus of Influenza. Nature *157*, 263.

Murti, K.G., Webster, R.G., and Jones, I.M. (1988). Localization of RNA polymerases on influenza viral ribonucleoproteins by immunogold labeling. Virology *164*, 562–566.

N'Diaye, E.N., and Brown, E.J. (2003). The ubiquitin-related protein PLIC-1 regulates heterotrimeric G protein function through association with Gβγ. J. Cell Biol.

Nath, P.R., Gangaplara, A., Pal-Nath, D., Mandal, A., Maric, D., Sipes, J.M., Cam, M., Shevach, E.M., and Roberts, D.D. (2018). CD47 Expression in Natural Killer Cells Regulates Homeostasis and Modulates Immune Response to Lymphocytic Choriomeningitis Virus. Front. Immunol. *9*, 2985.

Nath, P.R., Pal-Nath, D., Mandal, A., Cam, M.C., Schwartz, A.L., and Roberts, D.D. (2019). Natural killer cell recruitment and activation are regulated by cd47 expression in the tumor microenvironment. Cancer Immunol. Res.

Navarathna, D.H.M.L.P., Stein, E. V., Lessey-Morillon, E.C., Nayak, D., Martin-Manso, G., and Roberts, D.D. (2015). CD47 promotes protective innate and adaptive immunity in a mouse model of disseminated candidiasis. PLoS One *10*, 1–24.

Novel Swine-Origin Influenza A (H1N1) Virus Investigation Team (2009). Emergence of a Novel Swine-Origin Influenza A (H1N1) Virus in Humans. N. Engl. J. Med. *360*, 2605–2615.

O'Neill, R.E., Talon, J., and Palese, P. (1998). The influenza virus NEP (NS2 protein) mediates the nuclear export of viral ribonucleoproteins. EMBO J.

Oldenborg, P.-A. (2004). Role of CD47 in Erythroid Cells and in Autoimmunity. Leuk. Lymphoma *45*, 1319–1327.

Oldenborg, P.A., Zheleznyak, A., Fang, Y.F., Lagenaur, C.F., Gresham, H.D., and Lindberg, F.P. (2000). Role of CD47 as a marker of self on red blood cells. Science (80-.). *288*, 2051–2054.

Osterholm, M.T., Kelley, N.S., Sommer, A., and Belongia, E.A. (2012). Efficacy and effectiveness of influenza vaccines: A systematic review and meta-analysis. Lancet Infect. Dis. *12*, 36–44.

Palese, P., and Compans, R.W. (1976). Inhibition of Influenza Virus Replication in Tissue Culture by 2-deoxy-2,3-dehydro-N-trifluoroacetylneuraminic acid (FANA): Mechanism of Action. J. Gen. Virol. *33*, 159–163.

Palese, P., Tobita, K., Ueda, M., and Compans, R.W. (1974). Characterization of temperature sensitive influenza virus mutants defective in neuraminidase. Virology *61*, 397–410.

Pang, I.K., Ichinohe, T., and Iwasaki, A. (2013). IL-1R signaling in dendritic cells replaces pattern-recognition receptors in promoting $CD8^+$ T cell responses to influenza A virus. Nat. Immunol. *14*, 246–253.

Paquette, S.G., Banner, D., Zhao, Z., Fang, Y., Huang, S.S.H., León, A.J., Ng, D.C.K., Almansa, R., Martin-Loeches, I., Ramirez, P., et al. (2012). Interleukin-6 is a potential biomarker for severe pandemic H1N1 influenza a infection. PLoS One.

Parkins, A.C., Sharpe, A.H., and Orkin, S.H. (1995). Lethal β-thalassaemia in mice lacking the erythroid CACCC-transcription factor EKLF. Nature *375*, 318–322.

Parkinson, J.E., Sanderson, C.M., and Smith, G.L. (1995). The vaccinia virus A38L gene product is a 33-kDa integral membrane glycoprotein. Virology.

Paus, D., Tri, G.P., Chan, T.D., Gardam, S., Basten, A., and Brink, R. (2006). Antigen recognition strength regulates the choice between extrafollicular plasma cell and germinal center B cell differentiation. J. Exp. Med.

Pearson, R., Fleetwood, J., Eaton, S., Crossley, M., and Bao, S. (2008). Krüppel-like transcription factors: A functional family. Int. J. Biochem. Cell Biol. *40*, 1996–2001.

Perrone, L.A., Belser, J.A., Wadford, D.A., Katz, J.M., and Tumpey, T.M. (2013). Inducible Nitric Oxide Contributes to Viral Pathogenesis Following Highly Pathogenic Influenza Virus Infection in Mice. J. Infect. Dis. *207*, 1576–1584.

Pettersen, R.D., Hestdal, K., Olafsen, M.K., Lie, S.O., and Lindberg, F.P. (1999). CD47 signals T cell death. J. Immunol.

Phelps, D.S., and Floros, J. (1988). Localization of Surfactant Protein Synthesis in Human Lung by In Situ Hybridization. Am. Rev. Respir. Dis. *137*, 939–942.

Piccio, L., Vermi, W., Boles, K.S., Fuchs, A., Strader, C.A., Facchetti, F., Cella, M., and Colonna, M. (2005). Adhesion of human T cells to antigen-presenting cells through SIRPβ2-CD47 interaction costimulates T-cell proliferation. Blood *105*, 2421–2427.

Pichlmair, A., Schulz, O., Tan, C.P., Näslund, T.I., Liljeström, P., Weber, F., and Reis e Sousa, C. (2006). RIG-I-Mediated Antiviral Responses to Single-Stranded RNA Bearing 5'-Phosphates. Science (80-.). *314*, 997 LP – 1001.

Pinto, L.H., Holsinger, L.J., and Lamb, R.A. (1992). Influenza virus M2 protein has ion channel activity. Cell *69*, 517–528.

Potter, C.W. (2001). A history of influenza. In Journal of Applied Microbiology, p.

Prabhu, N., Ho, A.W., Wong, K.H.S., Hutchinson, P.E., Chua, Y.L., Kandasamy, M., Lee, D.C.P., Sivasankar, B., and Kemeny, D.M. (2013). Gamma interferon regulates contraction of the influenza virus-specific CD8 T cell response and limits the size of the memory population. J. Virol. *87*, 12510–12522.

Raugi, G.J., Mumby, S.M., Abbott-Brown, D., and Bornstein, P. (1982). Thrombospondin: Synthesis and secretion by cells in culture. J. Cell Biol.

Reading, P.C., Whitney, P.G., Pickett, D.L., Tate, M.D., and Brooks, A.G. (2010). Influenza viruses differ in ability to infect macrophages and to induce a local inflammatory response following intraperitoneal injection of mice. Immunol. Cell Biol. *88*, 641–650.

Rebres, R.A., Kajihara, K., and Brown, E.J. (2005). Novel CD47-dependent intercellular adhesion modulates cell migration. J. Cell. Physiol.

Rehwinkel, J., Tan, C.P., Goubau, D., Schulz, O., Pichlmair, A., Bier, K., Robb, N., Vreede, F., Barclay, W., Fodor, E., et al. (2010). RIG-I Detects Viral Genomic RNA during Negative-Strand RNA Virus Infection. Cell *140*, 397–408.

Reinhold, M.I., Lindberg, F.P., Plas, D., Reynolds, S., Peters, M.G., and Brown, E.J. (1995). In vivo expression of alternatively spliced forms of integrin-associated protein (CD47). J. Cell Sci. *108*, 3419–3425.

Reinhold, M.I., Lindberg, F.P., Kersh, G.J., Allen, P.M., and Brown, E.J. (1997). Costimulation of T cell activation by integrin-associated protein (CD47) is an adhesion-dependent, CD28-independent signaling pathway. J. Exp. Med. *185*, 1–11.

Richardson, J.C., and Akkina, R.K. (1991). NS2 protein of influenza virus is found in purified virus and phosphorylated in infected cells. Arch. Virol. *116*, 69–80.

Ridley, C., Kouvatsos, N., Raynal, B.D., Howard, M., Collins, R.F., Desseyn, J.-L., Jowitt, T.A., Baldock, C., Davis, C.W., Hardingham, T.E., et al. (2014). Assembly of the Respiratory Mucin MUC5B: A New Model for a Gel-forming Mucin. J. Biol. Chem. *289*, 16409–16420.

van Riel, D., Munster, V.J., de Wit, E., Rimmelzwaan, G.F., Fouchier, R.A.M., Osterhaus, A.D.M.E., and Kuiken, T. (2007). Human and avian influenza viruses target different cells in the lower respiratory tract of humans and other mammals. Am. J. Pathol. *171*, 1215–1223.

Rimmelzwaan, G.F., Baars, M., Fouchier, R.A.M., and Osterhaus, A.D.M.E. (2001). Inhibition of influenza virus replication by nitric oxide. Int. Congr. Ser. *1219*, 551–555.

Rodgers, B.C., and Mims, C.A. (1982). Influenza virus replication in human alveolar macrophages. J. Med. Virol. *9*, 177–184.

Rodríguez-Jiménez, P., Chicharro, P., Llamas-Velasco, M., Cibrian, D., Trigo-Torres, L., Vara, A., Jiménez-Fernández, M., Sevilla-Montero, J., Calzada, M.J., Sánchez-Madrid, F., et al. (2019). Thrombospondin-1/CD47 interaction regulates Th17 and treg differentiation in psoriasis. Front. Immunol. *10*, 1–10.

Rodriguez Boulan, E., and Sabatini, D.D. (1978). Asymmetric budding of viruses in epithelial monlayers: a model system for study of epithelial polarity. Proc. Natl. Acad. Sci. U. S. A. *75*, 5071–5075.

Román, E., Miller, E., Harmsen, A., Wiley, J., Von Andrian, U.H., Huston, G., and Swain, S.L. (2002). CD4 effector T cell subsets in the response to influenza: Heterogeneity, migration, and function. J. Exp. Med. *196*, 957–968.

van Rooijen, N., and Sanders, A. (1994). Liposome mediated depletion of macrophages: mechanism of action, preparation of liposomes and applications. J. Immunol. Methods *174*, 83–93.

Rosseau, S., Selhorst, J., Wiechmann, K., Leissner, K., Maus, U., Mayer, K., Grimminger, F., Seeger, W., and Lohmeyer, J. (2000). Monocyte Migration Through the Alveolar Epithelial Barrier: Adhesion Molecule Mechanisms and Impact of Chemokines. J. Immunol. *164*, 427–435.

Sangwung, P., Zhou, G., Lu, Y., Liao, X., Wang, B., Mutchler, S.M., Miller, M., Chance, M.R., Straub, A.C., and Jain, M.K. (2017). Regulation of endothelial hemoglobin alpha expression by Kruppel-like factors. Vasc. Med. *22*, 363–369.

Schmitz, N., Kurrer, M., Bachmann, M.F., and Kopf, M. (2005). Interleukin-1 Is Responsible for Acute Lung Immunopathology but Increases Survival of Respiratory Influenza Virus Infection. J. Virol. *79*, 6441 LP – 6448.

Schneider, C., Nobs, S.P., Heer, A.K., Kurrer, M., Klinke, G., van Rooijen, N., Vogel, J., and Kopf, M. (2014). Alveolar Macrophages Are Essential for Protection from Respiratory Failure and Associated Morbidity following Influenza Virus Infection. PLoS Pathog. *10*.

Scholtissek, C., Rohde, W., Von Hoyningen, V., and Rott, R. (1978). On the origin of the human influenza virus subtypes H2N2 and H3N2. Virology *87*, 13–20.

Schrauwen, E.J.A., de Graaf, M., Herfst, S., Rimmelzwaan, G.F., Osterhaus, A.D.M.E., and Fouchier, R.A.M. (2014). Determinants of virulence of influenza A virus. Eur. J. Clin. Microbiol. Infect. Dis. *33*, 479–490.

Seiffert, M., Cant, C., Chen, Z., Rappold, I., Brugger, W., Kanz, L., Brown, E.J., Ullrich, A., and Bühring, H.J. (1999). Human signal-regulatory protein is expressed on normal, but not on subsets of leukemic myeloid cells and mediates cellular adhesion involving its counterreceptor CD47. Blood.

Seiffert, M., Brossart, P., Cant, C., Cella, M., Colonna, M., Brugger, W., Kanz, L., Ullrich, A., and Bühring, H.J. (2001). Signal-regulatory protein α (SIRPα) but not SIRPβ is involved in T-cell activation, binds to CD47 with high affinity, and is expressed on immature CD34+CD38- hematopoietic cells. Blood *97*, 2741–2749.

Shaman, J., and Kohn, M. (2009). Absolute humidity modulates influenza survival, transmission, and seasonality. Proc. Natl. Acad. Sci. *106*, 3243–3248.

Sheu, T.G., Deyde, V.M., Okomo-Adhiambo, M., Garten, R.J., Xu, X., Bright, R.A., Butler, E.N., Wallis, T.R., Klimov, A.I., and Gubareva, L. V (2008). Surveillance for Neuraminidase Inhibitor Resistance among Human Influenza A and B Viruses Circulating Worldwide from 2004 to 2008. Antimicrob. Agents Chemother. *52*, 3284 LP – 3292.

Shi, C., and Pamer, E.G. (2011). Monocyte recruitment during infection and inflammation. Nat. Rev. Immunol. *11*, 762–774.

Shimizu, T., Takizawa, N., Watanabe, K., Nagata, K., and Kobayashi, N. (2011). Crucial role of the influenza virus NS2 (NEP) C-terminal domain in M1 binding and nuclear export of vRNP. FEBS Lett.

Shope, R.E. (1931a). Swine influenza: III. filtration experiments and etiology. J. Exp. Med.

Shope, R.E. (1931b). Swine influenza: I. Experimental transmission and pathology. J. Exp. Med.

Sidorenko, Y., and Reichl, U. (2004). Structured model of influenza virus replication in MDCK cells. Biotechnol. Bioeng. *88*, 1–14.

Simon, S.I., Burns, A.R., Taylor, A.D., Gopalan, P.K., Lynam, E.B., Sklar, L.A., and Smith, C.W. (1995). L-selectin (CD62L) cross-linking signals neutrophil adhesive functions via the Mac-1 (CD11b/CD18) beta 2-integrin. J. Immunol. *155*, 1502 LP – 1514.

Skowronski, D.M., Janjua, N.Z., De Serres, G., Sabaiduc, S., Eshaghi, A., Dickinson, J.A., Fonseca, K., Winter, A.L., Gubbay, J.B., Krajden, M., et al. (2014). Low 2012-13 influenza vaccine effectiveness associated with mutation in the egg-adapted H3N2 vaccine strain not antigenic drift in circulating viruses. PLoS One *9*.

Smith, D.J., Lapedes, A.S., de Jong, J.C., Bestebroer, T.M., Rimmelzwaan, G.F., Osterhaus, A.D.M.E., and Fouchier, R.A.M. (2004). Mapping the Antigenic and Genetic Evolution of Influenza Virus. Science (80-.). *305*, 371 LP – 376.

Smith, G.J.D., Vijaykrishna, D., Bahl, J., Lycett, S.J., Worobey, M., Pybus, O.G., Ma, S.K., Cheung, C.L., Raghwani, J., Bhatt, S., et al. (2009). Origins and evolutionary genomics of the 2009 swine-origin H1N1 influenza a epidemic. Nature.

Smith, W., Andrewes, C.H., and Laidlaw, P.P. (1933). A Virus obtained from Influenza Patients. Lancet.

Snelgrove, R.J., Edwards, L., Rae, A.J., and Hussell, T. (2006). An absence of reactive oxygen species improves the resolution of lung influenza infection. Eur. J. Immunol.

Snelgrove, R.J., Goulding, J., Didierlaurent, A.M., Lyonga, D., Vekaria, S., Edwards, L., Gwyer, E., Sedgwick, J.D., Barclay, A.N., and Hussell, T. (2008). A critical function for CD200 in lung immune homeostasis and the severity of influenza infection. Nat. Immunol. *9*, 1074–1083.

Soema, P.C., Kompier, R., Amorij, J.P., and Kersten, G.F.A. (2015). Current and next generation influenza vaccines: Formulation and production strategies. Eur. J. Pharm. Biopharm. *94*, 251–263.

Soroosh, P., Doherty, T.A., Duan, W., Mehta, A.K., Choi, H., Adams, Y.F., Mikulski, Z., Khorram, N., Rosenthal, P., Broide, D.H., et al. (2013). Lung-resident tissue macrophages generate Foxp3+ regulatory T cells and promote airway tolerance. J. Exp. Med. *210*, 775–788.

Soto-Pantoja, D.R., Kaur, S., and Roberts, D.D. (2015). CD47 signaling pathways controlling cellular differentiation and responses to stress. Crit Rev Biochem Mol Biol. *50*, 212–230.

Stegemann-Koniszewski, S., Jeron, A., Gereke, M., Geffers, R., Kröger, A., Gunzer, M., and Bruder, D. (2016). Alveolar Type II Epithelial Cells Contribute to the Anti-Influenza A Virus Response in the Lung by Integrating Pathogen- and Microenvironment-Derived Signals. MBio *7*, e00276-16.

Stein, E. V., Miller, T.W., Ivins-O'Keefe, K., Kaur, S., and Roberts, D.D. (2016). Secreted Thrombospondin-1 Regulates Macrophage Interleukin-1β Production and Activation through CD47. Sci. Rep. *6*, 1–14.

Su, X., Johansen, M., Looney, M.R., Brown, E.J., and Matthay, M.A. (2008). CD47 Deficiency Protects Mice from Lipopolysaccharide-Induced Acute Lung Injury and Escherichia coli Pneumonia . J. Immunol. *180*, 6947–6953.

Sullivan, S.G., Price, O.H., and Regan, A.K. (2019). Burden, effectiveness and safety of influenza vaccines in elderly, paediatric and pregnant populations. Ther. Adv. Vaccines Immunother. *7*.

Takashita, E., Morita, H., Ogawa, R., Nakamura, K., Fujisaki, S., Shirakura, M., Kuwahara, T., Kishida, N., Watanabe, S., and Odagiri, T. (2018). Susceptibility of Influenza Viruses to the Novel Cap-Dependent Endonuclease Inhibitor Baloxavir Marboxil . Front. Microbiol. *9*, 3026.

Tal, M.C., Torrez Dulgeroff, L.B., Myers, L., Cham, L.B., Mayer-Barber, K.D., Bohrer, A.C., Castro, E., Yiu, Y.Y., Lopez Angel, C., Pham, E., et al. (2020). Upregulation of CD47 Is a Host Checkpoint Response to Pathogen Recognition. MBio *11*, e01293-20.

Tate, M.D., Deng, Y.-M., Jones, J.E., Anderson, G.P., Brooks, A.G., and Reading, P.C. (2009). Neutrophils Ameliorate Lung Injury and the Development of Severe Disease during Influenza Infection. J. Immunol. *183*, 7441–7450.

Tate, M.D., Pickett, D.L., van Rooijen, N., Brooks, A.G., and Reading, P.C. (2010). Critical Role of Airway Macrophages in Modulating Disease Severity during Influenza Virus Infection of Mice. J. Virol. *84*, 7569–7580.

Taubenberger, J.K., and Morens, D.M. (2008). The Pathology of Influenza Virus Infections. Annu Rev Pathol. *3*, 499–522.

Thomas, P.G., Dash, P., Aldridge, J.R., Ellebedy, A.H., Reynolds, C., Funk, A.J., Martin, W.J., Lamkanfi, M., Webby, R.J., Boyd, K.L., et al. (2009). The Intracellular Sensor NLRP3 Mediates Key Innate and Healing Responses to Influenza A Virus via the Regulation of Caspase-1. Immunity.

Ticchioni, M., Deckert, M., Mary, F., Bernard, G., Brown, E.J., and Bernard, A. (1997). Integrin-associated protein (CD47) is a comitogenic molecule on CD3-activated human T cells. J. Immunol. *158*, 677–684.

Ticchioni, M., Raimondi, V., Lamy, L., Wijdenes, J., Lindberg, F.P., Brown, E.J., and Bernard, A. (2001). Integrin-associated protein (CD47/IAP) contributes to T cell arrest on inflammatory vascular endothelium under flow. FASEB J.

Tisoncik, J.R., Korth, M.J., Simmons, C.P., Farrar, J., Martin, T.R., and Katze, M.G. (2012). Into the Eye of the Cytokine Storm. Microbiol. Mol. Biol. Rev. *76*, 16 LP – 32.

Topham, D.J., and Doherty, P.C. (1998). Clearance of an Influenza A Virus by CD4+ T Cells Is Inefficient in the Absence of B Cells. J. Virol.

Topham, D.J., Tripp, R.A., and Doherty, P.C. (1997). CD8+ T cells clear influenza virus by perforin or Fas-dependent processes. J. Immunol.

Treanor, J.J., Hayden, F.G., Vrooman, P.S., Barbarash, R., Bettis, R., Riff, D., Singh, S., Kinnersley, N., Ward, P., Mills, R.G., et al. (2000). Efficacy and Safety of the Oral Neuraminidase Inhibitor Oseltamivir in Treating Acute InfluenzaA Randomized Controlled Trial. JAMA *283*, 1016–1024.

Tripathi, S., Tecle, T., Verma, A., Crouch, E., White, M., and Hartshorn, K.L. (2013). The human cathelicidin LL-37 inhibits influenza A viruses through a mechanism distinct from that of surfactant protein D or defensins. J. Gen. Virol. *94*, 40–49.

Tripathi, S., Wang, G., White, M., Qi, L., Taubenberger, J., and Hartshorn, K.L. (2015). Antiviral Activity of the Human Cathelicidin, LL-37, and Derived Peptides on Seasonal and Pandemic Influenza A Viruses. PLoS One *10*, e0124706.

Tsai, R.K., and Discher, D.E. (2008). Inhibition of "self" engulfment through deactivation of myosin-II at the phagocytic synapse between human cells. J. Cell Biol.

Tumpey, T.M., Garcia-Sastre, A., Taubenberger, J.K., Palese, P., Swayne, D.E., Pantin-Jackwood, M.J., Schultz-Cherry, S., Solorzano, A., Van Rooijen, N., Katz, J.M., et al. (2005). Pathogenicity of Influenza Viruses with Genes from the 1918 Pandemic Virus: Functional Roles of Alveolar Macrophages and Neutrophils in Limiting Virus Replication and Mortality in Mice. J. Virol. *79*, 14933–14944.

Unkel, B., Hoegner, K., Clausen, B.E., Lewe-Schlosser, P., Bodner, J., Gattenloehner, S., Janßen, H., Seeger, W., Lohmeyer, J., and Herold, S. (2012). Alveolar epithelial cells orchestrate DC function in murine viral pneumonia. J. Clin. Invest. *122*, 3652–3664.

Upham, J.W., Strickland, D.H., Bilyk, N., Robinson, B.W., and Holt, P.G. (1995). Alveolar macrophages from humans and rodents selectively inhibit T-cell proliferation but permit T-cell activation and cytokine secretion. Immunology *84*, 142–147.

Van, V.Q., Lesage, S., Bouguermouh, S., Gautier, P., Rubio, M., Levesque, M., Nguyen, S., Galibert, L., and Sarfati, M. (2006). Expression of the self-marker CD47 on dendritic cells governs their trafficking to secondary lymphoid organs. EMBO J. *25*, 5560–5568.

Van, V.Q., Baba, N., Rubio, M., Wakahara, K., Panzini, B., Richard, C., Soucy, G., Franchimont, D., Fortin, G., Torres, A.C.M., et al. (2012). CD47Low status on CD4 effectors is necessary for the contraction/resolution of the immune response in humans and mice. PLoS One *7*, 2–11.

Varghese, J.N., Laver, W.G., and Colman, P.M. (1983). Structure of the influenza virus glycoprotein antigen neuraminidase at 2.9 Å resolution. Nature *303*, 35–40.

Veillette, A., and Chen, J. (2018). SIRPα–CD47 Immune Checkpoint Blockade in Anticancer Therapy. Trends Immunol. *39*, 173–184.

Veillette, A., Thibaudeaut, E., and Latour, S. (1998). High expression of inhibitory receptor SHPS-1 and its association with protein-tyrosine phosphatase SHP-1 in macrophages. J. Biol. Chem. *273*, 22719–22728.

Verdrengh, M., Lindberg, F.P., Ryden, C., and Tarkowski, A. (1999). Integrin-associated protein (IAP)-deficient mice are less susceptible to developing Staphylococcus aureus-induced arthritis. Microbes Infect.

Vreede, F.T., Jung, T.E., and Brownlee, G.G. (2004). Model Suggesting that Replication of Influenza Virus Is Regulated by Stabilization of Replicative Intermediates. J. Virol. *78*, 9568 LP – 9572.

de Vries, H.E., Hendriks, J.J.A., Honing, H., de Lavalette, C.R., van der Pol, S.M.A., Hooijberg, E., Dijkstra, C.D., and van den Berg, T.K. (2002). Signal-Regulatory Protein α-CD47 Interactions Are Required for the Transmigration of Monocytes Across Cerebral Endothelium. J. Immunol. *168*, 5832–5839.

Walsh, J.J., Dietlein, L.F., Low, F.N., Burch, G.E., and Mogabga, W.J. (1961). Bronchotracheal response in human influenza. Type A, Asian strain, as studied by light and electron microscopic examination of bronchoscopic biopsies. Arch. Intern. Med.

Wang, H., Madariaga, M.L., Wang, S., Van Rooijen, N., Oldenborg, P.A., and Yang, Y.G. (2007). Lack of CD47 on nonhematopoietic cells induces split macrophage tolerance to CD47null cells. Proc. Natl. Acad. Sci. U. S. A. *104*, 13744–13749.

Wang, J., Nikrad, M.P., Travanty, E.A., Zhou, B., Phang, T., Gao, B., Alford, T., Ito, Y., Nahreini, P., Hartshorn, K., et al. (2012). Innate immune response of human alveolar macrophages during influenza a infection. PLoS One *7*.

Wareing, M.D., Shea, A.L., Inglis, C.A., Dias, P.B., and Sarawar, S.R. (2007). CXCR2 Is Required for Neutrophil Recruitment to the Lung during Influenza Virus Infection, But Is Not Essential for Viral Clearance. Viral Immunol. *20*, 369–378.

Van Weemen, B.K., and Schuurs, A.H.W.M. (1971). Immunoassay using antigen—enzyme conjugates. FEBS Lett. *15*, 232–236.

Weibel, E.R. (1973). Morphological basis of alveolar-capillary gas exchange. Physiol. Rev. *53*, 419–495.

Weinheimer, V.K., Becher, A., Tönnies, M., Holland, G., Knepper, J., Bauer, T.T., Schneider, P., Neudecker, J., Rückert, J.C., Szymanski, K., et al. (2012). Influenza A Viruses Target Type II Pneumocytes in the Human Lung. J. Infect. Dis. *206*, 1685–1694.

White, J., Helenius, A., and Gething, M.J. (1982). Haemagglutinin of influenza virus expressed from a cloned gene promotes membrane fusion. Nature.

WHO (2017). Review of global influenza activity, October 2016–October 2017. *50*, 761–780.

WHO (2018). The top 10 causes of death. Https://Www.Who.Int/En/News-Room/Fact-Sheets/Detail/the-Top-10-Causes-of-Death Accessed: 2020-03-24.

WHO (2020). Weekly epidemiological record Relevé épidémiologique hebdomadaire. *95*, 105–116.

Willingham, S.B., Volkmer, J.P., Gentles, A.J., Sahoo, D., Dalerba, P., Mitra, S.S., Wang, J., Contreras-Trujillo, H., Martin, R., Cohen, J.D., et al. (2012). The CD47-signal regulatory protein alpha (SIRPa) interaction is a therapeutic target for human solid tumors. Proc. Natl. Acad. Sci. U. S. A. *109*, 6662–6667.

Wilson, I.A., Skehel, J.J., and Wiley, D.C. (1981). Structure of the haemagglutinin membrane glyco˚ resolution. Nature, protein of influenza virus at 3. A *289*, 366–373.

Winternitz, M.C., Wason, I.M., and McNamara, F.P. (1920). The Pathology of Influenza. New Haven Yale Univ. Press.

Wise, H.M., Foeglein, A., Sun, J., Dalton, R.M., Patel, S., Howard, W., Anderson, E.C., Barclay, W.S., and Digard, P. (2009). A Complicated Message: Identification of a Novel PB1-Related Protein Translated from Influenza A Virus Segment 2 mRNA. J. Virol. *83*, 8021–8031.

Wu, A.-L., Wang, J., Zheleznyak, A., and Brown, E.J. (1999). Ubiquitin-Related Proteins Regulate Interaction of Vimentin Intermediate Filaments with the Plasma Membrane. Mol. Cell *4*, 619–625.

Xiao, H., Killip, M.J., Staeheli, P., Randall, R.E., and Jackson, D. (2013). The Human Interferon-Induced MxA Protein Inhibits Early Stages of Influenza A Virus Infection by Retaining the Incoming Viral Genome in the Cytoplasm. J. Virol. *87*.

Xing, T., Wang, Y., Ding, W. jie, Li, Y. ling, Hu, X. dong, Wang, C., Ding, A., and Shen, J. long (2017). Thrombospondin-1 Production Regulates the Inflammatory Cytokine Secretion in THP-1 Cells Through NF-κB Signaling Pathway. Inflammation *40*, 1606–1621.

Yamamoto, N., Suzuki, S., Suzuki, Y., Shirai, A., Nakazawa, M., Suzuki, M., Takamasu, T., Nagashima, Y., Minami, M., and Ishigatsubo, Y. (2001). Immune Response Induced by Airway Sensitization after Influenza A Virus Infection Depends on Timing of Antigen Exposure in Mice. J. Virol. *75*, 499 LP – 505.

Yamao, T., Noguchi, T., Takeuchi, O., Nishiyama, U., Morita, H., Hagiwara, T., Akahori, H., Kato, T., Inagaki, K., Okazawa, H., et al. (2002). Negative Regulation of Platelet Clearance and of the Macrophage Phagocytic Response by the Transmembrane Glycoprotein SHPS-1. J. Biol. Chem. *277*, 39833–39839.

Yap, K.L., Ada, G.L., and McKenzie, I.F.C. (1978). Transfer of specific cytotoxic T lymphocytes protects mice inoculated with influenza virus. Nature.

Ye, Z.W., Yuan, S., Poon, K.M., Wen, L., Yang, D., Sun, Z., Li, C., Hu, M., Shuai, H., Zhou, J., et al. (2017). Antibody-dependent cell-mediated cytotoxicity epitopes on the hemagglutinin head region of pandemic H1N1 influenza virus play detrimental roles in H1N1-infected mice. Front. Immunol.

York, A., Hengrung, N., Vreede, F.T., Huiskonen, J.T., and Fodor, E. (2013). Isolation and characterization of the positive-sense replicative intermediate of a negative-strand RNA virus. Proc. Natl. Acad. Sci. U. S. A. *110*, E4238-45.

Zambon, M.C. (2001). The pathogenesis of influenza in humans. Rev. Med. Virol.

Zhang, J., Miao, J., Hou, J., and Lu, C. (2015). The effects of H3N2 swine influenza virus infection on TLRs and RLRs signaling pathways in porcine alveolar macrophages. Virol. J. *12*, 61.

Zhang, M., Hutter, G., Kahn, S.A., Azad, T.D., Gholamin, S., Xu, C.Y., Liu, J., Achrol, A.S., Richard, C., Sommerkamp, P., et al. (2016). Anti-CD47 treatment stimulates phagocytosis of glioblastoma by M1 and M2 polarized macrophages and promotes M1 polarized macrophages in vivo. PLoS One *11*, 1–21.

Zhirnov, O.P. (1990). Solubilization of matrix protein M1/M from virions occurs at different pH for orthomyxo- and paramyxoviruses. Virology.

Zost, S.J., Parkhouse, K., Gumina, M.E., Kim, K., Perez, S.D., Wilson, P.C., Treanor, J.J., Sant, A.J., Cobey, S., and Hensley, S.E. (2017). Contemporary H3N2 influenza viruses have a glycosylation site that alters binding of antibodies elicited by egg-adapted vaccine strains. Proc. Natl. Acad. Sci. U. S. A. *114*, 12578–12583.

Acknowledgments

At this point I would like to thank all those who have contributed to the success of this work by their professional and personal support. First, I want to thank Prof. Dr. Jan Buer and Dr. Torben Knuschke, who gave me the opportunity to perform my PhD thesis on this exciting project and to grow and further develop with this challenge. Particular thanks are owed to my supervisor Torben Knuschke, who has always advised, supported, and motivated me in the last years. It was a great pleasure to work together with him and I am very grateful for all the time he spent on me and my work. Furthermore, I would like to thank Prof. Dr. Astrid Westendorf for her continued versed guidance. A special thanks also applies to Prof. Dr. Ulf Dittmer for his professional support and the commitment to be my second supervisor. Moreover, I would like to thank Prof. Dr. Wiebke Hansen for her knowledgeable support. A special thanks also goes to Christina Liebig for her support in the performance of the experiments and the humorous times we enjoyed. Besides, I would also like to thank Prof. Dr. Robert Klopfleisch at the Institute of Veterinary Pathology in Berlin, Dr. Robert Geffers at the Helmholtz Centre for Infection Research in Braunschweig, Prof. Dr. Dunja Bruder at the Helmholtz Centre for Infection Research in Braunschweig, Dr. Julia Boehme at the Helmholtz Centre for Infection Research in Braunschweig, Dr. Florian Wirsdörfer at the Institute of Cell Biology (Cancer Research) in Essen, and Prof. Dr. Karl Lang at the Institute for Immunology in Essen for their time and effort supporting my project. Thanks also go to the research training group 1949 for all the opportunities offered by the program and the great time I could spent with the other members. Furthermore, I would like to thank the entire working group for their professional and personal support. The friendly and open atmosphere has always motivated me in my work. Finally, I would like to thank friends and family for their constant support.

Curriculum vitae

Der Lebenslauf ist in der Online-Version aus Gründen des Datenschutzes nicht enthalten.

Der Lebenslauf ist in der Online-Version aus Gründen des Datenschutzes nicht enthalten.

Der Lebenslauf ist in der Online-Version aus Gründen des Datenschutzes nicht enthalten.

Erklärung

Hiermit erkläre ich, gem. § 7 Abs. (2) d) + f) der Promotionsordnung der Fakultät für Biologie zur Erlangung des Dr. rer. nat., dass ich die vorliegende Dissertation selbstständig verfasst und mich keiner anderen als der angegebenen Hilfsmittel bedient, bei der Abfassung der Dissertation nur die angegebenen Hilfsmittel benutzt und alle wörtlich oder inhaltlich übernommenen Stellen als solche gekennzeichnet habe.

Essen, den 07.10.20202 C. Wenzek

Unterschrift des/r Doktoranden/in

Erklärung

Hiermit erkläre ich, gem. § 7 Abs. (2) e) + g) der Promotionsordnung der Fakultät für Biologie zur Erlangung des Dr. rer. nat., dass ich keine anderen Promotionen bzw. Promotionsversuche in der Vergangenheit durchgeführt habe und dass diese Arbeit von keiner anderen Fakultät/Fachbereich abgelehnt worden ist.

Essen, den 07.10.20202 C. Wenzek

Unterschrift des/r Doktoranden/in

Erklärung

Hiermit erkläre ich, gem. § 6 Abs. (2) g) der Promotionsordnung der Fakultät für Biologie zur Erlangung des Dr. rer. nat., dass ich das Arbeitsgebiet, dem das Thema „CD47 impedes Antiviral Alveolar Macrophage Responses during Influenza A Virus Infection“ zuzuordnen ist, in Forschung und Lehre vertrete und den Antrag von Christina Wenzek befürworte und die Betreuung auch im Falle eines Weggangs, wenn nicht wichtige Gründe dem entgegenstehen, weiterführen werde.

Jan Byer

Name des Mitglieds der Universität Duisburg-Essen in Druckbuchstaben

Essen, den 07.10.20202

Unterschrift eines Mitglieds der Universität Duisburg-Essen